




Review

Indirect methods with transfer reactions: The Trojan Horse method and the Asymptotic Normalization Coefficient

A. Tumino ^{a,b} ^{*}, C.A. Bertulani ^c, S. Cherubini ^{d,b}, G.F. D'Agata ^{d,b}, A. Di Pietro ^b, P. Figuera ^b, G.L. Guardo ^b, M. Gulino ^{a,b}, S. Hayakawa ^e, M. La Cognata ^b, M. La Commara ^{f,g}, L. Lamia ^{d,b}, D. Lattuada ^{a,b}, M. Mazzocco ^{i,h}, A.M. Moro ^j, J. Mraček ^k, A.A. Oliva ^b, S. Palmerini ^{l,m}, R.G. Pizzone ^{d,b}, G.G. Rapisarda ^{d,b}, S. Romano ^{d,b}, M.L. Sergi ^{d,b}, R. Sparta ^{a,b}, S. Typel ^{n,o}, H. Yamaguchi ^e

^a Dipartimento di Ingegneria e Architettura, Università degli Studi di Enna "Kore", Enna, 94015, Italy

^b INFN, Laboratori Nazionali del Sud, Catania, 95123, Italy

^c Department of Physics and Astronomy, East Texas A&M University, Commerce, TX 75429, USA

^d Dipartimento di Fisica e Astronomia "E. Majorana", Università degli Studi di Catania, Catania, 95123, Italy

^e Center for Nuclear Study, the University of Tokyo, Wako, Saitama, Japan

^f Dipartimento di Farmacia, Università degli Studi di Napoli Federico II, Napoli, Italy

^g INFN, sezione di Napoli, Napoli, Italy

^h Dipartimento di Fisica e Astronomia, Università degli Studi di Padova, Padova, Italy

ⁱ INFN, sezione di Padova, Padova, Italy

^j Departamento de FAMN, Universidad de Sevilla, Apartado 1065, 41080 Sevilla, Spain

^k Nuclear Physics Institute of the CAS, 250 68 Řež near Prague, Czech Republic

^l Dipartimento di Fisica e Geologia, Università degli Studi di Perugia, Perugia, Italy

^m INFN, sezione di Perugia, Perugia, Italy

ⁿ GSI Helmholtzzentrum für Schwerionenforschung GmbH, Darmstadt, Germany

^o Technische Universität Darmstadt, Fachbereich Physik, Institut für Kernphysik, Darmstadt, Germany

ARTICLE INFO

Keywords:

Nuclear reactions
Transfer processes
Stellar burning
Stellar evolution

ABSTRACT

We review the status and perspectives of indirect methods that make use of transfer reactions. We focus on two of them that have been extensively used in the past decades to determine cross sections of reactions of astrophysical relevance: the Trojan Horse method and the Asymptotic Normalization Coefficients method. We provide a comprehensive description of the theory behind each of these techniques, followed by an overview of a selection of experiments carried out using these indirect tools.

Contents

1. Introduction	2
2. Theory of indirect methods for nuclear astrophysics	4
2.1. Notation and kinematics	4
2.2. Cross sections of nuclear rearrangement reactions	6
2.3. T-matrix elements and relation of cross sections in the THM	7
2.3.1. Plane-wave impulse approximation	7
2.3.2. Modified distorted-wave and plane-wave Born approximations	8

* Corresponding author at: Dipartimento di Ingegneria e Architettura, Università degli Studi di Enna "Kore", Enna, 94015, Italy.

E-mail address: tumino@lns.infn.it (A. Tumino).

<https://doi.org/10.1016/j.ppnp.2025.104164>

Available online 24 February 2025

0146-6410/© 2025 Elsevier B.V. All rights reserved, including those for text and data mining, AI training, and similar technologies.

2.3.3.	Other approaches	11
2.4.	T-matrix elements and cross sections in the ANC method	11
3.	Experimental application of the ANC method	13
3.0.1.	The $^{18}\text{O}(p, \gamma)^{19}\text{F}$ reaction	14
3.0.2.	The $^3\text{He}(\alpha, \gamma)^7\text{Be}$ reaction	15
3.0.3.	The $^{26}\text{Si}(p, \gamma)^{27}\text{P}$ reaction	17
4.	Experimental application of the THM	17
4.1.	Kinematic conditions	18
4.2.	General steps of data analysis	19
4.3.	Recent applications	21
4.3.1.	The contribution to the standard BBN reaction network	21
4.3.2.	Status of the $^7\text{Be}+n$ measurements and the THM experiment at CRIB	22
4.3.3.	Status of the $d+d$ fusion measurements and the THM experiments	23
4.3.4.	The $^{27}\text{Al}(p, \alpha)^{24}\text{Mg}$ reaction: astrophysical scenarios and measurements	24
4.3.5.	The Coulomb-free p-p scattering cross section and the fundamental symmetries in the NN interaction	26
4.3.6.	Status of the $^{12}\text{C}+^{12}\text{C}$ fusion measurements and the THM experiment	28
5.	Advances addressing next challenges	31
5.1.	Astrophysical cross sections from the surrogate method	32
5.1.1.	Reminder of the surrogate method	32
5.1.2.	Determination of the formation probability in the IAV model	32
6.	Summary and outlook	33
	Declaration of competing interest	33
	Acknowledgments	33
	References	34

1. Introduction

Nuclear reactions are crucial ingredients in describing how stars evolve. Beside of representing the stellar energy engine, nuclear reactions are also responsible for the chemical evolution of the universe and the production of the elements. To understand how elements are synthesized in stellar phenomena, it is fundamental to study the relevant reactions that govern the nucleosynthesis paths and to quantify their cross sections [1–5]. This is one of the main goals yet a critical issue of nuclear astrophysics since the extremely high temperatures in the stellar interiors correspond to amounts of energy usually much smaller than the Coulomb barrier between the nuclei involved in the relevant reactions. The Coulomb repulsion is thus responsible for the exponential decrease of the cross section $\sigma(E)$ at energies corresponding to stellar temperatures. This makes the majority of astrophysical reactions proceeding in stellar environments difficult or impossible to measure directly under the same conditions in the laboratory as in the stars. What is usually done is to carry out direct measurements at as low energies as possible (usually $E > 100$ keV) and then extrapolate the behavior of $\sigma(E)$ down to the astrophysical region using the definition of the astrophysical $S(E)$ factor

$$S(E) = E\sigma(E)\exp(2\pi\eta) \quad (1.1)$$

with the Sommerfeld parameter $\eta = \alpha Z_1 Z_2 \sqrt{\mu c^2 / 2E}$, where α is the fine-structure constant, Z_1 and Z_2 are the atomic numbers of the two colliding nuclei, μ is their reduced mass and c is the speed of light.

It removes the energy dependence of $\sigma(E)$ due to the barrier tunneling given by the Gamow factor $\exp(-2\pi\eta)$. However, even a simple extrapolation can easily lead to absolutely misleading/wrong results, due, for instance, to the missing contribution of unexpected resonances or sub-threshold ones. Resonances may change by orders of magnitude the extrapolated cross-section at astrophysical energies.

Another critical issue in laboratory measurements of nuclear reactions is represented by the electron screening effect. Indeed both target and projectile are usually embedded in neutral/ionized atoms or molecules or in a lattice of a solid-state system, whose electron clouds give rise to an attractive potential responsible for a reduction of the Coulomb barrier. This, in turn, leads to an increased cross section for screened nuclei, $\sigma_s(E)$, compared to the cross section for bare nuclei [6,7] $\sigma_b(E)$. Therefore, a correction factor has to be introduced to determine the unscreened or bare nucleus cross section. It is called screening factor, defined as

$$f_{\text{lab}}(E) = \frac{\sigma_s(E)}{\sigma_b(E)} \approx \exp\left(\pi\eta \frac{U_e}{E}\right), \quad (1.2)$$

with U_e the “electron screening potential”. The expression holds true when the energy of the incident particle is large compared to the screening energy, i.e., $E \gg U_e$. The electron screening potential, U_e , is assumed to be independent of energy. In a stellar plasma, a similar enhancement factor is considered:

$$f_{pl}(E) = \frac{\sigma_{pl}(E)}{\sigma_b(E)} \approx \exp\left(\pi\eta \frac{U_{pl}}{E}\right) \quad (1.3)$$

with $\sigma_{pl}(E)$ the cross section in the plasma. It can be calculated once the plasma screening potential U_{pl} is known. It depends on important properties of the plasma such as the Debye–Hückel radius. A measurement of U_e , which is needed to calculate $\sigma_s(E)$ from Eq. (1.2), would also be beneficial to better understand U_{pl} .

Low-energy charged particle fusion reactions measured so far have accordingly shown the exponential enhancement predicted by Eq. (1.2), see also [7]. However, the deduced U_e values are often larger than the adiabatic limit, defined in atomic physics as the difference between the electron binding energies of the separate atoms in the entrance channel and that of the composite atom [7,8]. This disagreement in laboratory experiments is yet to be understood, and prevents the effects under astrophysical conditions to be fully assessed. A weak point in the laboratory approach - and thus in the deduced U_e value - is the need to make an assumption for the energy dependence of $\sigma_b(E)$ at ultra-low energies.

Moreover, it was pointed out that Eq. (1.2) is not appropriate to correct the measured resonance strengths of narrow resonances, while it is emphasized that screening is responsible of the shift of the resonance energy compared to the case of unscreened nuclei [9].

These arguments are not so strong for reactions involving radioactive nuclei, which do play a role in explosive nucleosynthesis known for its higher energy dynamics. Consequently, these reactions are less impacted by Coulomb suppression or electron screening [10,11]. In reactions induced by radioactive nuclei, astrophysical timescales should typically align with the half-life of the nuclear species being studied [10]. Shorter timescales are commonly linked to explosive environments, where energies surpass those of quiescent nuclear burning, reaching the scale of about MeV. At such energies, the penetration probability of the Coulomb barrier is a smoothly varying function of the energy, as demonstrated in [12], for instance. Likewise, even considering the upper limit for the electron screening potential, the enhancement factor rapidly stabilizes around 1 with increasing energy at the MeV scale as exemplified in Ref. [13].

However, the study of reactions involving radioactive nuclei requires either the existence of radioactive beams, whose intensity is often very low, rarely exceeding 10^6 pps, or the production of radioactive targets when nuclei have relatively long lifetimes, something not easy to realize with a sufficiently large areal density. Therefore, again direct measurements are very challenging, if not impossible, as in the case of r-process reactions, due to the lack of neutron targets.

To overcome all these difficulties, indirect techniques have been introduced, see, e.g., [14,15] for recent reviews. They make use of direct reaction mechanisms, such as transfer processes, e.g. stripping, pick-up or knock-out. In particular, two indirect methods have been devised in this respect: the Asymptotic Normalization Coefficients (ANC) and the Trojan Horse Method (THM). In the ANC method, a virtual nucleon or nucleus x is transferred from a nucleus a to another nucleus A forming a bound state B leaving a nucleus b in the exit channel. This reaction

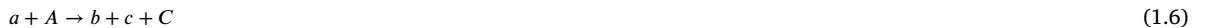


is depicted diagrammatically in the left panel of Fig. 1.1 with two vertices representing the breakup of a and the formation of the bound state B . The measured cross section of this process gives information on the asymptotic radial dependence of the wave function of Ax relative motion in B provided the transfer is peripheral. It can then be used in the analytic calculation of the cross section of the radiative capture reaction



at ultra-low energies.

The THM starts with the same entrance channel as the ANC method but a reaction



with three bodies in the exit channel is studied as shown in the right panel of Fig. 1.1. The main goal of the THM is to extract information on the asymptotic form of the $c + C$ scattering wave functions and hence the cross section of the reaction



determined by the corresponding S matrix. The particle x that is transferred between the two subsystems is considered virtual, not being “on the energy shell”. This means that the relation between its energy and momentum is not given by the typical dispersion relation $E_x = p_x^2/(2m_x)$ of freely propagating particles.

The ANC and THM share the common feature that reactions at high energies much above the Coulomb barrier, and thus far surpassing the screening potential energy, are studied to access the cross sections of a radiative capture or a rearrangement reaction at very low energies much below the Coulomb barrier. As a result, these cross-sections are inherently insensitive to both Coulomb suppression and screening enhancement effects. This feature holds substantial significance in the field of nuclear astrophysics since the two main effects preventing access to the energies of astrophysical interest in direct measurements are the Coulomb suppression of cross sections and the electron screening effects. The possibility to use energies of several tens of MeV makes the indirectly measured cross sections of a radiative capture or a rearrangement reaction free of Coulomb suppression and, from stronger argument, of electron screening effects as previously discussed in this section.

A proper knowledge of nuclear reaction theory is essential to understand the operation of the ANC and THM. The relation of the cross sections of the reactions (1.4) and (1.5) or (1.6) and (1.7), respectively, is found with the theory of direct transfer reactions. Approximations are needed to express the cross sections of the “surrogate” reactions as the product of a contribution that can be calculated from theory and a quantity that gives directly the cross section of the two-body reaction of interest. This factorization is related to the appearance of two vertices in the diagrams of Fig. 1.1. The approximations exploit the fact that the reaction mechanisms are dominated by peripheral processes where only the asymptotic part of the wave functions is relevant. This also leads to a selection of specific kinematic conditions in indirect experiments.

The Section 1 is devoted to the presentation of the theory of direct reactions, an indispensable ingredient for the application of indirect methods. In particular, topics related to the wave functions, transition matrix elements, and cross section with the employed

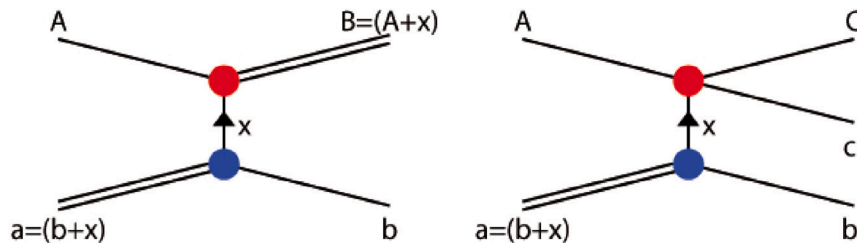


Fig. 1.1. Vertex diagrams of transfer reactions to a bound state B as applied in the ANC method (left panel) and to a scattering state $c + C$ with regard to the THM (right panel).

approximations will be discussed. The following sections are dedicated to the experimental application of the indirect methods. In particular, the kinematic conditions, specific features and tests of the methods and an overview over experiments will be given. Each application will be preceded by a brief astrophysical introduction when applicable. Finally, the work concludes with further discussion and conclusions.

2. Theory of indirect methods for nuclear astrophysics

In many cases, it is beneficial to measure cross sections of astrophysical reactions not only directly, if possible at all, but to consider indirect approaches. They are often more advantageous from an experimental point of view but require support from nuclear reaction theory (for recent reviews, see [15–18]).

The selected surrogate method depends on the reaction of interest. In case of rearrangement reactions $A(x, c)C$, the Trojan Horse method (THM) can be exploited to extract the energy dependence of the cross section, however, absolute values are not given and a normalization to direct data at high energies is needed [17,18]. For radiative capture reactions $A(a, \gamma)D$, there are two indirect methods that are utilized: the ANC method [19] and the Coulomb dissociation (CD) method [20].

The ANC method can be used to determine the zero-energy S factor of the radiative capture reaction. Absolute cross sections over a certain range of energies are provided by the CD method. In this review, the THM and ANC methods are discussed because they are based on similar concepts of nuclear reaction theory with processes involving the strong interaction.

The main goal of the THM is to extract the cross section of the two-body reaction (1.7) from the experimentally measured cross section of the reaction (1.6) with three particles in the exit channel. The connection of the cross sections can be established with the help of the theory of direct reactions following the traditional approaches for transfer reactions. The distinctive feature of the THM is a particular choice of the kinematic conditions that corresponds to a quasi-free reaction mechanism for the subreaction (1.7) within the reaction (1.6), i.e., a small momentum transfer to the spectator nucleus b that is originally bound inside the Trojan-horse nucleus a . It allows to apply certain approximations that finally lead to a factorization of the cross section of the three-body reaction with a kinematic factor, a momentum distribution of the bx relative motion inside the nucleus a and a cross section of the two-body reaction (1.7). The latter is, however, not the on-energy-shell (OES) cross section of the reaction of interest but a half-off-the-energy-shell (HOES) cross section that needs to be related to the OES cross section [17,18].

The derivation of the relation between the cross sections in the THM proceeds in several steps. First, general expressions for the cross sections of the two reactions with two and three particles in the final state are devised that connect them to the transition or T -matrix elements of the processes which contain the essential information of the reactions. These matrix elements can be evaluated in different approximations. Here, two approaches will be presented: the plane-wave impulse approximation (PWIA) and the modified distorted-wave and plane-wave Born approximations (MDWBA and MPWBA) that finally allow to deduce the connection between the HOES and OES cross section of the reaction (1.7). More details on these approaches can be found in some basic THM references, e.g., see [21–23] and review articles, e.g., [17,18,24]. Finally, other theoretical descriptions of the THM method will be briefly summarized.

The ANC method uses traditional transfer reactions with two particles in the initial and final states. These are often exploited to extract spectroscopic factors for specific states from the comparison of experimental cross sections to theoretical values employing simple single-particle descriptions of nuclear many-body wave functions. However, the goal of the ANC method is to determine the absolute amplitude of the asymptotic bound-state wave functions in the entrance ($a + A$) or exit channels ($c + C$). Thus, experimental conditions have to be selected that guarantee the dominance of peripheral processes. The ANC can then be used in a theoretical calculation of the astrophysical S factor for a radiative capture reaction that involves the channel $a + A$ or $c + C$ [15,19,24].

2.1. Notation and kinematics

The theoretical formulation usually employs center-of-mass coordinates (cm) in a non-relativistic description where \vec{r}_i and \vec{p}_i denote the spatial coordinate and the momentum of a particle i with mass m_i . It is convenient to introduce relative coordinates and momenta

$$\vec{r}_{ij} = \vec{r}_i - \vec{r}_j, \quad \vec{p}_{ij} = \mu_{ij} \left(\frac{\vec{p}_i}{m_i} - \frac{\vec{p}_j}{m_j} \right), \quad (2.1)$$

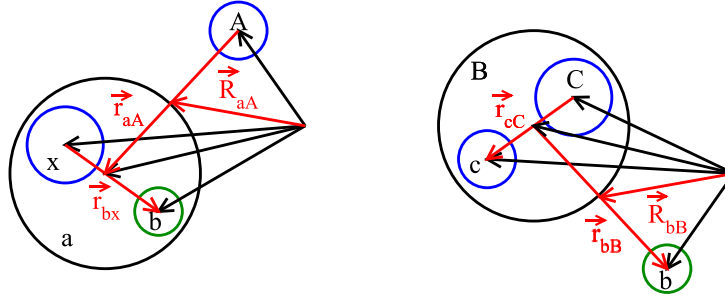


Fig. 2.1. Spatial Jacobi coordinates in the initial (left) and final (right) state of the TH reaction are given in red color. The spectator b is colored green and the nuclei participating in the two-body reaction of interest are colored blue.

in a two-body system $i + j$ as well as the cm position and momentum

$$\vec{R}_{ij} = \frac{1}{M_{ij}} (m_i \vec{r}_i + m_j \vec{r}_j), \quad \vec{P}_{ij} = \vec{p}_i + \vec{p}_j, \quad (2.2)$$

of the total system. In these definitions, the reduced mass and the total mass

$$\mu_{ij} = \frac{m_i m_j}{M_{ij}}, \quad M_{ij} = m_i + m_j, \quad (2.3)$$

appear. Denoting the system $i + j$ with k and defining $\vec{r}_k = \vec{R}_{ij}$, $\vec{p}_k = \vec{P}_{ij}$ and $m_k = M_{ij}$, further coordinates and momenta can be introduced recursively for systems with more than two particles, defining the usual Jacobi coordinates. The spatial Jacobi coordinates \vec{r}_{bx} , \vec{r}_{aA} , \vec{R}_{aA} and \vec{r}_{cC} , \vec{r}_{bB} , \vec{R}_{bB} are depicted in Fig. 2.1 for the initial and final state of the TH reaction, respectively. The Jacobi coordinates in momentum space can be used favorably to express the energies in the entrance and exit channels of the two reactions of interest. In particular, one has

$$E_{xA} = E_x + E_A = \frac{p_{xA}^2}{2\mu_{xA}} + \frac{P_{xA}^2}{2M_{xA}}, \quad E_{cC} = E_c + E_C = \frac{p_{cC}^2}{2\mu_{cC}} + \frac{P_{cC}^2}{2M_{cC}}, \quad (2.4)$$

with $\vec{P}_{xA} = \vec{P}_{cC} = 0$ in the cm system for reaction (1.7) and

$$E_{aA} = E_a + E_A = \frac{p_{aA}^2}{2\mu_{aA}} + \frac{P_{aA}^2}{2M_{aA}}, \quad E_{bcC} = E_b + E_c + E_C = \frac{p_{cC}^2}{2\mu_{cC}} + \frac{p_{bB}^2}{2\mu_{bB}} + \frac{P_{bB}^2}{2M_{bB}}, \quad (2.5)$$

with $\vec{P}_{aA} = \vec{P}_{bB} = 0$ in the cm system for reaction (1.6). Here, B stands for the system $c + C$. Energy conservation can be expressed as

$$E_{xA} + Q_{xA \rightarrow cC} = E_{cC}, \quad E_{aA} + Q_{aA \rightarrow bcC} = E_{bcC}, \quad (2.6)$$

with the Q values

$$Q_{xA \rightarrow cC} = m_x + m_A - m_c - m_C, \quad Q_{aA \rightarrow bcC} = m_a + m_A - m_b - m_c - m_C, \quad (2.7)$$

for the two reactions.

It is instructive to explore the kinematic condition of the THM in more detail. Combining the two equations gives

$$E_{xA} = E_{aA} - E_{bB} - B_a \quad (2.8)$$

with the binding energy

$$B_a = m_b + m_x - m_a > 0 \quad (2.9)$$

of the Trojan-horse nucleus a with respect to the breakup into $b + x$ and kinetic energy of relative motion $E_{bB} = p_{bB}^2 / (2\mu_{bB})$ of the spectator b and the system $B = c + C$. In the cm system, momentum conservation can be written as

$$0 = \vec{p}_a + \vec{p}_A = \vec{p}_b + \vec{p}_c + \vec{p}_C = \vec{p}_b + \vec{p}_B. \quad (2.10)$$

Then the momenta of relative motion are determined by

$$\vec{p}_{bB} = \vec{p}_b = -\vec{p}_B \quad \vec{p}_{aA} = \vec{p}_a = -\vec{p}_A \quad (2.11)$$

and the energy

$$E_{bB} = \frac{p_b^2}{2\mu_{bB}} = \left(\frac{m_b}{m_a}\right)^2 \frac{p_a^2}{2\mu_{bB}} = \left(\frac{m_b}{m_a}\right)^2 \frac{\mu_{aA}}{\mu_{bB}} E_{aA} \quad (2.12)$$

can be expressed as a multiple of the energy E_{aA} . Under quasi-free scattering conditions, there is no momentum transfer to the spectator nucleus and its original velocity inside the Trojan-horse nucleus a will not change during the reaction. Thus, its momentum in the final state is given by

$$\vec{p}_b^{af} = \frac{m_b}{m_a} \vec{p}_a \quad (2.13)$$

if the Fermi motion of b inside a is neglected. As a result, the quasi-free energy in the initial state of the two-body reaction (1.7) takes the value

$$E_{xA}^{qf} = \left[1 - \left(\frac{m_b}{m_a} \right)^2 \frac{\mu_{aA}}{\mu_{bB}} \right] E_{aA} - B_a \quad (2.14)$$

which can be much smaller than the energy E_{aA} in the entrance channel of the Trojan-horse (TH) reaction. Thus, it is possible to study reactions at energies below the Coulomb barrier, even at negative energies, with a surrogate reaction at much higher energies without being affected by Coulomb suppression of the cross section or electron screening effects. The quasi-free scattering condition also leads to a constraint for the momenta of the particles in the final state, in particular, an angular correlation of the detected nuclei. This condition has to be considered in the planning of a TH experiment.

In practical applications, the energy E_{aA} is not changed to cover a certain range in E_{xA} since it is determined by the energy of the projectile in the TH experiment. Instead, a limited range for the momentum transfer to the spectator is allowed, typically of the order of a few ten MeV/c and smaller than the bound-state momentum $q_{bx} = \sqrt{2\mu_{bx}B_a}$ of the nucleus Trojan-horse nucleus a . This approach was first described in [25] and is different compared to the procedure envisaged in the original introduction of the THM in [26] where it was proposed to use the tail of the Fermi motion of x inside a to compensate for the energy in the $a + A$ relative motion. The required dominance of the quasi-free reaction mechanism also affects the choice of the Trojan-horse nuclei. Their momentum distribution should peak near zero momentum transfer to the spectator and thus nuclei like ${}^2\text{H}$ or ${}^6\text{Li}$ with a dominant s-wave component in their ground state are most favorable to investigate reactions with neutrons, protons, deuterons or α particles.

2.2. Cross sections of nuclear rearrangement reactions

For the reaction (1.7) with two particles in the entrance and exit channels, the general expression for the cross section for particles with total angular momentum J_i is given by

$$d\sigma(x + A \rightarrow c + C) = \frac{2\pi}{\hbar} \frac{\mu_{xA}}{p_{xA}} \frac{1}{(2J_x + 1)(2J_A + 1)} \sum_{M_x M_A} \sum_{M_c M_C} \int \frac{d^3 p_{cC}}{(2\pi\hbar)^3} |T_{xA \rightarrow cC}|^2 \delta(E_{xA} + Q_{xA \rightarrow cC} - E_{cC}) \quad (2.15)$$

with an averaging and summation over the unobserved spin projections M_i in the initial and final states. The prefactor $2\pi/\hbar$ is known from Fermi's golden rule and μ_{xA}/p_{xA} is the inverse relative velocity in the entrance channel corresponding to the required flux factor. The integrand contains the squared modulus of the T-matrix element $T_{xA \rightarrow cC}$ and a δ function that represents the energy conservation. An explicit factor for momentum conservation does not appear because the formulation above is expressed with the cm relative momentum p_{cC} . The expression (2.15) is valid if the scattering waves that enter the calculation of the T-matrix element are normalized to plane waves + in/outgoing spherical waves.

A simple integration over E_{cC} with $d^3 p_{cC} = p_{cC}^2 dp_{cC} d\Omega_{cC} = (p_{cC} \mu_{cC}) dE_{cC} d\Omega_{cC}$ yields the usual differential cross section

$$\frac{d^2\sigma}{d\Omega_{cC}}(x + A \rightarrow c + C) = \frac{\mu_{xA} \mu_{cC}}{(2\pi)^2 \hbar^4} \frac{p_{cC}}{p_{xA}} \frac{1}{(2J_x + 1)(2J_A + 1)} \sum_{M_x M_A} \sum_{M_c M_C} |T_{xA \rightarrow cC}|^2 \quad (2.16)$$

where $d\Omega_{cC}$ defines the solid angle of the relative momentum \vec{p}_{cC} in the final state. Due to time-reversal symmetry of the reaction, one has $|T_{xA \rightarrow cC}|^2 = |T_{cC \rightarrow xA}|^2$ and the theorem of detailed balance

$$(2J_x + 1)(2J_A + 1) p_{xA}^2 \frac{d\sigma}{d\Omega_{cC}}(x + A \rightarrow c + C) = (2J_c + 1)(2J_C + 1) p_{cC}^2 \frac{d\sigma}{d\Omega_{xA}}(c + C \rightarrow x + A) \quad (2.17)$$

with the differential cross section of the inverse reaction easily obtained.

The general expression for the reaction with three particles in the exit channel

$$d\sigma(a + A \rightarrow b + c + C) = \frac{2\pi}{\hbar} \frac{\mu_{aA}}{p_{aA}} \frac{1}{(2J_a + 1)(2J_A + 1)} \sum_{M_a M_A} \sum_{M_b M_c M_C} \int \frac{d^3 p_{cC}}{(2\pi\hbar)^3} \frac{d^3 p_{bB}}{(2\pi\hbar)^3} |T_{aA \rightarrow bcC}|^2 \delta(E_{aA} + Q_{aA \rightarrow bcC} - E_{bcC}) \quad (2.18)$$

is slightly more involved than the one given in (2.15) due to the additional momentum integration and summation over the angular momentum projection of the third particle. The δ function for energy conservation allows again to perform an explicit integration over E_{bB} . The result

$$\frac{d^5\sigma}{dE_{cC} d\Omega_{cC} d\Omega_{bB}}(a + A \rightarrow b + c + C) = \frac{\mu_{aA} \mu_{bB} \mu_{cC}}{(2\pi)^5 \hbar^7} \frac{p_{bB} p_{cC}}{p_{aA}} \frac{1}{(2J_a + 1)(2J_A + 1)} \sum_{M_a M_A} \sum_{M_b M_c M_C} |T_{aA \rightarrow bcC}|^2 \quad (2.19)$$

is a five-fold differential cross section that depends on the kinematic state of the $c + C$ subsystem (E_{cC} , Ω_{cC}) and the solid angle of the momentum \vec{p}_{bB} . In principle, also another variable than E_{cC} can be chosen for the integration but the one used above is most convenient in the theoretical formulation of the THM.

As soon as a relation between the T-matrix elements $T_{xA \rightarrow cC}$ and $T_{aA \rightarrow bcC}$ is found, it is possible to establish a relation between the cross sections (2.16) and (2.19). In order to keep the expressions simple, the spins of the particles will not be considered in the following. Equations with a full treatment of the angular momenta can be found in [23].

2.3. T-matrix elements and relation of cross sections in the THM

There are various possibilities to give explicit expression for the T-matrix elements $T_{xA \rightarrow cC}$ and $T_{aA \rightarrow bcC}$. Starting from exact forms, approximations have to be applied to arrive at tractable forms for an actual calculation. In the case of the THM, it is sufficient to find some formal expressions that allow to establish the required connection. All of them contain wave functions in the various channels. The internal wave functions of individual nuclei i are denoted by ϕ_i and the plane waves for their relative motion are written as $\Phi_{ij} = \exp(i\vec{p}_{ij} \cdot \vec{r}_{ij}/\hbar)$.

As first approach, the plane-wave impulse approximation is discussed in the following. It serves as a transparent means to obtain the characteristic factorization of the three-body cross section. The second approach considers the modified plane-wave Born approximation that is more involved but helps to take the off-shell effects into account that are essential in the application of the THM.

2.3.1. Plane-wave impulse approximation

The T-matrix elements for the reactions (1.7) and (1.6) can be written in the post and prior forms as

$$T_{xA \rightarrow cC} = \langle \phi_c \phi_C \Phi_{cC} | V_{cC} | \Psi_{xA}^{(+)} \rangle = \langle \Psi_{cC}^{(-)} | V_{xA} | \phi_x \phi_A \Phi_{xA} \rangle \quad (2.20)$$

$$T_{aA \rightarrow bcC} = \langle \phi_b \phi_B \Phi_{bB} | V_{bc} + V_{bC} | \Psi_{aA}^{(+)} \rangle = \langle \Psi_{bcC}^{(-)} | V_{xA} + V_{bA} | \phi_a \phi_A \Phi_{aA} \rangle \quad (2.21)$$

with the exact solutions of the scattering problem, $\Psi_{xA}^{(+)}$ and $\Psi_{aA}^{(+)}$ in the initial state or $\Psi_{cC}^{(-)}$ and $\Psi_{bcC}^{(-)}$ in the final state, respectively. (The full three-body wave function $\Psi_{bcC}^{(-)}$ is approximated here as the product $\Psi_{b(cC)}^{(-)} \phi_B$ where $\phi_B = \Psi_{cC}^{(-)}$ is a scattering state in the $B = c + C$ system.) Formally, T-matrix elements can be expressed as

$$T_{xA \rightarrow cC} = \langle \phi_c \phi_C \Phi_{cC} | \hat{t}_{xA \rightarrow cC} | \phi_x \phi_A \Phi_{xA} \rangle, \quad T_{aA \rightarrow bcC} = \langle \phi_b \phi_c \phi_C \Phi_{cC} \Phi_{bB} | \hat{t}_{aA \rightarrow bcC} | \phi_a \phi_A \Phi_{aA} \rangle, \quad (2.22)$$

with transition operators $\hat{t}_{xA \rightarrow cC}$ and $\hat{t}_{aA \rightarrow bcC}$, respectively, which are usually highly complex objects that act on the wave functions. They can be expressed explicitly with the Green's function $G(z) = 1/(z - H)$ depending on the Hamiltonian $H = T + V$. E.g., in case of the TH reaction one has

$$\hat{t}_{aA \rightarrow bcC} = (V - V_{cC}) \left[1 + \lim_{\epsilon \rightarrow 0} G(E + i\epsilon) (V - V_{bx}) \right] \quad (2.23)$$

with the full interaction

$$V = V_{bx} + V_{bA} + V_{xA} = V_{cC} + V_{bc} + V_{bC}. \quad (2.24)$$

In the impulse approximation, the rather drastic approximation

$$T_{aA \rightarrow bcC} \approx \langle \phi_b \phi_c \phi_C \Phi_{cC} \Phi_{bB} | \hat{t}_{xA \rightarrow cC} | \phi_a \phi_A \Phi_{aA} \rangle \quad (2.25)$$

is applied with a replacement of $\hat{t}_{aA \rightarrow bcC}$ by $\hat{t}_{xA \rightarrow cC}$. This is only permissible if the interaction of b with the other nuclei can be neglected during the reaction. A simple condition for the validity of this approach is a very small momentum transfer to b . Thus, the subreaction $xA \rightarrow cC$ proceeds independent of the presence of b , which is just an uninvolved spectator. From a kinematical point of view, this condition corresponds to a quasi-free scattering process of x and A . It limits the range of momenta in the final state of the $a + A \rightarrow b + c + C$ reaction that can be used in the analysis of a TH experiment. Furthermore, it suffices for the theoretical description of the TH reaction to be accurate solely within the small fraction of the full phase space under examination. Beyond this specific region of momenta combinations, the precision of the theoretical framework in describing the reaction is of no importance.

Another feature of the THM is the employment of a Trojan-horse nucleus a that has a high probability to be considered as a cluster configuration $b + x$ in its ground state. Thus it is reasonable to write the internal wave function ϕ_a of a in coordinate space as

$$\phi_a = \int \frac{d^3q}{(2\pi\hbar)^3} \varphi_a(\vec{q}) \exp(i\vec{q} \cdot \vec{r}_{bx}/\hbar) \phi_b \phi_x \quad (2.26)$$

neglecting other components of the many-body wave function. Introducing this form in the T-matrix element and gives

$$T_{aA \rightarrow bcC} \approx \int \frac{d^3q_{bx}}{(2\pi\hbar)^3} \varphi_a(\vec{q}_{bx}) \langle \phi_b \phi_c \phi_C \Phi_{cC} \Phi_{bB} | \hat{t}_{xA \rightarrow cC} | \exp(i\vec{q}_{bx} \cdot \vec{r}_{bx}/\hbar) \phi_b \phi_x \phi_A \Phi_{aA} \rangle \quad (2.27)$$

with the momentum amplitude $\varphi_a(\vec{q})$.

For a further reformulation of the T-matrix element $T_{aA \rightarrow bcC}$, it is convenient to use the transformation of the arguments

$$-\vec{p}_{bB} \cdot \vec{r}_{bB} + \vec{q}_{bx} \cdot \vec{r}_{bx} + \vec{p}_{aA} \cdot \vec{r}_{aA} = (\vec{q}_{bx} - \vec{Q}_{bB}) \cdot \vec{r}_{bB} + \left[\vec{Q}_{aA} - \frac{m_A}{m_x + m_A} (\vec{q}_{bx} - \vec{Q}_{bB}) \right] \cdot \vec{r}_{xA} \quad (2.28)$$

in the product $\Phi_{bB}^* \exp(i\vec{q}_{bx} \cdot \vec{r}_{bx}/\hbar) \Phi_{aA}$ with the new momenta

$$\vec{Q}_{aA} = \vec{p}_{aA} - \frac{m_A}{m_x + m_A} \vec{p}_{bB}, \quad \vec{Q}_{bB} = \vec{p}_{bB} - \frac{m_b}{m_x + m_b} \vec{p}_{aA}. \quad (2.29)$$

Then the T-matrix element assumes the form

$$\begin{aligned} T_{aA \rightarrow bcC} &\approx \int d^3 q_{bx} \varphi_a(\vec{q}_{bx}) \delta(\vec{q}_{bx} - \vec{Q}_{bB}) \langle \phi_c \phi_C \Phi_{cC} | \hat{t}_{xA \rightarrow cC} | \exp\left\{i \left[\vec{Q}_{aA} - \frac{m_A}{m_x + m_A} (\vec{q}_{bx} - \vec{Q}_{bB}) \right] \cdot \vec{r}_{xA}/\hbar \right\} \phi_x \phi_A \rangle \\ &= \varphi_a(\vec{Q}_{bB}) \langle \phi_c \phi_C \Phi_{cC} | \hat{t}_{xA \rightarrow cC} | \exp(i\vec{Q}_{aA} \cdot \vec{r}_{xA}/\hbar) \phi_x \phi_A \rangle \end{aligned} \quad (2.30)$$

since the integration over \vec{r}_{bx} is analytic and gives a δ function so that the integration over \vec{q}_{bx} can also be performed immediately. The remaining matrix element looks very similar to the two-body matrix element (2.22) except that the plane wave $\Phi_{xA} = \exp(i\vec{p}_{xA} \cdot \vec{r}_{xA}/\hbar)$ is replaced by $\tilde{\Phi}_{xA} = \exp(i\vec{Q}_{aA} \cdot \vec{r}_{xA}/\hbar)$. Since $\vec{Q}_{aA} \neq \vec{p}_{xA}$ in general and

$$\frac{Q_{aA}^2}{2\mu_{xA}} \neq \frac{p_{xA}^2}{2\mu_{xA}} = \frac{p_{cC}^2}{2\mu_{cC}} - Q_{xA \rightarrow cC}, \quad (2.31)$$

there is an energy mismatch and hence a HOES T-matrix element of the two-body reaction (1.7) appears in the T-matrix element

$$T_{aA \rightarrow bcC} \approx \varphi_a(\vec{Q}_{bB}) T_{xA \rightarrow cC}^{HOES} = \varphi_a(\vec{Q}_{bB}) \langle \phi_c \phi_C \Phi_{cC} | \hat{t}_{xA \rightarrow cC} | \tilde{\Phi}_{xA} \phi_x \phi_A \rangle \quad (2.32)$$

of the TH reactions (1.6). Finally, the cross section factorizes as

$$\frac{d^5 \sigma}{dE_{cC} d\Omega_{cC} d\Omega_{bB}} (a + A \rightarrow b + c + C) \approx K W(\vec{Q}_{bB}) \frac{d^2 \sigma^{HOES}}{d\Omega_{cC}} (x + A \rightarrow c + C) \quad (2.33)$$

with a kinematic factor

$$K = \frac{\mu_{aA} \mu_{bB}}{(2\pi\hbar)^3 \mu_{xA}} \frac{p_{xA} p_{bB}}{p_{aA}}, \quad (2.34)$$

and momentum distribution

$$W(\vec{Q}_{bB}) = \left| \varphi_a(\vec{Q}_{bB}) \right|^2, \quad (2.35)$$

and the HOES cross section

$$\frac{d^2 \sigma^{HOES}}{d\Omega_{cC}} (x + A \rightarrow c + C) = \frac{\mu_{xA} \mu_{cC}}{(2\pi)^2 \hbar^4} \frac{p_{cC}}{p_{xA}} \left| T_{xA \rightarrow cC}^{HOES} \right|^2 \quad (2.36)$$

of the two-body reaction. The argument \vec{Q}_{bB} of the momentum distribution has a simple interpretation. In the cm system it is given by $\vec{Q}_{bB} = \vec{p}_b - \vec{q}_b$, i.e., it is the momentum transfer to the spectator b , cf., (2.13), if $\vec{q}_b = \frac{m_b}{m_x + m_b} \vec{p}_a$ is identified with the momentum of b in the initial state. Thus, the condition $\vec{Q}_{bB} = 0$ characterizes the quasi-free scattering condition that leads to

$$\vec{Q}_{aA}^{qf} = \left(1 - \frac{m_A}{m_x + m_A} \frac{m_b}{m_x + m_b} \right) \vec{p}_{aA} \quad (2.37)$$

for the momentum appearing in the HOES cross section. The derivation of the cross section formula (2.33) is very transparent but no evident link between the HOES cross (2.36) and the sought-after OES cross section is found. For this, a more detailed treatment of the reaction with the help of the theory of direct reactions is required.

2.3.2. Modified distorted-wave and plane-wave Born approximations

The quasi-free reaction mechanism in the THM can be described as a transfer reaction in a similar way as usual in direct reaction theory. The main difference is that the transferred particle x is not captured to a bound state with the nucleus A in the exit channel but a reaction takes place to a scattering state $c + C$ with a different partition than before. The main aim is to express the T-matrix element $T_{aA \rightarrow bcC}$ of the TH reaction (1.6) in a form that allows to find a more direct connection to the cross section of the two-body reaction (1.7).

A possible starting point is the general post-form T-matrix element

$$\mathbf{T}_{aA \rightarrow bB} = \langle \phi_b \phi_B \Phi_{bB} | V_{bB} | \Psi_{aA}^{(+)} \rangle \quad (2.38)$$

that contains the full interaction V_{bB} between the spectator b and the system $B = c + C$ and the exact scattering wave function $\Psi_{aA}^{(\pm)}$ in the initial state. (The boundary conditions of outgoing or ingoing spherical waves in the reaction channels are denoted by the \pm symbol.) The wave function ϕ_B represents the full scattering wave function of the $c + C$ system in the final state. In an ordinary transfer reaction it was just the bound state after the pickup of the transferred particle x by the nucleus A . Since the expression (2.38) contains the unknown wave function $\Psi_{aA}^{(\pm)}$, it has to be transformed to a more suitable form. The potential V_{bB} is in general a rather complicated interaction that depends on the coordinates of all nucleons. It is convenient to introduce optical potentials U_{aA} and U_{bB} that depend only on the relative coordinates \vec{r}_{aA} and \vec{r}_{bB} . Then the Schrödinger equations

$$\left(\frac{\hat{p}_{aA}^2}{2\mu_{aA}} + U_{aA}(\vec{r}_{aA}) \right) \chi_{aA}^{(\pm)} = \frac{p_{aA}^2}{2\mu_{aA}} \chi_{aA}^{(\pm)}, \quad \left(\frac{\hat{p}_{bB}^2}{2\mu_{bB}} + U_{bB}(\vec{r}_{bB}) \right) \chi_{bB}^{(\pm)} = \frac{p_{bB}^2}{2\mu_{bB}} \chi_{bB}^{(\pm)}, \quad (2.39)$$

can be solved exactly with the distorted waves $\chi_{aA}^{(\pm)}$ and $\chi_{bB}^{(\pm)}$ that describe the relative motion in the $a + A$ and $b + B$ channels for elastic scattering. An application of the Gell-Mann–Goldberger relation allows to write

$$T_{aA \rightarrow bcC} = \langle \phi_b \phi_B \Phi_{bB} | U_{bB} | \phi_a \phi_A \chi_{aA}^{(+)} \rangle + \langle \phi_b \phi_B \chi_{bB}^{(-)} | V_{bB} - U_{bB} | \Psi_{aA}^{(+)} \rangle \quad (2.40)$$

for the T-matrix element with two contributions. The first term vanishes because $a + A \neq b + B$. Replacing the full scattering wave function $\Psi_{aA}^{(+)}$ with the distorted wave $\chi_{aA}^{(+)}$ in the second term leads to the distorted-wave Born approximation (DWBA)

$$T_{aA \rightarrow bcC} \approx \langle \phi_b \phi_B \chi_{bB}^{(-)} | V_{bB} - U_{bB} | \phi_a \phi_A \chi_{aA}^{(+)} \rangle \quad (2.41)$$

with the difference

$$V_{bB} - U_{bB} = V_{bc} + V_{bC} - U_{bB} = V_{bx} + V_{bA} - U_{bB} \quad (2.42)$$

of the potentials. Since it is assumed that the full potential V_{bA} and the optical potential U_{bB} have similar effects in the scattering of the spectator b on the nuclei A and B , the potential difference in (2.41) is replaced by V_{bx} . Considering that the wave function ϕ_B in the T-matrix element is given by the full scattering wave function $\Psi_{cC}^{(-)}$ in the final state, the approximate expression

$$T_{aA \rightarrow bcC} = \langle \phi_b \Psi_{cC}^{(-)} \chi_{bB}^{(-)} | V_{bx} | \phi_a \phi_A \chi_{aA}^{(+)} \rangle \quad (2.43)$$

is obtained. Similar as in the plane-wave impulse approximation, the bound-state wave function ϕ_a of the Trojan-horse nucleus a in coordinate space is replaced by a representation in momentum space also taking into account the action of the potential V_{bx} via the Schrödinger equation

$$\left(\frac{\hat{p}_{bx}^2}{2\mu_{bx}} + V_{bx} \right) \phi_a = \left(-\frac{\hbar^2}{2\mu_{bx}} \Delta_{\vec{r}_{bx}} + V_{bx} \right) \phi_a = -B_a \phi_a \quad (2.44)$$

with the binding energy B_a of the bound-state. Thus the expression

$$V_{bx} \phi_a = \int \frac{d^3 q_{bx}}{(2\pi\hbar)^3} w_{bx}^a(\vec{q}_{bx}) \exp(i\vec{q}_{bx} \cdot \vec{r}_{bx}/\hbar) \phi_b \phi_x \quad (2.45)$$

with the momentum amplitude

$$w_{bx}^a(\vec{q}_{bx}) = - \left(B_a + \frac{q_{bx}^2}{2\mu_{bx}} \right) \phi_a(\vec{q}_{bx}) \quad (2.46)$$

is obtained and the T-matrix assumes the form

$$T_{aA \rightarrow bcC} \approx \int \frac{d^3 q}{(2\pi\hbar)^3} w_{bx}^a(\vec{q}) \langle \Psi_{cC}^{(-)} \chi_{bB}^{(-)} | \exp(i\vec{q} \cdot \vec{r}_{bx}/\hbar) \phi_x \phi_A \chi_{aA}^{(+)} \rangle \quad (2.47)$$

in analogy to (2.27) but with the full scattering wave function $\Psi_{cC}^{(-)}$ and the distorted waves $\chi_{aA}^{(+)}$ and $\chi_{bB}^{(-)}$.

In order to find the relation of the cross section (2.19) with the T-matrix element (2.47) to the cross section of the two-body reaction (1.6), it is necessary to specify the scattering wave function $\Psi_{cC}^{(-)}$ in more detail. In partial-wave representation, its asymptotic form for large radii is given by

$$\Psi_{cC}^{(\pm)}(\vec{r}_{cC}) \rightarrow \frac{4\pi\hbar}{p_{cC}} \sum_{dD} \sum_{lm} \frac{i^l}{r_{dD}} \psi_{dDcC}^{(\pm)}(l, r_{dD}) Y_{lm}(\hat{r}_{dD}) Y_{lm}^*(\hat{p}_{cC}) \phi_d \phi_D \quad (2.48)$$

when all two-body channels with partitions $d + D = c + C, a + A, \dots$ are considered. The radial wave functions have the form

$$\psi_{dDcC}^{(\pm)}(l, \vec{r}_{dD}) = \psi_{dDcC}^{(-)*}(l, \vec{r}_{dD}) \rightarrow \frac{1}{2i} \sqrt{\frac{v_{cC}}{v_{dD}}} \left\{ \exp[2i\sigma_l(\eta_{dD})] S_{dDcC}^l u_l^{(+)}(\eta_{dD}, p_{dD} r_{dD}/\hbar) - \delta_{dDcC} u_l^{(-)}(\eta_{dD}, p_{dD} r_{dD}/\hbar) \right\} \quad (2.49)$$

for large radii with (nuclear) S-matrix elements S_{dDcC}^l for the reactions $c + C \rightarrow d + D$, Coulomb phase shifts $\sigma_l(\eta_{dD})$, and Sommerfeld parameter η_{dD} . The out- and ingoing Coulomb wave functions

$$u_l^{(\pm)}(\eta, z) = \exp[\mp i\sigma_l(\eta)] [G_l(\eta; z) \pm iF_l(\eta; z)] \quad (2.50)$$

are expressed with the help of the regular and irregular Coulomb wave functions F_l and G_l , respectively, and have the asymptotic form

$$u_l^{(\pm)}(\eta, z) \rightarrow \exp\left[\pm i\left(z - 2\eta \ln z - l\frac{\pi}{2}\right)\right] \quad (2.51)$$

for large argument $z \rightarrow \infty$. Comparing the boundary condition of the full wave function

$$\Psi_{cC}^{(\pm)} \rightarrow \phi_c \phi_C \exp(i\vec{p}_{cC} \cdot \vec{r}_{cC}/\hbar) + \sum_{dD} f_{cC \rightarrow dD}^{(\pm)} \phi_d \phi_D \frac{\exp(\pm i p_{dD} r_{dD}/\hbar)}{r_{dD}} \quad (2.52)$$

with the asymptotic form (2.48), the scattering amplitude

$$f_{cC \rightarrow xA}^{(+)} = \frac{\hbar}{2ip_{cC}} \sqrt{\frac{v_{cC}}{v_{xA}}} \sum_l (2l+1) \exp[2i\sigma_l(\eta_{xA})] S_{xAcC}^l P_l(\cos\vartheta) \quad (2.53)$$

for the two-body reaction $c + C \rightarrow x + A$ can be extracted. The Legendre polynomials P_l depend on the scattering angle ϑ with $\cos\vartheta = \hat{r}_{xA} \cdot \hat{p}_{cC}$. Then the differential cross section of this reaction is obtained from

$$\frac{d^2\sigma}{d\Omega_{xA}}(c + C \rightarrow x + A) = \frac{v_{xA}}{v_{cC}} \left| f_{cC \rightarrow xA}^{(+)} \right|^2 = \frac{\hbar^2}{4p_{cC}^2} \left| \sum_l (2l+1) \exp[2i\sigma_l(\eta_{xA})] S_{xAcC}^l P_l(\cos\vartheta) \right|^2 \quad (2.54)$$

that can be related directly to the cross section of the inverse reaction (1.7) of interest with the theorem of detailed balance (2.17). An angular integration gives the total reaction cross section

$$\sigma_{cC \rightarrow xA} = \frac{\pi \hbar^2}{p_{cC}^2} \sum_l (2l+1) \left| S_{xAcC}^l \right|^2 \quad (2.55)$$

with the contributions of individual partial waves.

The action of the optical potentials on the distorted waves will lead to a strong suppression of the contributions at small distances between the particles in the matrix element in (2.47) and thus it will be sufficient to consider only the asymptotic form of the full scattering wave function (2.48). The choice of the initial state $a + A$ in the matrix element will then select this channel from $\Psi_{cC}^{(-)}$. In this case, the T-matrix element (2.47) of the TH reaction can be written in a similar form as the scattering amplitude (2.53). It assumes the form

$$T_{aA \rightarrow bcC} \approx \frac{\hbar}{2ip_{cC}} \sqrt{\frac{v_{cC}}{v_{xA}}} \sum_l (2l+1) \exp[2i\sigma_l(\eta_{xA})] S_{xAcC}^l U_l^{(+)} \quad (2.56)$$

with the functions

$$U_l^{(\pm)} = \frac{4\pi i^{-l}}{(2l+1)} \sum_m Y_{lm}(\hat{p}_{cC}) \int \frac{d^3 q_{bx}}{(2\pi\hbar)^3} w_{bx}^a(\vec{q}_{bx}) \langle \theta(r_{xA} - R) r_{xA}^{-1} u_l^{(\mp)}(\eta_{xA}, p_{xA} r_{xA}/\hbar) Y_{lm}(\hat{r}_{xA}) \chi_{bB}^{(-)} \exp(i\vec{q}_{bx} \cdot \vec{r}_{bx}/\hbar) \chi_{aA}^{(+)} \rangle \quad (2.57)$$

in the various partial waves that depend on kinematic quantities, the momentum amplitude w_{bx}^a , and the distorted waves. The θ function in the matrix element limits the integration range to radii r_{xA} larger than a suitably selected cut-off radius R to select only the asymptotic part of the wave function. The similarity of (2.53) and (2.56) is obvious. In this modified distorted-wave Born approximation (MDWBA) it is still necessary to perform the integration over \vec{q}_{bx} in the functions $U_l^{(\pm)}$ and thus there is no factorization of the T-matrix element as in (2.32). However, if the distorted waves are replaced by plane waves

$$\chi_{aA}^{(+)} \rightarrow \exp[i(\vec{r}_{aA} \cdot \vec{p}_{aA})/\hbar], \quad \chi_{bB}^{(-)} \rightarrow \exp[i(\vec{r}_{bB} \cdot \vec{p}_{bB})/\hbar], \quad (2.58)$$

the same transformations as in the PWIA can be applied after a rearrangement of the arguments, cf., (2.28), in the matrix element. It is again possible to perform the integration over \vec{r}_{bB} and \vec{q}_{bx} analytically with the result

$$U_l^{(\pm)} = \frac{4\pi\hbar^2}{Q_{aA} p_{xA}} w_{bx}^a(\vec{Q}_{bB}) J_l^{(\pm)} P_l(\hat{p}_{cC} \cdot \hat{Q}_{aA}) \quad (2.59)$$

where the simple radial integrals

$$J_l^{(\pm)} = \frac{Q_{aA} p_{xA}}{\hbar^2} \int_R^\infty dr_{xA} r_{xA} u_l^{(\pm)}(\eta_{xA}, p_{xA} r_{xA}/\hbar) j_l(Q_{aA} r_{xA}/\hbar) \quad (2.60)$$

where spherical Bessel functions j_l appear. As a consequence, the T-matrix elements factorizes as

$$T_{aA \rightarrow bcC} \approx 4\pi w_{bx}^a(\vec{Q}_{bB}) \frac{\hbar}{2ip_{cC}} \sqrt{\frac{v_{cC}}{v_{xA}}} \sum_l (2l+1) \exp[2i\sigma_l(\eta_{xA})] S_{xAcC}^l J_l^{(\pm)} P_l(\hat{p}_{cC} \cdot \hat{Q}_{aA}) \quad (2.61)$$

with an angular dependence defined by the Legendre polynomial. This finally leads to the expression

$$\frac{d^5\sigma}{dE_{cC} d\Omega_{cC} d\Omega_{bB}}(a + A \rightarrow b + c + C) = \frac{K}{p_{Ax}^2} W(\vec{Q}_{bB}) \frac{v_{cC}}{v_{xA}} \frac{d^2\sigma^{HOES}}{d\Omega_{xA}}(c + C \rightarrow x + A) \quad (2.62)$$

for the cross section in the modified plane-wave Born approximation (MPWBA) with a kinematic factor

$$K = \frac{\mu_{aA} \mu_{bB} \mu_{cC}}{(2\pi\hbar)^3} \frac{p_{bB} p_{cC}}{p_{aA}} \frac{4}{Q_{aA}^2}, \quad (2.63)$$

the momentum distribution

$$W(\vec{Q}_{bB}) = \left| w_{bx}^a(\vec{Q}_{bB}) \right|^2 \quad (2.64)$$

and the HOES cross section

$$\frac{d^2\sigma_{cC \rightarrow xA}^{HOES}}{d\Omega_{xA}}(c + C \rightarrow x + A) = \frac{\hbar^2}{4p_{cC}^2} \left| \sum_l (2l+1) \exp[2i\sigma_l(\eta_{xA})] S_{xAcC}^l J_l^{(+)} P_l(\hat{p}_{cC} \cdot \hat{Q}_{aA}) \right|^2 \quad (2.65)$$

that can be compared to the cross (2.54) and thus quantifies the off-shell effects. The main difference is the appearance of the functions $J_l^{(\pm)}$ that are dimensionless quantities. They have been studied in detail in [23], their dependence on p_{xA} . In the limit of small energies E_{xA} in the entrance channel to the two-body reaction (1.7), i.e., $p_{xA} \rightarrow 0$, they behave as

$$J_l^{(\pm)} \propto p_{xA}^{3/2} \exp(\pi\eta_{xA}) \quad (2.66)$$

with a characteristic exponential factor depending on the Sommerfeld parameter of the $x + A$ system. So the approximate relation

$$\frac{d^2\sigma_{cC \rightarrow xA}^{HOES}}{d\Omega_{xA}}(c + C \rightarrow x + A) \approx p_{xA}^3 \exp(2\pi\eta_{xA}) \frac{d^2\sigma_{cC \rightarrow xA}}{d\Omega_{xA}}(c + C \rightarrow x + A) \quad (2.67)$$

can be established. Taking the theorem of detailed balance (2.17) into account, the final expression

$$\frac{d^5\sigma}{dE_{cC}d\Omega_{cC}d\Omega_{bB}}(a+A \rightarrow b+c+C) \approx \tilde{K} W(\bar{Q}_{bB}) \frac{p_{xA}^3}{v_{xA}} \exp(2\pi\eta_{xA}) \frac{d^2\sigma}{d\Omega_{cC}}(x+A \rightarrow c+C) \quad (2.68)$$

with the modified kinematic factor

$$\tilde{K} = K \frac{v_{cC}}{p_{cC}^2} = \frac{\mu_{aA}\mu_{bB}}{(2\pi\hbar)^3} \frac{p_{bB}}{p_{aA}} \frac{4}{Q_{aA}^2} \quad (2.69)$$

is found that relates the two cross sections of interest. The essential feature in formula (2.68) is the appearance of the factor

$$\frac{p_{xA}^3}{v_{xA}} \exp(2\pi\eta_{xA}) = 2\mu_{aX}^2 E_{xA} \exp(2\pi\eta_{xA}) \quad (2.70)$$

that is (except for the constant $2\mu_{aX}^2$) identical to the factor that appears in the relation of the astrophysical S factor to the cross section for reactions of astrophysical interest, cf., (1.1). It removes the strong energy dependence due to the Coulomb barrier in the entrance channel. Hence, the cross section of the TH reaction is also not affected by the Coulomb suppression and the S factor is essentially measured directly in the TH experiments.

2.3.3. Other approaches

In the discussion of the MDWBA/MPWBA, the post-form expression for the DWBA T-matrix element (2.41) has been used to derive the relation to the S-matrix elements and thus the cross section of the astrophysical reaction (1.7). But also the prior-form of the DWBA T-matrix element

$$T_{aA \rightarrow bC} \approx \langle \phi_b \Psi_{cC}^{(-)} \chi_{bB}^{(-)} | V_{aA} - U_{aA} | \phi_a \phi_A \chi_{aA}^{(+)} \rangle \quad (2.71)$$

in combination with a surface-integral approach can be used to find a connection to the two-body reaction cross section, see [27] for details.

If the TH reaction (1.6) proceeds via a resonance, the R-matrix formalism can be applied as a particular option as, e.g., discussed in [28,29]. In this case, the reduced width amplitudes γ in the entrance and exit channels appear explicitly in the HOES cross section for a resonant reaction. It assumes the form

$$\frac{d^2\sigma}{dE_{xA}d\Omega_b} = N \sum_i (2J_i + 1) \left| \sqrt{\frac{p_{cC}}{\hbar\mu_{cC}}} \frac{\sqrt{2P_{l_i}(p_{cC}R_{cC}/\hbar)} M_i(p_{xA}R_{xA}/\hbar) \gamma_{cC}^i \gamma_{xA}^i}{D_i(E_{xA})} \right|^2 \quad (2.72)$$

in the case of isolated non-interfering resonances i [30] with a normalization factor N and penetration factors P_{l_i} in the partial wave l_i . R_{xA} and R_{cC} are the channel radii in the initial and final state of the two-body reaction. If the use of plane waves is justified, the simple form

$$M_i(p_{xA}R_{xA}/\hbar) = \left[(B_{xA}^i - 1) j_{l_i}(\rho) - \rho \frac{\partial j_{l_i}(\rho)}{\partial \rho} \right]_{\rho=p_{xA}R_{xA}/\hbar}, \quad (2.73)$$

for the transfer amplitude in (2.72) can be deduced [31]. Here, $p_{xA} = \sqrt{2\mu_{xA}(E_{xA} + B_{bX}^a)}$ is the effective momentum, $j_{l_i}(\rho)$ is a spherical Bessel function, and B_{xA}^i is an arbitrary boundary condition. It can be chosen as in [32] to yield observable resonance parameters. Finally, the quantity $D_i(E_{xA})$ in (2.72) is the standard R-matrix denominator for the case of a one-level, two-channel R-matrix description [33]. The factorization of the THM cross section into a momentum distribution and a HOES cross section represents a two-step description of the reaction. However, this approach is not explicitly considered in the direct reaction theory outlined earlier, which employs a one-step process in its theoretical framework. To address this, it has been suggested to examine the propagation of the transferred particle x within a two-step framework, as exemplified in the inclusive nonelastic breakup theory [34,35]. Moreover, achieving a more precise calculation of the T-matrix element involving three particles in the exit channel might require the application of three-body scattering within the Faddeev theory [36]. This strategy could enable the exploration of the validity and limitations of simplified approximations. Nonetheless, adopting these advanced methodologies results in the loss of the convenient factorization of the TH cross section.

2.4. T-matrix elements and cross sections in the ANC method

In contrast to the THM, where the subsystem B in the exit channel of the transfer reaction is a scattering state $c + C$, a bound state B is considered in the ANC method. The T-matrix element is usually considered in the distorted-wave Born approximation

$$T_{aA \rightarrow bB} \approx \langle \phi_b \phi_B \chi_{bB}^{(-)} | W | \phi_a \phi_A \chi_{aA}^{(+)} \rangle \quad (2.74)$$

with $W = V_{bB} - U_{bB}$ or $W = V_{aA} - U_{aA}$ in the post or prior formulation, respectively, with optical potentials U_{ij} and distorted waves $\chi_{ij}^{(\pm)}$, cf. Section 2.3.2. As in the THM, it is supposed that the many-body wave functions ϕ_a and ϕ_B have a prominent cluster structure $a = x + b$ and $B = x + A$, respectively. Then one can write

$$\phi_a = \phi_x \phi_b \phi_{xb}^a, \quad \phi_B = \phi_x \phi_A \phi_{xA}^B, \quad (2.75)$$

with wave functions of relative motion

$$\phi_{xb}^a = \langle \phi_x \phi_b | \phi_a \rangle, \quad \phi_{xA}^B = \langle \phi_x \phi_A | \phi_B \rangle, \quad (2.76)$$

that are often denoted as overlap functions. The T-matrix element can then be expressed as

$$T_{aA \rightarrow bB} \approx \langle \phi_x \phi_b \phi_A \phi_{xA}^B \chi_{bB}^{(-)} | W | \phi_x \phi_b \phi_A \phi_{xA}^a \chi_{aA}^{(+)} \rangle \quad (2.77)$$

that reduces to the simplified form

$$T_{aA \rightarrow bB} \approx \langle \phi_{xA}^B \chi_{bB}^{(-)} | W | \phi_{xA}^a \chi_{aA}^{(+)} \rangle \quad (2.78)$$

if the integration over the internal coordinates of x , b and A can be performed. The overlap functions depend only on the relative coordinates \vec{r}_{xb} and \vec{r}_{xA} and can be expressed as

$$\phi_{xb}^a(\vec{r}_{xb}) = \frac{\varphi_{xb}^a(r_{xb})}{r_{xb}} Y_{l_{xb} m_{xb}}(\hat{r}_{xb}), \quad \phi_{xA}^B(\vec{r}_{xA}) = \frac{\varphi_{xA}^B(r_{xA})}{r_{xA}} Y_{l_{xA} m_{xA}}(\hat{r}_{xA}), \quad (2.79)$$

in a partial-wave representation with radial wave functions φ_{xb}^a , φ_{xA}^B and spherical harmonics $Y_{l_{xb} m_{xb}}$, $Y_{l_{xA} m_{xA}}$. Different to usual single-particle wave functions, they are not normalized to one but their norms

$$S_{xb}^a = \langle \phi_{xb}^a(\vec{r}_{xb}) | \phi_{xb}^a(\vec{r}_{xb}) \rangle, \quad S_{xA}^B = \langle \phi_{xA}^B(\vec{r}_{xA}) | \phi_{xA}^B(\vec{r}_{xA}) \rangle, \quad (2.80)$$

are the so-called spectroscopic factors that are smaller than one in most cases.

In actual calculations, the overlap functions are usually replaced by simple normalized single-particle wave functions ξ_{xb}^a and ξ_{xA}^B with radial wave functions $u_{xb}^a(r_{xb})$ and $u_{xA}^B(r_{xA})$. The latter are found by solving the Schrödinger equations of relative motion with nuclear potentials of Woods–Saxon form using standard parameters for the radius, diffuseness and depths adjusted to the correct energies. Thus the overlap functions are written as

$$\phi_{xb}^a = A_{xb}^a \xi_{xb}^a, \quad \phi_{xA}^B = A_{xA}^B \xi_{xA}^B, \quad (2.81)$$

with spectroscopic amplitudes A_{xb}^a and A_{xA}^B to account for the difference in the normalization. Then the T-matrix element factorizes as

$$T_{aA \rightarrow bB} = A_{xb}^a A_{xA}^B T_{aA \rightarrow bB}^{sp} \quad (2.82)$$

with the single-particle T-matrix element

$$T_{aA \rightarrow bB}^{sp} \approx \langle \xi_{xA}^B \chi_{bB}^{(-)} | W | \xi_{xb}^a \chi_{aA}^{(+)} \rangle \quad (2.83)$$

that enters in the cross section $d^2\sigma/d\Omega_{bB}$ of the transfer reaction $A(a, b)B$. Hence, one can write

$$\frac{d^2\sigma}{d\Omega_{bB}}(a + A \rightarrow b + B) = \left| A_{xb}^a \right|^2 \left| A_{xA}^B \right|^2 \frac{d^2\sigma^{sp}}{d\Omega_{bB}}(a + A \rightarrow b + B) \quad (2.84)$$

with the single-particle cross section

$$\frac{d^2\sigma^{sp}}{d\Omega_{bB}}(a + A \rightarrow b + B) = \frac{\mu_{aA} \mu_{bB}}{(2\pi)^2 \hbar^4} \frac{p_{bB}}{p_{aA}} \left| T_{aA \rightarrow bB}^{sp} \right|^2 \quad (2.85)$$

that can be calculated using well-known computer codes. Identifying the modulus squares of the spectroscopic amplitudes with spectroscopic factors, i.e.,

$$S_{xb}^a = \left| A_{xb}^a \right|^2, \quad S_{xA}^B = \left| A_{xA}^B \right|^2, \quad (2.86)$$

the latter can be determined from the ratio of experimentally measured cross sections to calculated single-particle cross sections (2.85). Since one of the two spectroscopic factors in the cross section is usually known, e.g., if a or B is a deuteron with $S_{np}^d = 1$, the other can be obtained.

The distinctive difference of the ANC method to the usual application of transfer reactions is the selection of peripheral reactions. In that case, only the asymptotic part of the overlap functions (2.79) contributes effectively in the T-matrix elements and the reaction cross section is, in fact, not proportional to the spectroscopic factors. For sufficiently large radii, the radial wave function in (2.79) behaves as

$$\phi_{xb}^a(r_{xb}) \rightarrow C_{xb}^a W_{-\eta_{xb}, l_{xb}}(2q_{xb}^a r_{xb}), \quad \phi_{xA}^B(r_{xA}) \rightarrow C_{xA}^B W_{-\eta_{xA}, l_{xA}}(2q_{xA}^B r_{xA}), \quad (2.87)$$

with Whittaker functions that depend on the Sommerfeld parameters η_{xb} , η_{xA} orbital angular momenta l_{xb} , l_{xA} , and bound-state wave numbers $q_{xb}^a = \sqrt{2\mu_{xb} B_{xb}^a}/\hbar$, $q_{xA}^B = \sqrt{2\mu_{xA} B_{xA}^B}/\hbar$ with binding energies B_{xb}^a , B_{xA}^B in the two channels. The asymptotic form of the radial wave functions is thus fully determined by known properties of the nuclei a and B , except for the quantities C_{xb}^a and C_{xA}^B that are the asymptotic normalization coefficients for the breakup of the nuclear ground states of a and B into $x + b$ and $x + A$, respectively. Similarly as in the determination of spectroscopic factors, T-matrix elements $T_{aA \rightarrow bB}^{asym}$ and single-particle cross sections $d^2\sigma^{asym}/d\Omega_{bB}$ can be introduced using only the asymptotic part of the radial wave functions (Whittaker functions) without the ANCs. Then the cross

$$\frac{d\sigma}{d\Omega_{bB}}(a + A \rightarrow b + B) = \left| C_{xb}^a \right|^2 \left| C_{xA}^B \right|^2 \frac{d\sigma^{asym}}{d\Omega_{bB}}(a + A \rightarrow b + B) \quad (2.88)$$

is proportional to the modulus squares of the ANCs and an ‘asymptotic’ single-particle cross section that is actually calculated. A comparison with experimental cross sections allows then to extract one of the two ANCs if the other is known.

In a final step, the cross section $\sigma(x+A \rightarrow B+\gamma)$ of the radiative capture reaction can be calculated numerically for low energies in the entrance channel. It involves the transition matrix element

$$M_{xA \rightarrow B\gamma} = \langle \phi_{xA}^B | \mathcal{M}(E\lambda\mu) | \Psi_{xA}^{(+)} \rangle \quad (2.89)$$

with the electric multipole operator that has the form

$$\mathcal{M}(E\lambda\mu) = Z_{xA}^{(\lambda)} e r_{xA}^\lambda Y_{\lambda\mu}(\hat{r}_{xA}) \quad (2.90)$$

with the effective charge number

$$Z_{xa}^{(\lambda)} = Z_x \left(\frac{m_A}{m_x + m_A} \right)^\lambda + Z_A \left(-\frac{m_x}{m_x + m_A} \right)^\lambda \quad (2.91)$$

for the relative motion between x and A . Then, adding the angular momenta and their projections in the notation, the reduced transition probability

$$\frac{dB}{dE_{xA}}(E\lambda, j_B \rightarrow j_x j_A) = \frac{1}{2j_B + 1} \sum_{m_B} \sum_{m_x m_A} \int d\Omega_{xA} \left| \langle \phi_{xA}^B(j_B m_B) | \mathcal{M}(E\lambda\mu) | \Psi_{xA}^{(+)}(\vec{p}_{xA}, j_x m_x j_A m_A) \rangle \right|^2 \frac{\mu_{xA} p_{xA}}{(2\pi\hbar)^3} \quad (2.92)$$

can be introduced. It enters the calculation of the photo absorption cross section

$$\sigma_{\text{abs}}(E\lambda, j_B \rightarrow j_x j_A) = \frac{\lambda + 1}{\lambda} \frac{(2\pi)^3}{[(2\lambda + 1)!!]^2} k_\gamma^{\lambda-1} \frac{dB}{dE_{xA}}(E\lambda, j_B \rightarrow j_x j_A) \quad (2.93)$$

with the photon momentum $\hbar k_\gamma$ that is related to the radiative capture cross section

$$\sigma_{\text{cap}}(E\lambda, j_x j_A \rightarrow j_B) = \frac{2(2j_B + 1)}{(2j_x + 1)(2j_A + 1)} \frac{k_\gamma^2}{k_{xA}^2} \sigma_{\text{abs}}(E\lambda, j_B \rightarrow j_x j_A) \quad (2.94)$$

via the theorem of detailed balance. Finally, the astrophysical S factor is obtained as

$$S_{E\lambda}(E_{xA}, j_x j_A \rightarrow j_B) = \sigma_{\text{cap}}(E\lambda, j_x j_A \rightarrow j_B) E_{xA} \exp(2\pi\eta_{xA}) \quad (2.95)$$

with the Sommerfeld parameter $\eta_{xA} = Z_x Z_A e^2 \sqrt{2E_{xA}/\mu_{xA}}/\hbar$. Due to its r_{xA}^λ dependence and the Coulomb suppression of the radial wave function in the scattering state for small radii in the calculation of (2.89), it is sufficient to use only the asymptotic form (2.87) of the radial wave function for the bound state of nucleus a . At very low energies, it is found that interaction effects in the scattering channel are also strongly reduced and the wave function of relative motion between x and A can be well approximated by the regular Coulomb scattering wave function. The transition matrix element is then easily calculated numerically with the analytical radial wave functions of the bound and scattering states for large radii. The reduced transition probability (2.92), the absorption cross (2.93), the radiative capture cross (2.94), and the S(E) factor (2.95) are proportional to $|C_{xA}^b|^2$. A detailed analysis of the energy dependence of the cross sections and the S(E) factor shows that $S_{E\lambda}(E_{xA})$ approaches a finite value in the limit $E_{xA} \rightarrow 0$ for the capture from an s -wave in the continuum to a p or d wave in the bound state via an $E1$ or $E2$ transition, respectively. Thus, $S_{E\lambda}(0, j_x j_A \rightarrow j_B)$ is given by $|C_{xA}^b|^2$ up to a numerical factor from theory, which presents a valuable constraint for the S factor from the known ANC.

3. Experimental application of the ANC method

The ANC technique [37] stems from the fact that capture reactions of astrophysical interest involve bound-state systems where the binding energy of the captured particle is low. In stars, these captures occur through the tail of the overlap function, being highly peripheral. The shape of this function is therefore insensitive to the details of the nuclear potential, and its amplitude (the ANC) dictates the strength of the capture reaction. To reduce the influence of the nucleus’s internal structure (phase shifts in the involved partial waves) in the scattering wave function, ANC measurements can only determine low-energy S(E) factors for peripheral direct radiative capture reactions. Traditional methods using nuclear transfer reactions can be used for this purpose [37,38], as long as the capture occurs with weakly bound states in the system $B = x + A$. For tightly bound states, the ANC technique is not suitable because the bound state wave function is confined to a small region and the influence of interactions at short distances becomes significant. This can bring non-negligible changes in the zero-energy S(E) factor.

The computation of the reduced differential cross section, as specified in Eq. (2.88) utilizing Whittaker functions, can be achieved through conventional DWBA codes such as FRESKO [39]. This process entails a meticulous selection of optical potentials for determining the distorted waves in the matrix element (2.89). In the context of the normalized single-particle wave function ξ_{xb}^a for the $a = x + b$ cluster configuration, under asymptotic conditions it takes the form

$$\xi_{xb}^a(r_{xb}) \rightarrow b_{xb}^a W_{-\eta_{xb}, l_{xb}}(2q_{xb}^a r_{xb}), \quad (3.1)$$

where the parameter b_{xb}^a represents the single-particle ANC (for a detailed discussion, refer to [15]). From Eq. (2.81) and (2.87) one can retrieve the connection between the ANC and the single-particle ANC (eq. (2.47) of ref. [15]):

$$C_{xb}^a = A_{xb}^a b_{xb}^a. \quad (3.2)$$

By using the single-particle ANC definition b_{xb}^a , the aforementioned equation can be reformulated in a manner commonly used in experimental applications:

$$\frac{d\sigma_{exp}}{d\Omega_{bB}}(a + A \rightarrow b + B) = \left| \frac{C_{xb}^a}{b_{xb}^a} \right|^2 \left| \frac{C_{xA}^B}{b_{xA}^B} \right|^2 \frac{d\sigma_{DWBA}}{d\Omega_{bB}}(a + A \rightarrow b + B) \quad (3.3)$$

where $\frac{d\sigma_{DWBA}}{d\Omega_{bB}}$ represents the transfer cross section calculated within the DWBA formalism, linked to the experimental one through the spectroscopic factors according to Eq. (3.2).

The ANC technique can also be used to determine the γ widths Γ_γ for resonant capture processes, see, e.g., [31] for neutron, [40], proton and [41] α captures of astrophysical interest. The method has also been applied to mirror reactions to study proton/neutron captures [42–45]. In summary, the ANC method is valuable for both resonant and nonresonant capture amplitudes and it can be used to determine astrophysical S(E) factors when the capture occurs through a subthreshold resonance. [37].

When resonance parameters are known, which can be obtained from measurements or calculations, R-matrix calculations can be performed to determine the capture cross section.

For practical applications of the ANC method, the following steps need to be taken into account:

- The transfer reaction has to be peripheral. This requirement can be achieved in two ways: by using reactions with large impact parameters — this can be achieved by selecting events with small scattering angles; by performing reactions at sub-Coulomb energies to secure the peripherality of the process due to the Coulomb repulsion. With the assistance of DWBA calculations, cross checks can be done by changing the values of the radius and diffuseness parameters in the potentials describing the binding of the transferred particle x to the cores A . Peripherality is then verified by assessing the dependence of C_{xb}^a on b_{xb}^a (Eq. (3.2)). While A_{xb}^a and b_{xb}^a depend on the choice of the potentials used in the calculations, their product is a model independent quantity, provided that the experimental conditions necessary for its deduction are satisfied. Specifically, this entails the possibility to describe the experimental transfer cross section using Eq. (3.3).
- After confirming that the ANC reaction is peripheral, the experiment needs to measure the absolute differential cross section accurately. This involves carefully considering all factors that might influence the results and estimating the associated uncertainties.
- The last step involves comparing measured results with calculations to extract the ANC we need. This comparison relies on accurate descriptions of how particles interact with the nucleus, which are captured by the optical model parameters. For stable nuclei, these parameters can be easily obtained by measuring elastic scattering cross sections in the entrance and exit channels. However, for unstable nuclei, obtaining good optical potentials is more challenging. In these cases, one might need to rely on data from broader studies also involving similar nuclei.

The ANC method has proven valuable in studying various reactions relevant to key astrophysical problems. Table 3.1 showcases some of the most studied reactions using ANC, highlighting both the astrophysical and the ANC reactions. Here below, we will report on some recent applications: $^{18}\text{O}(p, \gamma)^{19}\text{F}$, $^3\text{He}(\alpha, \gamma)^7\text{Be}$ and $^{26}\text{Si}(p, \gamma)^{27}\text{P}$ reaction studies.

3.0.1. The $^{18}\text{O}(p, \gamma)^{19}\text{F}$ reaction

Astrophysical background. The $^{18}\text{O}(p, \gamma)^{19}\text{F}$ radiative capture finds its importance in the nucleosynthesis, given that such a reaction can play an important role in mixing stages of the AGB environment. The (p, γ) process, in fact, allows the escape from the CNO cycle, and its branching ratio against $^{18}\text{O}(p, \alpha)^{15}\text{N}$ (that is the dominant one) has an impact on both ^{15}N and ^{19}F abundances. This ratio represents an important parameter for different nucleosynthesis environments, and can be crucial to determine the origin of presolar grains [46,47].

The direct capture of the $^{18}\text{O}(p, \gamma)^{19}\text{F}$ reaction constitutes the most important part of the total cross section of astrophysical interest, and its behavior has been thoroughly investigated: its excitation function has been evaluated theoretically and experimentally [48], and the presence of three resonances at low energies have been confirmed [49,50]. Nonetheless discrepancies in the behavior of the direct component at low energies have been found [51], showing an increasing trend with energy, instead of the decreasing one present in the literature at the time [48].

Experimental set-up and astrophysical S(E) factor extraction. For the reasons above, the $^{18}\text{O}(p, \gamma)^{19}\text{F}$ has been investigated by means of the ANC method [52]. The radiative part of the total cross section has been retrieved from the $^{18}\text{O}(^3\text{He}, d)^{19}\text{F}$ transfer reaction, using the ^3He beam available at the U-120M iso-chronous cyclotron of the Nuclear Physics Institute of the Czech Academy of Sciences. In order to study the transfer reaction, a gas target composed by a chamber filled with 99% purity ^{18}O , with an output window that covers the angular range $-65^\circ +40^\circ$, has been used. The detection set-up was composed by eight ΔE -E telescopes made by thin (250 μm) Si and thick (5 mm) Si(Li) detectors, in order to detect the deuterons of interest, as well as the scattered ^3He from the beam.

The optical model parameters (OMP's) for the entrance channel have been extracted from the elastic scattering, and are consistent with previous publications [53,54]. Eleven peaks belonging to excited states related to the deuterons coming from the reaction of interest, corresponding to the transitions to the ground state of ^{19}F , have been identified. For the OMP's in the exit channels, those were taken from the global formula in [55] at the proper energy. An example of the angular distribution fitting procedure can be found in the left panel of Fig. 3.1, showing the angular distributions for the transitions to the ^{19}F ground and first (0.197 MeV) excited states. The black solid squares represent the experimental data, while the lines refer to the sets of optical model parameters taken from Table 1 of [52] (fit A: solid line, fit B: dashed line).

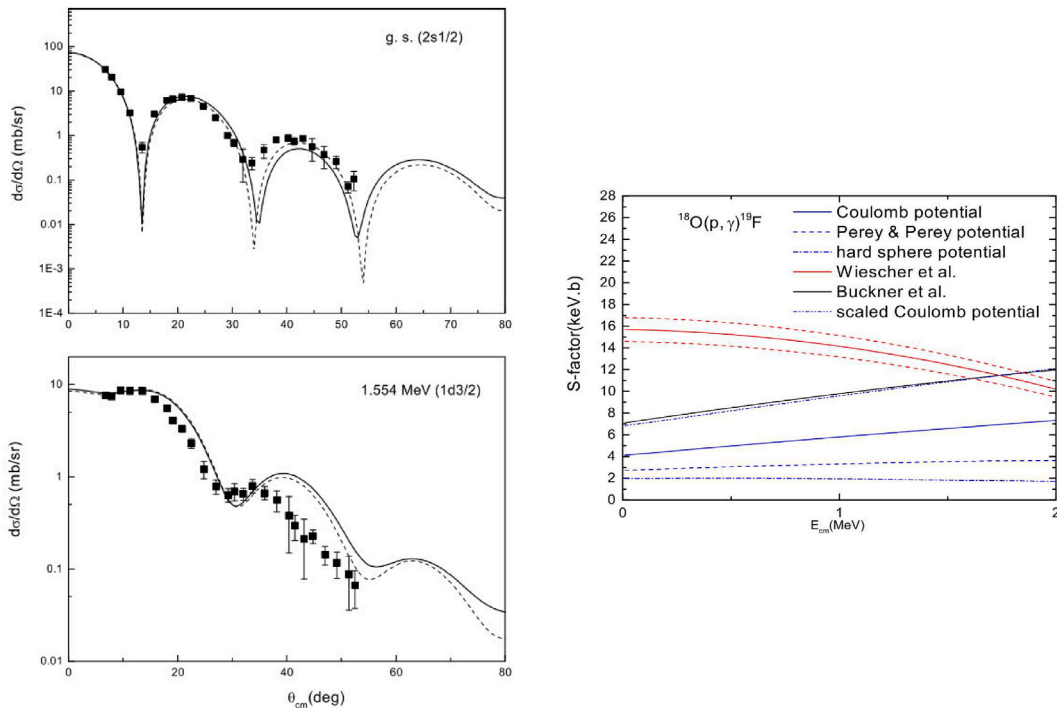


Fig. 3.1. Left panel: angular distribution for the $^{18}\text{O}(^3\text{He},d)^{19}\text{F}$ in the ^{19}F ground and first excited state. Right panel: $S(E)$ factor for the total proton direct capture $^{18}\text{O}(p, \gamma)^{19}\text{F}$ for three different potentials, compared with literature (see text for details).

Source: The figure is adapted from Ref. [40].

Using three different potentials, the ANC's for the twelve states (ground state and eleven excited ones) have been calculated (see Table 3 from [52]). Resulting $S(E)$ factors for the $^{18}\text{O}(p, \gamma)^{19}\text{F}$ total direct capture are shown in the right panel of Fig. 3.1 as blue solid (Coulomb potential), dashed (Perey & Perey potential) and dash-dotted (hard sphere potential) lines. Calculations from [51] and measurement by [48] are shown as solid black and red lines, respectively. In two out of three cases the resulting astrophysical $S(E)$ factor has been found having the same trend found by [51], but with a lower contribution than the one given in [48,51]. This is due to the fact that the ANC method addresses only the direct part of the capture process. To address this discrepancy, the $S(E)$ factor calculated with the Coulomb potential was normalized to the absolute cross-section value measured by Wiescher et al. at $E_{c.m.} = 1.75$ MeV. The normalized curve (blue dotted line) closely matches the Buckner et al. calculations. Also it has been found that the Coulomb potential contribution to the direct part constitutes up to 57% or more of the contribution determined in [51]. Refer to [52] for more details.

3.0.2. The $^3\text{He}(\alpha, \gamma)^7\text{Be}$ reaction

Astrophysical background. The $^3\text{He}(\alpha, \gamma)^7\text{Be}$ reaction is critically important in nuclear astrophysics. The reaction is significant for understanding the lithium problem in Big Bang Nucleosynthesis [56] and especially to constrain the Standard Solar Model from precise measurements of the neutrino flux from the Sun's core, if accurate nuclear reaction cross sections are known. However, current uncertainties in these parameters are too high due to the low cross sections at the relevant energies. Improving our knowledge of the low-energy cross section of the $^3\text{He}(\alpha, \gamma)^7\text{Be}$ reaction would significantly reduce uncertainties in solar neutrino flux predictions and, in turn, on the Standard Solar Model parameters [3].

The reaction has been extensively studied using different experimental methods, such as gamma ray detection, measuring ^7Be activity, and counting ^7Be recoils (see, e.g. [57] and references therein for works published after 2004). Despite the extensive number of dedicated experimental studies, it has remained a challenge to measure it directly because the energy range relevant to astrophysics, known as the Gamow window, falls between approximately 15 keV and 30 keV for a temperature of 15 MK, which characterizes the core of the Sun [3]. At these temperatures, the cross-section of the $^3\text{He}(\alpha, \gamma)^7\text{Be}$ reaction becomes exceedingly small, making the direct measurement presently unfeasible or very uncertain. For applications to the lithium problem in Big Bang Nucleosynthesis, it plays a role particularly at energies around 100 keV, where more data are available, though sometimes with scattered absolute values.

For these reasons, extrapolation from higher energies is often necessary, in particular using the R-matrix approach (see, for instance, the compilation [58]). Furthermore, various theoretical models, including external capture models, potential models, and ab initio approaches, have been used to describe the reaction (see [57] for an inexhaustive list). Different models yield varying values for the astrophysical $S(E)$ factor of the reaction, especially with respect to the absolute value. Recent studies have focused

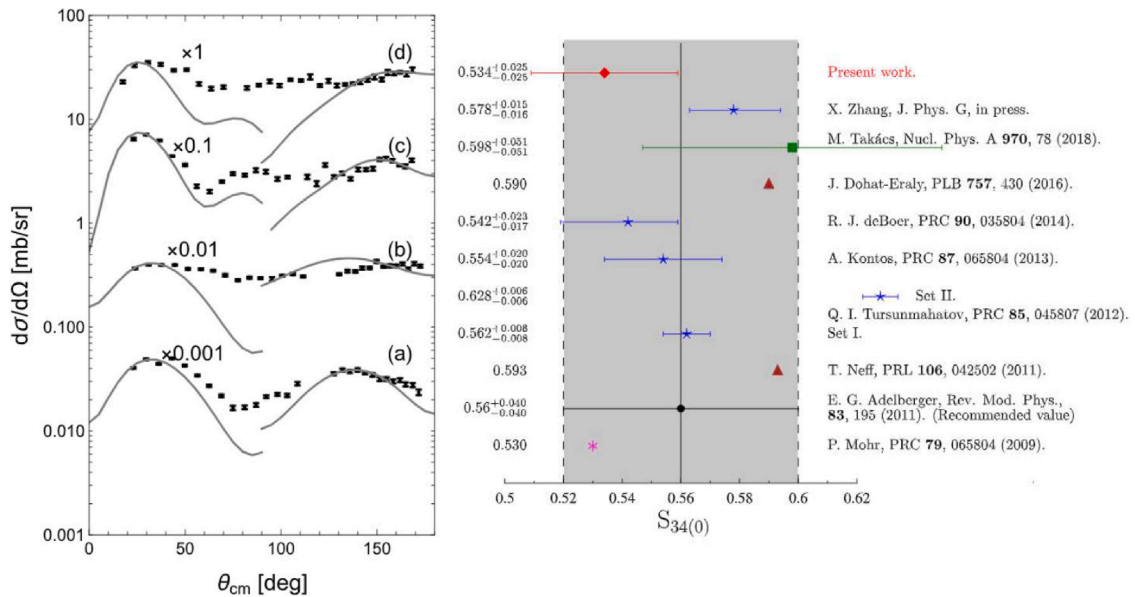


Fig. 3.2. Left panel: angular distribution for the ${}^6\text{Li}({}^3\text{He}, \alpha){}^7\text{Be}$ populating the ground ((a) and (c), beam energy 3 MeV) and first (0.429 MeV, (b) and (d), beam energy 5 MeV) along with the calculated differential cross sections (gray lines, see text for details). Right panel: Summary of the most recent ${}^3\text{He}(\alpha, \gamma){}^7\text{Be}$ $S_{34}(0)$ results. The central value represents the recommended one.

Source: The figure is adapted from Ref. [57].

on using the asymptotic normalization coefficient (ANC) technique to derive the zero-energy astrophysical factor $S_{34}(0)$ factor of the ${}^3\text{He}(\alpha, \gamma){}^7\text{Be}$ reaction without extrapolation [59]. This approach takes advantage of the pure external direct capture process of the reaction and to the possibility to derive the absolute normalization from measurements easier to carry out.

From the experiment to the astrophysical factor. The ${}^3\text{He}(\alpha, \gamma){}^7\text{Be}$ reaction was studied through the ANC approach by measuring the near-barrier transfer reaction ${}^6\text{Li}({}^3\text{He}, d){}^7\text{Be}$, populating both the ${}^7\text{Be}$ ground state and first excited state (excitation energy 429 keV). The angular distributions of the emitted deuterons were measured in two experiments performed using the 3 MV singletron accelerator of the Department of Physics and Astronomy (DFA) of the University of Catania (Italy) and the FN tandem accelerator at the John. D. Fox Superconducting Accelerator Laboratory at the Florida State University (FSU), Tallahassee, USA, at ${}^3\text{He}$ beam energies of 3 and 5 MeV. Details on the experiment and on the analysis are given in [57,60]. In the analysis, the ANCs for the ${}^6\text{Li}-p$ channel were deduced as well, to provide an independent assessment of the accuracy of the method.

The ANCs of the ${}^3\text{He}-\alpha$ channels were extracted from the analysis of the deuteron angular distributions (Fig. 3.2, left panel) at backward angles in the center of mass, focusing in particular on the main peak, where the peripherality of the process is more pronounced. The angular distributions were fitted using the post form of the modified DWBA, taking into account the channel coupling effects (CCE). Two separate calculations were carried out (originating the two sets of gray lines in Fig. 3.2, left panel), assuming two different reaction mechanisms, p -transfer at forward center-of-mass angles ($\theta_{\text{cm}} \leq 90^\circ$) and α -transfer at backward center-of-mass angles ($\theta_{\text{cm}} \geq 90^\circ$). Focusing on α -transfer, the contribution of p -transfer is negligible at large θ_{cm} angles, as well as the interference of the two mechanisms. To minimize and quantify the systematic error introduced by the dependence on optical model parameters, several sets of optical potentials were tested in the ingoing and outgoing channels. From these, the one providing the most accurate description for the experimental data was used in the data analysis. Furthermore, the geometrical parameters of the Woods–Saxon potential of the bound state wave function were varied within a broad range to test the peripheral nature of the reaction. The ANCs were found to have a very weak dependence on the single particle ANCs, showing that the peripherality condition is satisfied within a 2%–3% level [60].

As discussed in [57], the values of the square of the ANCs for the ${}^3\text{He} + \alpha \rightarrow {}^7\text{Be}(\text{g.s.})$ and ${}^3\text{He} + \alpha \rightarrow {}^7\text{Be}(0.429 \text{ MeV})$ were found to be $C^2 = 20.84 \pm 1.12$ [0.82; 0.77] fm^{-1} and $C^2 = 12.86 \pm 0.50$ [0.35; 0.36] fm^{-1} , respectively. Square parentheses show the components of the error budget: it includes both experimental uncertainties on the $d\sigma^{\text{exp}}/d\Omega$ (first term in square brackets) and the uncertainty due to the ANC of $d + {}^4\text{He} \rightarrow {}^6\text{Li}$, as well as the uncertainties from the adopted optical model (second term in square brackets). Using the deduced ANCs and within the modified two-body potential model (MTBPM) [57,60], the direct capture ${}^3\text{He}({}^4\text{He}, \gamma){}^7\text{Be}$ astrophysical factor was calculated and the resulting $S_{34}(0)$ (Fig. 3.2) and $S_{34}(23 \text{ keV})$ factors (23 keV being the Gamow energy for Solar fusion) turned out to be $S_{34}(0) = 0.534 \pm 0.025$ [0.015; 0.019] keVb and $S_{34}(23 \text{ keV}) = 0.525 \pm 0.022$ [0.016; 0.016] keVb. The comparison with the values in the literature shows an improved accuracy with respect to the present-day recommended value in [3], $S_{34}(0) = 0.56 \pm 0.02(\text{expt}) \pm 0.02(\text{theor})$ keVb, but with an uncertainty still higher than the target value of 3%, calling for further improved determinations of the ${}^6\text{Li}({}^3\text{He}, d){}^7\text{Be}$ transfer cross section.

Table 3.1
Reactions studied with the ANC method.

	Indirect reaction	Direct reaction	References
[1]	$^{10}\text{B}(^7\text{Be}, ^8\text{B})^9\text{Be}$	$^1\text{H}(^7\text{Be}, \gamma)^8\text{B}$	Azhari et al 2001 [76]
[2]	$^{14}\text{N}(^7\text{Be}, ^8\text{B})^{13}\text{C}$	$^1\text{H}(^7\text{Be}, \gamma)^8\text{B}$	Azhari et al 2001[76]
[3]	$^{13}\text{C}(^7\text{Li}, ^8\text{Li})^{12}\text{C}$	$^1\text{H}(^7\text{Be}, \gamma)^8\text{B}$	Trache et al 2003 [43]
[4]	$^{16}\text{O}(^3\text{He}, d)^{17}\text{F}$	$^1\text{H}(^{16}\text{O}, \gamma)^{17}\text{F}$	Gagliardi et al 1998 [77]
[5]	$^{14}\text{N}(^3\text{He}, d)^{15}\text{O}$	$^1\text{H}(^{14}\text{N}, \gamma)^{15}\text{O}$	Bertone et al 2002 [78]
[6]	$^{12}\text{C}(d, p)^{13}\text{C}$	$n(^{12}\text{C}, \gamma)^{13}\text{C}$	Imai et al 2000 [79]
[7]	$^{13}\text{C}(^6\text{Li}, d)^{17}\text{O}$	$^4\text{He}(^{13}\text{C}, n)^{16}\text{O}$	Kubono et al 2003 [80]
[8]	$^{14}\text{N}(^{13}\text{N}, ^{14}\text{O})^{13}\text{C}$	$^1\text{H}(^{13}\text{N}, \gamma)^{14}\text{O}$	Motobayashi et al 1991 [81]
[9]	$^{12}\text{N}(^3\text{He}, d)^{13}\text{O}$	$^1\text{H}(^{12}\text{N}, \gamma)^{13}\text{O}$	Skorodumov et al 2007 [82]
[10]	$^{15}\text{N}(^3\text{He}, d)^{16}\text{O}$	$^1\text{H}(^{15}\text{N}, \gamma)^{16}\text{O}$	Mukhamedzhanov et al 2010 [83]
[11]	$^{13}\text{C}(^{14}\text{C}, ^{15}\text{C})^{12}\text{C}$	$^{14}\text{C}(n, \gamma)^{15}\text{O}$	McCleskey et al 2014 [44]
[12]	$^{14}\text{C}(d, p)^{15}\text{C}$	$^{14}\text{C}(n, \gamma)^{15}\text{O}$	McCleskey et al 2014 [44]
[13]	$^{18}\text{O}(^3\text{He}, d)^{19}\text{F}$	$^{18}\text{O}(p, \gamma)^{19}\text{F}$	Burjan et al 2019 [40]
[14]	$^6\text{Li}(^3\text{He}, d)^7\text{Be}$	$^3\text{He}(\alpha, \gamma)^7\text{Be}$	Kiss et al 2020 [41]
[15]	$^{26}\text{Mg}(d, p)^{27}\text{Mg}$	$^{26}\text{Si}(p, \gamma)^{27}\text{P}$	Guo et al 2006, Timofeyuk et al 2008, D'Agata et al 2021 [45,69,70]
[16]	$^6\text{Li}(^3\text{He}, d)^7\text{Be}$	$^6\text{Li}(p, \gamma)^7\text{Be}$	Kiss et al 2021 [84]

3.0.3. The $^{26}\text{Si}(p, \gamma)^{27}\text{P}$ reaction

Astrophysical background. The production and destruction channels of ^{26}Si are strongly correlated with one of the most studied topics in nuclear astrophysics: the ^{26}Al abundance in our Galaxy. Such element ($T_{1/2} = 0.75$ Mys, $J^\pi = 5^+$) can be produced in a number of different stellar scenarios, such as core-collapse Supernovae [61], Novae [62], Wolf-Rayet objects and AGB-stars [63]. All these sites have been addressed as possible sites of proton capture, therefore ^{26}Al can be produced from ^{24}Mg following the reaction chain $^{24}\text{Mg}(p, \gamma)^{25}\text{Al}(\beta^+)^{25}\text{Mg}(p, \gamma)^{26}\text{Al}$, with the ^{26}Al that then decays in ^{26}Mg 1st, that almost immediately (476 fs) falls in its ground state, emitting the well-known 1.807 MeV γ -ray line. Such a scenario is made more complicated by the presence of the well-known isomeric state $^{26}\text{Al}^m$ ($T_{1/2} = 6.34$ s, $J^\pi = 0^+$), that can swiftly decay in $^{26}\text{Mg}_{g.s.}$. Such an isomer can be produced from ^{25}Al via proton capture, following the reaction chain $^{25}\text{Al}(p, \gamma)^{26}\text{Si}(\beta^+)^{26}\text{Al}^m$, thus reducing the quantity of ^{26}Al produced. In this second reaction chain, the unstable ($T_{1/2} = 2.24$ s) ^{26}Si can also capture a proton, producing ^{27}P via the $^{26}\text{Si}(p, \gamma)^{27}\text{P}$ reaction.

The $^{26}\text{Si}(p, \gamma)^{27}\text{P}$ proton capture has been studied many times in the past [64–70]. In particular, in [69], the authors re-analyzed old published data available in literature [71] regarding the $^{26}\text{Mg}(d, p)^{27}\text{Mg}$ reaction, and using the well established extension of the ANC method for the mirror nuclei ([72], see also [73] for more details), were able to calculate the ANC's for the $^{26}\text{Si}(p, \gamma)^{27}\text{P}$ capture in the ground, first and second excited states. Such results were nonetheless challenged by [70], that retrieved the ANC's for the ground and 1st excited states of ^{27}P from the $^{26}\text{Mg}(t, d)^{27}\text{Mg}$ reaction, again using the mirror nuclei technique. In this last work, the ANC's for the ground and first excited states for the $^{26}\text{Mg}(n, \gamma)^{27}\text{Mg}$ neutron capture have been found to be a factor of 2 and a factor of 3 smaller, respectively, and the S(E) factor at zero energies – $S(0)$ – has been found to be 1.7 times smaller than [69].

Experimental apparatus and reaction rate calculation. To address this discrepancies, another ANC experiment involving mirror nuclei has been performed, using the deuteron beam available at the U120-M isochronous cyclotron of the Nuclear Physics Institute of the Czech Academy of sciences [45]. The $^{26}\text{Mg}(d, p)^{27}\text{Mg}$ reaction has been then used to study the $^{26}\text{Si}(p, \gamma)^{27}\text{P}$ one.

The experimental setup consisted of five ΔE -E telescopes, made with thin (250 μm) Si and thick (5 mm) Si(Li) surface detectors. Three of those were positioned on a rotating plate with a 10° step between each other, in order to cover the region between 7° and 60° in the laboratory reference frame. On the other side of the beam, the remaining two ΔE -E telescopes were placed at 15° and 35° , and have been used as monitors to check beam purity and alignment.

The OMP's for the entrance channel have been obtained from the elastic scattering $^{26}\text{Mg}(d, d)^{26}\text{Mg}$, while for the exit one the code FRESKO has been used to fit the experimental angular distributions of the protons coming from the $^{26}\text{Mg}(d, p)^{27}\text{Mg}$ in the ground and 1st excited states (Fig. 3.3, left panel), using the OMP's from [69] as seed values (see dashed and dotted lines in the figure referring to potentials P1 and P2 from Table I of Ref. [45]).

Once the peripherality for the process has been ascertained by checking the small dependency of the ANC from the single-particle ANC (Fig. 3.3, right panel), following the discussion in section 3 and in Ref. [15] (section 2.1.3), the calculated ANC's in this work have been found to be 28.26 ± 4.9 fm $^{-1}$ and 1.41 ± 0.25 fm $^{-1}$ for the $^{26}\text{Mg}(n, \gamma)^{27}\text{Mg}$ capture in the ground state and in the first excited state, respectively. Those values – in reasonable agreement with [70] – have then been used to calculate the $|C_{Si+p}^{1/2+}|^2 = 1420 \pm 255$ fm $^{-1}$, value in agreement with [70] if the different separation energies for the system $^{26}\text{Si}+p$ used in [45,70] are considered. For the first excited state of ^{27}P , the total width Γ_p has been calculated – $\Gamma_p = (5.23 \pm 1.5) \times 10^{-9}$ – and there is again a fair agreement between [45,70]. Finally, the reaction rates for proton capture in both the ground and 1st excited states of ^{27}P have been calculated and compared with the results coming from [74], using the Γ_γ value coming from the Γ_γ/Γ_p ratio from [75]: an increasing by a factor 1.4 and 2.2 has been found for the reaction rates of the $^{26}\text{Si}(p, \gamma)^{27}\text{P}$ capture in the ground and first excited states, respectively.

4. Experimental application of the THM

The Theory of the THM relies on the principles of direct reactions and is utilized to establish a connection between the cross sections of two closely related reactions. In this approach, the reaction of astrophysical interest (Eq. (1.7)) can be viewed as a

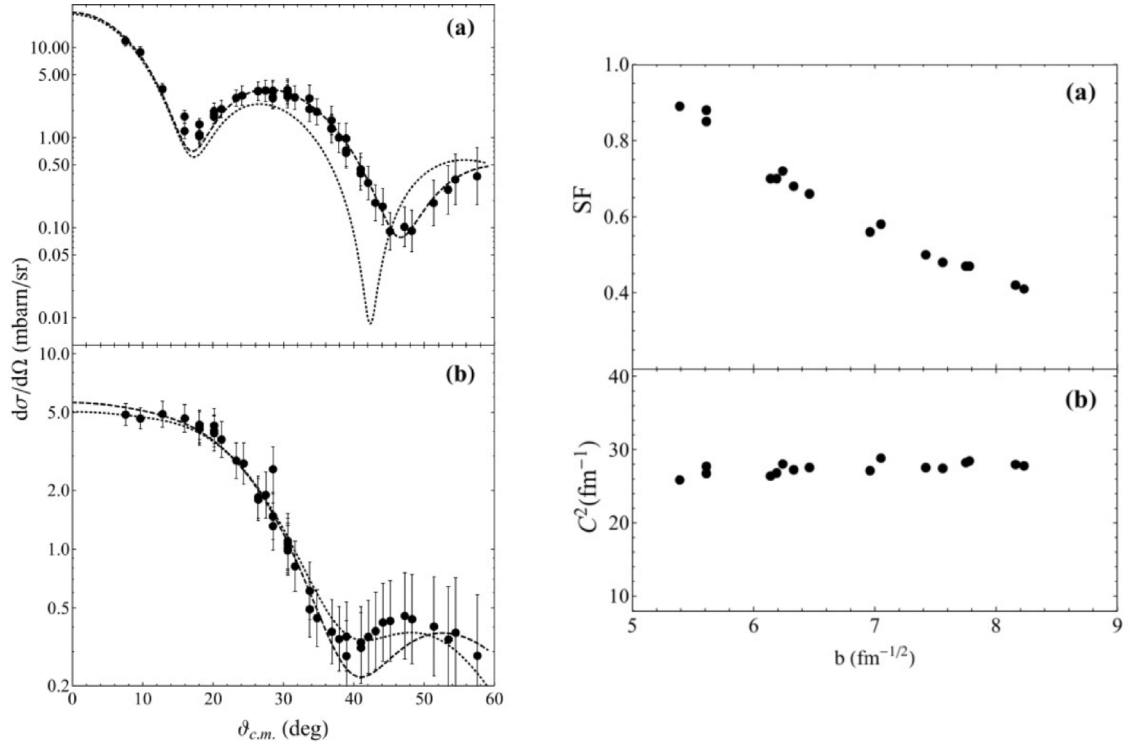


Fig. 3.3. Left Panel: angular distribution for the $^{26}\text{Mg}(d,p)^{27}\text{Mg}$ transfer reaction for the ground (a) and first excited (b) states. Fitting dashed and dotted lines in the figure refer to potentials P1 and P2 from Table I of Ref. [45]. Right panel: comparison between the variation of the spectroscopic factor (a) and ANC (b) as a function of the single-particle ANC. The small variation of the latter is a strong hint of a peripheral process, allowing the application of the ANC method. Source: The figure is adapted from Ref. [45].

subprocess of the actual Trojan-Horse (TH) reaction (Eq. (1.6)). The nucleus a possesses a prominent cluster structure $b + x$ in its ground state and acts as a Trojan horse, drawing an analogy to the tale from Homer's *Odyssey*. The nucleus b is considered a spectator, essentially unaffected by the TH reaction, and therefore, only a minimal momentum transfer to b is expected. The theory of the THM has been developed and discussed in multiple papers employing various alternative formalisms [17,21,23,26,85]

However, despite the differences in notation, introduced quantities, and specific details, the general features of the THM remain essentially the same. In the previous section on transfer reactions, an approach was chosen to provide a direct understanding of the key aspects of the THM. The TH reaction (Eq. (1.6)) is assumed to be dominated by surface effects, and the reduction of the cross section for the sub-process (Eq. (1.7)) due to Coulomb interactions is suppressed. This suppression occurs because the particle x is brought close to nucleus A within the Trojan horse a at a high energy. Despite the high energy in the $a + A$ channel, it is possible to achieve low energies in the relative motion of x and A . Initially, it was proposed an explanation for this phenomenon by considering the momentum distribution of the clusters x and b inside the Trojan horse a [26]. However, this interpretation, which relied on compensating the energy of $a + A$ with the Fermi motion of x within a , was later superseded by the experimental work carried out by the nuclear astrophysics group at INFN-Laboratori Nazionali del Sud in Catania, known as the ASFIN group. Historical developments and reviews of this work can be found in [15,17,85–87]. In order to successfully apply the THM in actual experiments, the TH reaction (Eq. (1.6)) is typically studied under quasi-free (QF) scattering conditions. Under these kinematic conditions, the momentum transfer \bar{Q}_{bB} to the spectator b , as described in Eq. (2.29), is small and close to the peak of the momentum distribution. This particular region in the three-body phase space is where the quasi-free (QF) process makes the most significant contribution to the cross section of the reaction (1.6), in comparison to other mechanisms such as sequential or compound-nucleus reactions. Consequently, the momentum transfer is not large and does not correspond to the tail of the momentum distribution, as initially assumed in the original presentation of the method.

4.1. Kinematic conditions

The conservation of energy in the center-of-mass (c.m.) system for the TH reaction (1.6) can be expressed as:

$$E_{aA} = E_{cC} + E_{bB} - Q_{a+A \rightarrow b+c+C} \quad (4.1)$$

with the Q value (2.7) and the kinetic energies of the relative motion (2.4).

Additionally, we introduce the binding energy B_a of the Trojan horse a , defined in Eq. (2.9). By utilizing the energy conservation of the two-body reaction (1.7), we can further analyze the energy relationships involved in the TH reaction:

$$E_{cC} + m_c + m_C = E_{xA} + m_x + m_A, \quad (4.2)$$

and the effective kinetic energy

$$E_{xA} = E_{aA} - E_{bB} - B_a \quad (4.3)$$

in the initial state of the sub-process (1.7) is expressed by means of the energies of the TH reaction (1.6).

The positivity of both E_{bB} and B_a implies that the energy E_{xA} is significantly smaller than the energy E_{aA} in the entrance channel of the TH reaction. This observation underscores the fact that the Trojan horse mechanism allows for the extraction of low-energy information from a higher-energy entrance channel. Moreover, momentum conservation in the quasi-free scattering condition, where $\vec{Q}_{bB} = 0$ or $\vec{p}_{bB} = m_b \vec{p}_{aA} / (m_x + m_b)$, can be utilized to impose an additional constraint on the kinematics of the reaction.

The expression

$$E_{bB} = \frac{p_{bB}^2}{2\mu_{bB}} = \left(\frac{m_b}{m_x + m_b} \right)^2 \frac{\mu_{aA}}{\mu_{bB}} E_{aA} \quad (4.4)$$

allows us to define the quasi-free energy

$$E_{xA}^{qf} = \left[1 - \left(\frac{m_b}{m_x + m_b} \right)^2 \frac{\mu_{aA}}{\mu_{bB}} \right] E_{aA} - B_a \quad (4.5)$$

in the entrance channel of the astrophysical reaction (1.7). This quasi-free energy is completely determined by the energy in the initial state of the TH reaction (1.6). It is important to note that E_{xA}^{qf} can become very small or even negative depending on the binding energy B_a of the Trojan horse a and the choice of E_{aA} , as the pre-factor of E_{aA} is smaller than one. However, in real experiments, the quasi-free energy E_{xA}^{qf} is not changed by changing E_{aA} .

Typically, it is more suitable to maintain a constant value for the beam energy while exploring a specific range in Q_{bB} around zero. By utilizing the definition of Jacobi momenta and disregarding the binding energies of the nuclei relative to their masses, we can establish $\vec{Q}_{bB} = -\vec{p}_{xb}$. To ensure a reasonable approach, it is advisable to confine the range to $Q_{bB} < \hbar \kappa_{xb}$, where $\kappa_{xb} = \sqrt{2\mu_{xb} B_a} / \hbar$ denotes the OES wave number for the bound state of a . The method described here, initially outlined in [88], represents a distinct approach to the THM (Three-Body Model) in contrast to the original concept presented in [26], where the pertinent values of p_{xb} were substantially higher, reaching hundreds of MeV/c. This high p_{xb} value was necessary to compensate for the energy associated with the relative motion of $A + a$. At such large momenta, the magnitude of the momentum distribution can be significantly smaller compared to that at $p_{xb} = 0$, necessitating a careful separation of the quasi-free process from other competing reaction mechanisms. Furthermore, given that the analysis of experimental data relies on the shape of the momentum distribution, it is crucial to have a reliable theoretical description. This becomes more challenging for the tail of the distribution compared to a limited region at small p_{xb} values.

The finite range of p_{xb} in the inter-cluster motion is employed to ensure access to the astrophysical energy region in the TH experiment. Typically, this range is on the order of a few tens of MeV/c. Fig. 4.1 illustrates a typical shape analysis of the momentum distribution, conducted for the $^{17}\text{O}(p, \alpha)^{14}\text{N}$ reaction by employing ^2H as the TH nucleus [89,90]. The experimental momentum distribution is represented by black full circles and is compared with theoretical distributions. Theoretical distributions are obtained using the square of the Hulthén wave function in momentum space, based on the plane-wave impulse approximation (shown as a black solid line), as well as calculations performed within the distorted-wave Born approximation (DWBA) using the FRESKO code [39] and optical potential parameters extrapolated from [55] (represented by a red dotted line). Both curves are scaled to the experimental maximum for comparison purposes. A noticeable agreement within experimental uncertainties is observed for neutron momentum values $p_b \leq 50$ MeV/c, which corresponds to the matching κ_{xb} value for the deuteron. This criterion determines the selection of quasi-free (QF) events for further analysis of the data.

The quasi-free condition $\vec{p}_{xb} = 0$ can be expressed as $m_x \vec{p}_b = m_b \vec{p}_x$, leading to the following equations:

$$\vec{p}_x = \left(1 + \frac{m_b}{m_x} \right)^{-1} \vec{p}_a = \frac{m_x}{m_a} \vec{p}_a \quad (4.6)$$

These equations are derived from the fact that $\vec{p}_a = \vec{p}_x + \vec{p}_b$. Furthermore, this provides the energy expression:

$$E_{xA} = \frac{p_{xA}^2}{2\mu_{xA}} = \frac{1}{2\mu_{xA}} \left[\mu_{xA} \left(\frac{\vec{p}_x}{m_x} - \frac{\vec{p}_A}{m_A} \right) \right]^2 = \frac{\mu_{xA}}{\mu_{aA}} E_{aA} \quad (4.7)$$

This energy expression, derived through the usual dispersion relation, is distinct from E_{xA}^{qf} calculated in Eq. (2.14). Consequently, the sub-process of transferring x in the TH (Transfer-Hydrogen) reaction occurs off the energy shell, and x must be regarded as a virtual particle. In TH experiments, the quasi-free condition, where p_{xb} is close to zero, also determines the selection of the TH nuclei. TH nuclei that exhibit a significant cluster component in an s -wave of relative motion are preferred, such as ^2H for two-body reactions involving protons or neutrons, or ^6Li for the transfer of deuterons or α particles.

4.2. General steps of data analysis

Now the methodology for data analysis in TH experiments is discussed, which requires careful considerations regarding the choice of the TH nucleus, kinematic conditions (to satisfy Eq. (2.14) regarding beam energy), detection angles, choice of detected

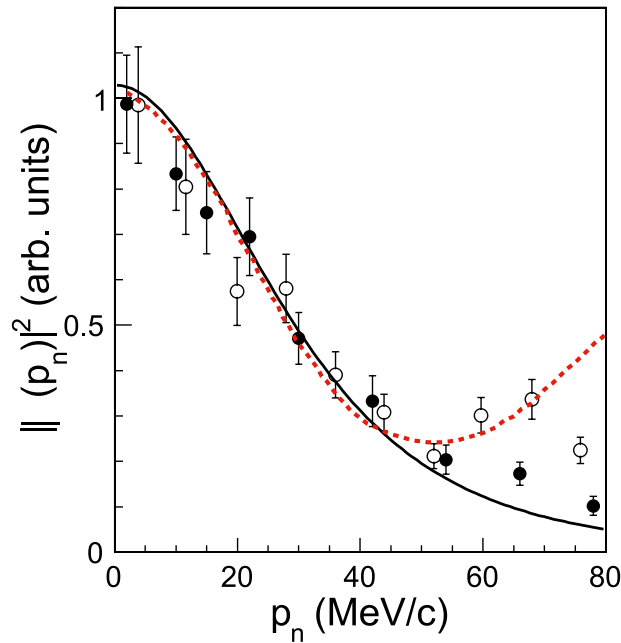


Fig. 4.1. Experimental momentum distribution for the spectator (full black and open circles) from [89,90] compared with theoretical ones, given in plane wave impulse approximation (black solid line) and DWBA (red dotted line) normalized to the experimental maximum.

particles, and the experimental setup. Successful TH experiments necessitate relatively simple experimental setups with high energy and angular resolutions (typically less than 1% and less than 0.2 degrees, respectively) to minimize uncertainties in E_{xA} . For TH reactions, all kinematic variables can be calculated using the energies and angles of any two out of the three particles in the exit channel. This feature is particularly advantageous when the breakup occurs in the target or when one of the three particles involved is a neutron. In such cases, the detection of very low-energy particles, which may be limited by detection thresholds, or the use of neutron detectors with poor angular resolution can be avoided. A typical detection setup consists of two or more pairs of coincidence telescopes positioned on opposite sides of the beam direction at relatively forward angles. TH experiments are often conducted in inverse kinematics. Several steps are involved in the data analysis process before extracting the two-body cross section relevant to astrophysics:

- identification of the three-body reaction channel of interest, typically accomplished using the standard ΔE - E technique or through kinematic calculations;
- validity tests on selected events and the selection of the quasi-free (QF) mechanism;
- extraction of the binary cross section from the measured TH cross section in arbitrary units. At sub-Coulomb energies, the penetrability factor needs to be considered;
- normalization procedure using available direct data to obtain the cross section $\sigma_b(E)/S_b(E)$ in absolute units. In cases where ultra-low energy data from direct measurements are available, the electron screening potential can be extracted using Eq. (1.2);
- validity tests comparing direct and indirect data in terms of excitation functions, including resonances, and angular distributions.

After these validations, THM data can be considered reliable in cases where direct data are not available. The general procedure for applying the TH method is summarized in Fig. 4.2. Starting with the selection of a specific TH nucleus with a particular momentum distribution (top panel) and determining the entrance channel energy E_{aA} , the quasi-free energy (2.14) in the astrophysical reaction (1.7) is calculated (bottom panel). The chosen momentum distribution cutoff, denoted as Q_{cut} , defines the accessible range of energies E_{xA} . The cross section extracted from the TH experiment needs to be scaled to direct data since it provides only the energy dependence and not the absolute normalization.

Recently, the selection of suitable nuclei for TH experiments has expanded to include ^{14}N in addition to the commonly used nuclei ^2H , ^3He , and ^6Li , which have been extensively employed in numerous TH experiments. The inclusion of ^{14}N in recent applications [30] opens up new possibilities for future experiments using THM with heavier stable nuclei and even with radioactive beams. The utilization of heavier TH nuclei, such as ^{13}C , ^{14}N , ^{20}Ne , ^{23}Na , and ^{26}Mg , holds promise for investigating crucial reactions that contribute to energy generation and the production of heavy elements in the late stages of massive star evolution. These experiments can provide valuable insights into the dynamics and role of clusters within the THM framework. For more detailed information on the influence of clusters and their dynamics in THM, refer to [91]. Additionally, some of the potential TH nuclei

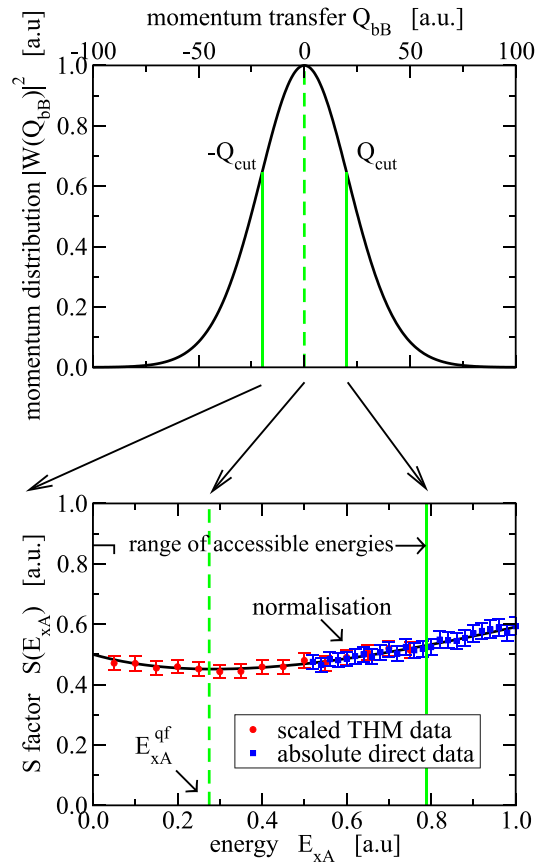


Fig. 4.2. Connection of the momentum distribution of the Trojan-Horse nucleus (top panel) to the range of accessible energies for the astrophysical $S(E)$ factor (lower panel) in the THM.

exhibit p-wave intercluster motion configurations, and focused studies in this area are anticipated in the near future to broaden the applicability of the method.

4.3. Recent applications

The THM has demonstrated successful applications to various reactions of astrophysical importance. A comprehensive list of the most significant reactions investigated thus far, along with relevant bibliographical references, can be found in Table 4.1. For a more detailed analysis of the specific characteristics of each experimental study, it is recommended to refer to the corresponding articles. Here, we will provide an overview of recent results, highlighting the versatility of the THM. The method has been employed to study a wide range of reactions, including those involving charged particles (resonant or non-resonant) and neutron-induced reactions. These investigations have utilized both stable and radioactive ion beams (see, for example, [92,93]). TH investigations typically focus on processes that are relevant to stellar nucleosynthesis scenarios, spanning from the early universe to advanced and explosive phases of evolved stars. In some cases, these studies serve the purpose of understanding crucial aspects of nuclear interactions. They also play a significant role in investigating fusion dynamics in plasmas for energy production. Notable examples include the d+d reaction [94] and the $^{10,11}\text{B}+p$ reaction [95,96]. In these cases, the availability of unscreened low-energy data allows for testing the consistency of existing models in determining electron screening effects. In the following, we will review recent studies, most of them triggered by the nuclear astrophysics interest. In particular, we will focus on the $^7\text{Be}(n, \alpha)$ and $^7\text{Be}(n, p)$ reactions, $^{27}\text{Al}(n, \alpha)$ reaction, Coulomb-free $p-p$ scattering cross section and $^{12}\text{C}+^{12}\text{C}$ fusion reaction.

4.3.1. The contribution to the standard BBN reaction network

The Big Bang Nucleosynthesis (BBN) occurred during the time span when our universe was capable of producing nuclei, just after baryogenesis, most likely 1–20 min after the *Bang*. BBN has been extensively studied for decades due to its significance in understanding the entire Big Bang Model. It serves as one of the three main evidences supporting the model, along with galactic recession and the Cosmic Microwave Background (CMB). BBN allows us to explore the universe during its earliest stages, making it a valuable tool for constraining the physical evolution of the Big Bang. By studying the primordial abundances of ^2H , ^3He , ^4He , ^7Li ,

Table 4.1

Reactions studied with the THM.

	Indirect reaction	Direct reaction	References
[1]	${}^2\text{H}({}^7\text{Li}, \alpha\alpha)\text{n}$	${}^1\text{H}({}^7\text{Li}, \alpha){}^4\text{He}$	Spitaleri et al 1999, Lattuada et al 2001 [97]
[2]	${}^3\text{He}({}^7\text{Li}, \alpha\alpha)\text{d}$	${}^2\text{H}({}^7\text{Li}, \alpha){}^4\text{He}$	Tumino et al 2006 [98]
[3]	${}^2\text{H}({}^6\text{Li}, \alpha){}^3\text{He}\text{n}$	${}^1\text{H}({}^6\text{Li}, \alpha){}^3\text{He}$	Tumino et al 2003 [88]
[4]	${}^6\text{Li}({}^6\text{Li}, \alpha\alpha){}^4\text{He}$	${}^2\text{H}({}^6\text{Li}, \alpha){}^4\text{He}$	Spitaleri et al 2001 [22]
[5]	${}^2\text{H}({}^9\text{Be}, \alpha){}^6\text{Li}\text{n}$	${}^1\text{H}({}^9\text{Be}, \alpha){}^6\text{Li}$	Wen et al 2008 [99]
[6]	${}^2\text{H}({}^{10}\text{B}, \alpha){}^7\text{Be}\text{n}$	${}^1\text{H}({}^{10}\text{B}, \alpha){}^7\text{Be}$	Lamia et al 2008, Rapisarda et al 2018, Cvetinovic et al 2018 [100–102]
[7]	${}^2\text{H}({}^{11}\text{B}, \alpha_0){}^8\text{Be}\text{n}$	${}^1\text{H}({}^{11}\text{B}, \alpha){}^8\text{Be}$	Spitaleri et al 2004, Lamia et al 2011 [103,104]
[8]	${}^2\text{H}({}^{15}\text{N}, \alpha){}^{12}\text{C}\text{n}$	${}^1\text{H}({}^{15}\text{N}, \alpha){}^{12}\text{C}$	La Cognata et al 2007 [105]
[9]	${}^2\text{H}({}^{18}\text{O}, \alpha){}^{15}\text{N}\text{n}$	${}^1\text{H}({}^{18}\text{O}, \alpha){}^{15}\text{N}$	La Cognata et al 2009 [106]
[10]	${}^2\text{H}({}^{17}\text{O}, \alpha){}^{14}\text{N}\text{n}$	${}^1\text{H}({}^{17}\text{O}, \alpha){}^{14}\text{N}$	Sergi et al 2010, Sergi et al. 2015 [89,90]
[11]	${}^6\text{Li}({}^3\text{He}, \text{p}^4\text{He}){}^4\text{He}$	${}^2\text{H}({}^3\text{He}, \text{p}){}^4\text{He}$	La Cognata et al 2005 [107]
[12]	${}^2\text{H}({}^6\text{Li}, \text{p}^3\text{H}){}^4\text{He}$	${}^2\text{H}(\text{d}, \text{p}){}^3\text{H}$	Rinollo et al 2005 [108]
[13]	${}^6\text{Li}({}^{12}\text{C}, \alpha){}^{12}\text{C}^2\text{H}$	${}^4\text{He}({}^{12}\text{C}, {}^{12}\text{C}){}^4\text{He}$	Spitaleri et al 2000 [109]
[14]	${}^2\text{H}({}^6\text{Li}, \text{t}^4\text{He}){}^1\text{H}$	$\text{n}({}^6\text{Li}, \text{t}){}^4\text{He}$	Tumino et al 2005, Gulino et al 2010 [110,111]
[15]	${}^2\text{H}(\text{p}, \text{pp})\text{n}$	${}^1\text{H}(\text{p}, \text{p}){}^1\text{H}$	Tumino et al 2007, Tumino et al 2008 [112,113]
[16]	${}^2\text{H}({}^3\text{He}, \text{p}^3\text{H}){}^1\text{H}$	${}^2\text{H}({}^3\text{He}, \text{p}){}^3\text{H}$	Tumino et al 2011, Tumino et al 2014 [94,114]
[17]	${}^2\text{H}({}^3\text{He}, \text{n}^3\text{He}){}^1\text{H}$	${}^2\text{H}({}^3\text{He}, \text{n}){}^3\text{He}$	Tumino et al 2011, Tumino et al 2014 [94,114]
[18]	${}^2\text{H}({}^{19}\text{F}, \alpha){}^{16}\text{O}\text{n}$	${}^1\text{H}({}^{19}\text{F}, \alpha){}^{16}\text{O}$	La Cognata et al 2011, Indelicato et al 2017 [32,115]
[19]	${}^{13}\text{C}({}^6\text{Li}, \text{n}){}^{16}\text{O}^2\text{H}$	${}^{13}\text{C}(\alpha, \text{n}){}^{16}\text{O}$	La Cognata et al 2014 [116]
[20]	${}^2\text{H}({}^{18}\text{F}, \alpha){}^{15}\text{O}\text{n}$	${}^1\text{H}({}^{18}\text{F}, \alpha){}^{15}\text{O}$	Cherubini et al 2015, Pizzone et al. 2016, La Cognata et al. 2017 [92,117,118]
[21]	${}^2\text{H}({}^{10}\text{B}, \alpha){}^7\text{Li}^1\text{H}$	$\text{n}({}^{10}\text{B}, \alpha){}^7\text{Li}$	Guardo et al 2019, Sparta et al 2021 [119,120]
[22]	${}^2\text{H}({}^7\text{Be}, \alpha\alpha){}^1\text{H}$	$\text{n}({}^7\text{Be}, \alpha){}^4\text{He}$	Lamia et al 2017, Lamia et al 2019, Hayakawa et al 2021 [121–123]
[23]	${}^{12}\text{C}({}^{14}\text{N}, \alpha){}^{20}\text{Ne}^2\text{H}$	${}^{12}\text{C}({}^{14}\text{N}, \alpha){}^{20}\text{Ne}$	Tumino et al 2018 [30]
[24]	${}^{12}\text{C}({}^{14}\text{N}, \text{p}^{23}\text{Na})^2\text{H}$	${}^{12}\text{C}({}^{12}\text{C}, \text{p})^{23}\text{Na}$	Tumino et al 2018 [30]
[25]	${}^6\text{Li}({}^{19}\text{F}, \text{p}^{22}\text{Ne})^2\text{H}$	${}^4\text{He}({}^{19}\text{F}, \text{p})^{22}\text{Ne}$	Pizzone et al 2017, Dagata et al 2018 [117,124]
[26]	${}^2\text{H}({}^{17}\text{O}, \alpha){}^{14}\text{C}^1\text{H}$	${}^{17}\text{O}(\text{n}, \alpha){}^{14}\text{C}$	Oliva et al 2020 [125]
[27]	${}^2\text{H}({}^3\text{He}, \text{pt}){}^1\text{H}$	${}^3\text{He}(\text{n}, \text{p}){}^3\text{H}$	Pizzone et al 2021 [126]
[28]	${}^2\text{H}({}^7\text{Be}, \text{p}^7\text{Li}){}^1\text{H}$	$\text{n}({}^7\text{Be}, \text{p}){}^7\text{Li}$	Hayakawa et al 2021 [123]
[29]	${}^2\text{H}({}^{27}\text{Al}, \alpha){}^{24}\text{Mg}\text{n}$	${}^{27}\text{Al}(\text{p}, \alpha){}^{24}\text{Mg}$	Palmerini et al 2021, La Cognata et al. 2022 [127–129]

we can gather information about the physical conditions in the primordial era. For a recent review and references, refer to [130]. To investigate the abundances, origin, and evolution of light elements, we must consider various processes in addition to the Big Bang, such as production by cosmic rays, stellar destruction, and nucleosynthesis. However, understanding the light element abundances in stars is limited by our incomplete knowledge of many astrophysical processes, including convection, microscopic diffusion, and the possible presence of additional mixing mechanisms. Furthermore, the destruction of light elements strongly depends on the chosen physical inputs, particularly the nuclear reaction rates. One well-studied case is the discrepancy between the predicted and observed abundances of ${}^7\text{Li}$ in the Sun, as well as in open clusters and halo or disk stars. However, a complete understanding of lithium burning in stars also involves considering the role of the less abundant ${}^6\text{Li}$ [88,131]. It is important to note that, except for ${}^7\text{Li}$, the predicted and observed abundances of other primordial isotopes generally match within uncertainties, considering the appropriate astrophysical sites. Despite the efforts made to reduce uncertainties, in most cases, directly measured cross-section data exhibit inadequate accuracy in the energy range relevant for BBN. This is due to inherent limitations, such as the presence of the Coulomb barrier for charged particle-induced reactions, which reduces cross-section values to such small values that they are nearly impossible to measure. Additionally, there is a need for neutron beams that cover the energy region relevant to astrophysics.

Recently, indirect measurements have been performed to overcome these difficulties, particularly using the THM. This has been applied to some of the most relevant reactions of the SBBN network, such as ${}^2\text{H}(\text{d}, \text{p}){}^3\text{H}$ [94,114,132], ${}^2\text{H}(\text{d}, \text{n}){}^3\text{He}$ [94,114], ${}^3\text{He}(\text{d}, \text{p}){}^4\text{He}$ [133], ${}^7\text{Li}(\text{p}, \alpha){}^4\text{He}$ [134,135], and then extended to ${}^7\text{Be}(\text{n}, \alpha){}^4\text{He}$, ${}^7\text{Be}(\text{n}, \text{p}){}^7\text{Li}$ and ${}^3\text{He}(\text{n}, \text{p}){}^3\text{H}$ [136] in [137]. These studies open up new avenues for the application of the Trojan Horse Method (THM) to neutron-induced reactions on radioactive ion beams. This significantly expands the utility of THM to encompass almost all the reactions that are relevant for astrophysics.

4.3.2. Status of the ${}^7\text{Be}+\text{n}$ measurements and the THM experiment at CRIB

Background. The nucleosynthesis of the radioactive ${}^7\text{Be}$ isotope impacts the final abundance of ${}^7\text{Li}$ predicted by the cosmological Big Bang Nucleosynthesis (BBN) model. BBN is a critical probe to understand the early universe, describing the primordial production of light nuclides such as ${}^4\text{He}$, D, ${}^3\text{He}$, and ${}^7\text{Li}$ [138,139]. Besides the fair agreement found nowadays for ${}^3\text{He}$, ${}^4\text{He}$ and D, a factor of 2.5–3.5 of discrepancy is still present between the predicted BBN ${}^7\text{Li}$ primordial abundances at the value of the baryon-to-photon ratio η deduced by CMB studies and the observed ones deduced by halo objects observations [130]. Among the possible nuclear physics solutions proposed for shedding light on the so-called “cosmological lithium problem”, those involving the radioactive ${}^7\text{Be}$ nucleus were hampered in the very recent years with particular regard to its destruction during BBN because of neutron-induced reactions by using both direct and indirect approaches [121–123,140–143].

Recent THM investigation. ${}^7\text{Be}+\text{n}$ interaction at BBN energies has to be investigated for both of the two competing channels, (n,p) and (n, α). Although the (n,p) channel dominates the ${}^7\text{Be}$ destruction, the (n, α) ones had large uncertainties, now reduced because of the improved experimental studies. In order to complement the already available information on the (n, p_0) and (n, p_1) cross section

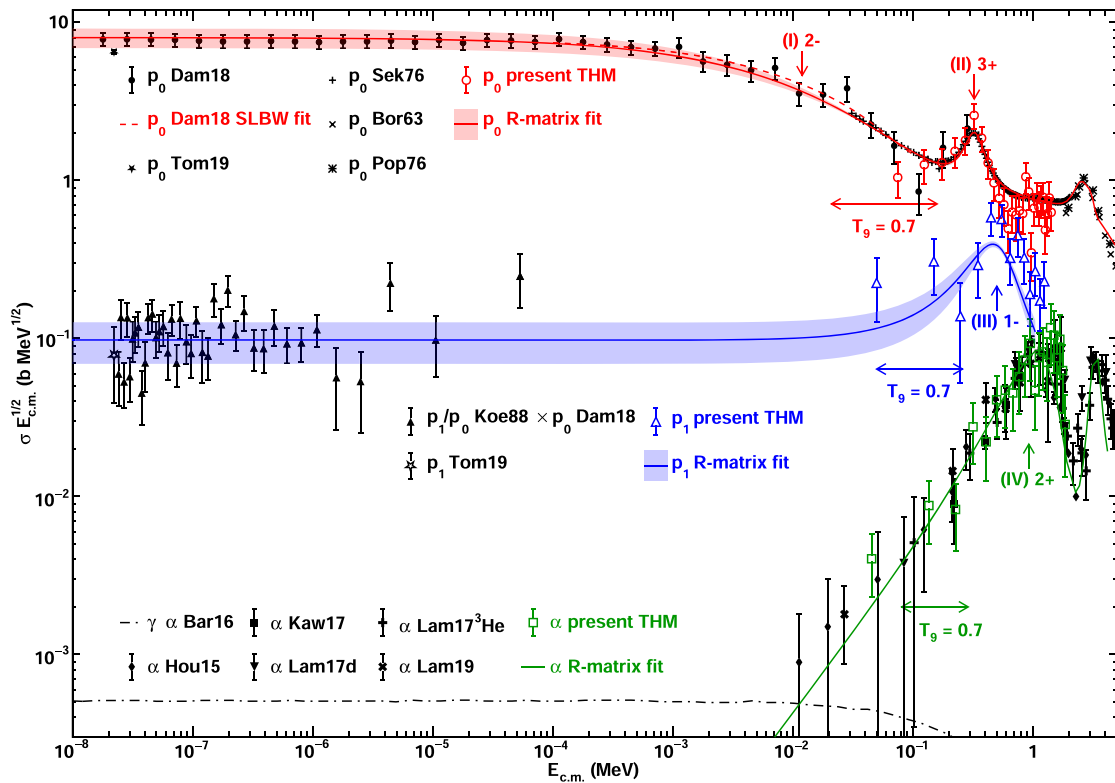


Fig. 4.3. THM cross sections for the ${}^7\text{Be}(n,p_0){}^7\text{Li}$, ${}^7\text{Be}(n,p_1){}^7\text{Li}$ and ${}^7\text{Be}(n,\alpha){}^4\text{He}$ nuclear reactions as discussed in [123].
 Source: The figure is adapted from Ref. [123].

measurements of [142,144,145] and those referring to the (n,α) channels [140,141], devoted THM studies have been performed by applying the method to the ${}^7\text{Be}+{}^2\text{H}$ quasi-free reaction [122,123].

The most recent THM application of [123] allowed to deduce both the (n,p) and (n,α) channels cross sections via a single experiment performed at the Center-for-Nuclear-Study RI Beam separator (CRIB) of the University of Tokyo, located at the RI Beam Factory, RIKEN [146–148]. A $64\ \mu\text{g}/\text{cm}^2$ thick deuterated polyethylene (CD_2) target was irradiated by a ${}^7\text{Be}$ beam at 3.16 MeV per nucleon with a typical intensity of $\sim 10^6$ pps produced. The adopted experimental setup has an expanded capability to detect, besides α -particles, also the ${}^7\text{Li}$ recoils, enabling the ${}^7\text{Be}(n,p){}^7\text{Li}$ reaction measurement via ${}^2\text{H}({}^7\text{Be}, {}^7\text{Li } p){}^1\text{H}$. Beam tracking was ensured by using two parallel plate avalanche counters installed in front of the target. Particle detection has been accomplished by using six ΔE -E silicon telescopes having charge-division position-sensitive detectors with $45 \times 45\ \text{mm}^2$ active areas, surrounding the target at distances of 20 cm placed at central angles of 12° , 34° and 56° with respect the beam direction in a symmetric configuration to double the statistics. The most forward telescopes were equipped with a $20\ \mu\text{m}$ ΔE silicon layer optimized for lithium detection while at backward angles α -particles and protons were detected through a $300\ \mu\text{m}$ ΔE silicon detector.

As in deep discussed in [123], the selection of the three-body channels have been accomplished via the standard approach foreseen by THM analysis and described elsewhere, such as experimental Q-value reconstruction. In details, because of the focus on the (n,p) channels, the experiment allowed for unambiguously derive results on both p_0 ($Q = -0.580\ \text{MeV}$) and p_1 ($Q = -1.058\ \text{MeV}$) channels in a single experiment. The occurrence of the QF-mechanism has been provided by detailed study on the experimental momentum distribution that, in the present case of using a deuteron as TH-nucleus, was compared with the theoretical Hulthén-wave function in momentum space. For the analysis only the events below $60\ \text{MeV}/c$ were selected as those belonging to pure QF-mechanism. The derived HOES cross section for the (n,p) and (n,α) channels were corrected for the dominant partial waves intervening in the penetrability function, i.e. s-wave component for both the (n,p) channels and p-wave for the (n,α) one [123]. The obtained THM cross section for the ${}^7\text{Be}(n,p_0){}^7\text{Li}$, ${}^7\text{Be}(n,p_1){}^7\text{Li}$ and ${}^7\text{Be}(n,\alpha){}^4\text{He}$ are reported in Fig. 4.3 with solid lines representing R-matrix fits with light-colored bands as their uncertainties (see Ref. [123] for details).

4.3.3. Status of the $d+d$ fusion measurements and the THM experiments

Background. The outstanding relevance of ${}^2\text{H}(d,p){}^3\text{H}$ and ${}^2\text{H}(d,n){}^3\text{He}$ cross section at energies of less than 1 MeV reaches both astrophysics and applications. These two channels, in fact, are at the base of the chain of the twelve most important reactions that lead to BBN, thus being greatly effective on the primordial abundances. Furthermore, they are part of the chain of reactions in the

Pre Main Sequence phase of the stellar evolution and their possible application for energy production in fusion power plants makes these reactions been measured several times in the last century, as well as the extraction of electron screening potential, studied also in metals, to ultimately understand this process in details.

The THM measurement. The ${}^2\text{H}(d,p){}^3\text{H}$ and ${}^2\text{H}(d,n){}^3\text{He}$ have also been studied using the THM [94], with a simple experimental setup consisting of silicon telescopes placed on both sides of the beam direction and using a single beam energy to cover a center of mass energy between 2 keV and 1.1 MeV. According to the THM features, the bare nucleus (unscreened) $S(E)$ factor has been determined, also valuable to be compared with the screened measurements to obtain the screening potential. The measured reactions were ${}^2\text{H}({}^3\text{He},p){}^3\text{H}$ and ${}^2\text{H}({}^3\text{He},n){}^3\text{He}$ with ${}^3\text{He}$ as projectile with a beam energy of 18 MeV. This was the first application of the THM with the coincidence detection of ${}^3\text{H}/{}^3\text{He}$ with the proton that acts as a spectator to both ${}^2\text{H}(d, n) {}^3\text{He}$ and ${}^2\text{H}(d, p) {}^3\text{H}$ binary processes. This technique was very convenient for the ${}^3\text{He}+n$ fusion channel to avoid the limitation of standard neutron detectors. However, it was also suitable for the ${}^3\text{H}+p$ channel, preventing detection of unwanted QF events from target break-up. A detailed account of the measurement and related data analysis is given in [94,114]. Here, we briefly report on the final results.

The $S(E)$ factor of the ${}^2\text{H}(d,p){}^3\text{H}$ channel is shown in Fig. 4.4. TH data are shown as black full dots, with uncertainties accounting for statistical and normalization errors. Direct data from [149–152] are shown as colored symbols. The various datasets exhibit significant dispersion, displaying deviations of over 15% in both energy dependence and absolute values. This contrasts with the smooth trend observed in THM data.

The THM parameterizations of the $S(E)$ factors lead to new values of $S(0) = 57.4 \pm 1.8$ keVb for ${}^3\text{H}+p$ and 60.1 ± 1.9 keVb for ${}^3\text{He}+n$, with uncertainties including the 1% normalization error and 3% coming from the theory, combined in quadrature. A comparison between the THM $S(0)$ factors to the ${}^2\text{H}(d, p) {}^3\text{H}$ direct data below 15 keV provides further insight into the electron screening effect. Low-energy direct data at 14.95 keV from [150] were first normalized to the THM $S_{\text{bare}}(E)$ (black solid line) and then fitted with the screening function [13] leaving U_e as a free parameter. This provides a value of $U_e = 13.2 \pm 1.8$ eV, not exceeding the adiabatic limit (14 eV) for a molecular deuteron target (gas target), but covering it with its uncertainty. Further improvements in the precision of direct low-energy data would help to pin point the electron screening potential.

The deduced ${}^2\text{H}(d, p) {}^3\text{H}$ and ${}^2\text{H}(d, n) {}^3\text{He}$ reaction rates undergo significant changes. At the SBBN temperature, the rate for the ${}^3\text{H}+p$ (${}^3\text{He}+n$) channel increases (decreases) by up to 15% with respect to previous studies [58,153,154] while at the temperatures relevant for PMS and future fusion power plants it undergoes a larger increase by up to 20% for both channels. Using the sensitivity studies reported in [154,155], the rate variations at the SBBN temperatures lead to a decrease in the production of lithium by up to 10%.

New insights. The results shown in [94] provided the calculation of the reaction rates with an error of 5%. In the last decades, BBN has moved to the so-called precision era, and since 2018 D/H is known from observations with a 1.2% precision [156]. Correspondingly, a new cross section measurement by the LUNA collaboration [157] of the ${}^2\text{H}(p, \gamma){}^3\text{He}$ has made it possible a rate calculation with a 2% error [158]. For this reason, a more accurate ${}^2\text{H}(d,p){}^3\text{H}$ and ${}^2\text{H}(d,n){}^3\text{He}$ measurement is now foreseen. From the THM side, data in [94] are undergoing a revision with an improved theoretical support based on new inputs from the recent literature.

4.3.4. The ${}^{27}\text{Al}(p, \alpha){}^{24}\text{Mg}$ reaction: astrophysical scenarios and measurements

The astrophysical thread. Measurements of Mg and Al isotopic abundances play an important role in advancing our understanding of astrophysical processes. Recent observations reveal an intriguing anti-correlation between Mg and Al abundances in red-giant-branch stars located in globular clusters like NGC 2808, $\omega - \text{Cen}$, and M4. This anti-correlation is of particular interest because it suggests a complex interplay of nucleosynthesis processes in these stars [159–161]. Advanced high-resolution stellar spectroscopy has contributed to our understanding by showing that these globular clusters host various stellar populations. This has further complicated our understanding of Mg-Al abundances, indicating that different types of stars, including massive, fast-rotating stars, intermediate-mass asymptotic giant branch (AGB) stars, and super AGB stars, all contribute to the observed abundance patterns. Furthermore, these observations underscore the necessity for fine-tuning theoretical models to account for the observed variations in Mg isotopes. The production, destruction, or accumulation of ${}^{24}\text{Mg}$ is highly sensitive to the temperature of stellar H-burning, particularly within the narrow temperature range of 0.07 to 0.08 GK. In this framework, the Mg-Al cycle is a fundamental process to tag Mg and Al isotopic abundances in high-temperature H-burning in evolved stars. This cycle involves a set of nuclear reactions, with the ${}^{27}\text{Al}(p, \alpha){}^{24}\text{Mg}$ reaction playing a central role [162,163]. It contributes to both the destruction of ${}^{27}\text{Al}$ and the production of ${}^{24}\text{Mg}$, and it is a key component in closing the Mg-Al cycle. The reliability of astrophysical predictions depends on the rate of this reaction being higher than the competing ${}^{27}\text{Al}(p, \gamma){}^{28}\text{Si}$ reaction, especially in the energy range typical of stellar nucleosynthesis (around 100 keV). The significant uncertainties in these rates present a challenge in making precise predictions.

High-precision investigations of the nucleosynthesis of ${}^{27}\text{Al}$ and ${}^{24}\text{Mg}$ influences our understanding of ${}^{26}\text{Al}$ production as well. ${}^{26}\text{Al}$ is especially important in astrophysics. While its presence in the Milky Way is established through the detection of gamma emissions from ${}^{26}\text{Mg}$ following the β decay of ${}^{26}\text{Al}$ [164], its initial presence in the Early Solar System is indicated by the excesses of ${}^{26}\text{Mg}$ observed in presolar grains, meteorites, and early solar system materials [165]. These excesses, when measured in relation to the most abundant Mg isotope (${}^{24}\text{Mg}$), provide crucial insights into the ${}^{26}\text{Al}/{}^{27}\text{Al}$ ratio in the ancient Galaxy and the ages of ancient solids within meteorites and early solar system materials. Also in this case the ${}^{27}\text{Al}(p, \alpha){}^{24}\text{Mg}$ reaction intervene in the complex interplay of Mg and Al isotopes. However, precise measurements in the energy region of astrophysical interest are still lacking. Indeed, direct and indirect investigation could only set upper limits to the resonance strengths below about 300 keV in the ${}^{27}\text{Al}$ -p center of mass [162].

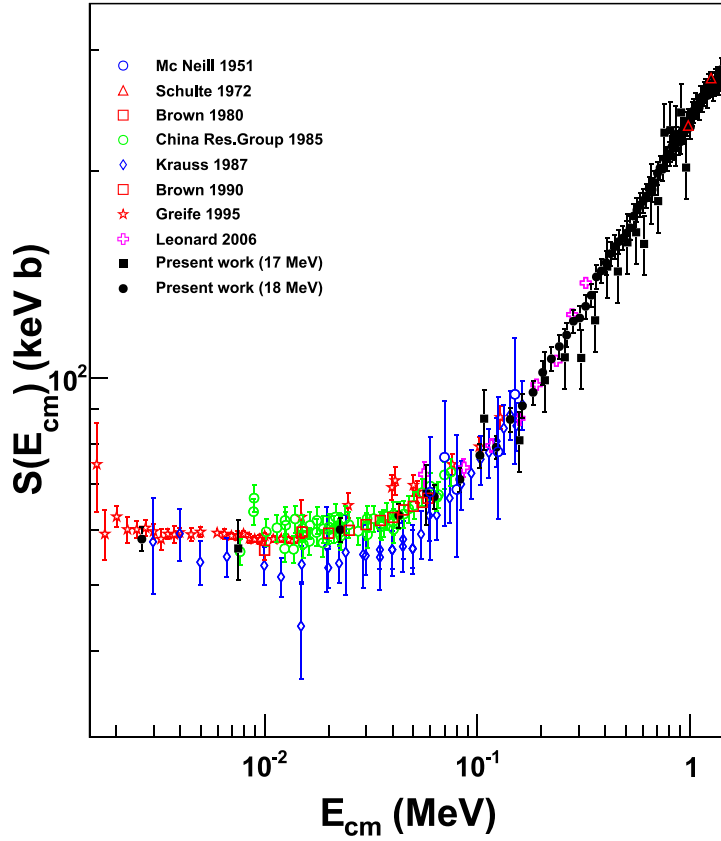


Fig. 4.4. THM ${}^2\text{H}(d,p){}^3\text{H}$ $S(E)$ factor (black solid circles and squares) from [94] compared with direct data sets (colored symbols). Source: The figure is adapted from Ref. [94].

Extraction of the resonance strengths using the narrow-resonance approximation. Since the astrophysical factor of the ${}^{27}\text{Al}(p, \alpha){}^{24}\text{Mg}$ reaction is dominated by narrow resonances, the THM in its formulation for the resonant reaction case [29] was applied, selecting the QF contribution to the $d({}^{27}\text{Al}, \alpha{}^{24}\text{Mg})n$ reaction. Assuming that a single resonance is present (a more generalized treatment can be found in [17,29,128,129]), the double differential cross section integrated over $d\Omega_{\mathbf{k}_{\alpha^{24}\text{Mg}}}$ is given by:

$$\frac{d^2\sigma^{\text{TH}}}{dE_{\alpha^{24}\text{Mg}} d\Omega_{\mathbf{k}_{n^{28}\text{Si}}}} = \frac{1}{2\pi} \frac{\Gamma_{\alpha^{24}\text{Mg}}(E_{\alpha^{24}\text{Mg}})}{(E_{\alpha^{24}\text{Mg}} - E_R)^2 + \frac{1}{4}\Gamma^2(E_{\alpha^{24}\text{Mg}})} \times \frac{d\sigma_{d({}^{27}\text{Al},n){}^{28}\text{Si}}}{d\Omega_{\mathbf{k}_{n^{28}\text{Si}}}} \quad (4.8)$$

where $\frac{d\sigma_{d({}^{27}\text{Al},n){}^{28}\text{Si}}}{d\Omega_{\mathbf{k}_{n^{28}\text{Si}}}}$ is the differential cross section for the stripping $d({}^{27}\text{Al}, n){}^{28}\text{Si}$ to the resonant state of ${}^{28}\text{Si}$, $E_{\alpha^{24}\text{Mg}}$ is the α - ${}^{24}\text{Mg}$ relative energy, Γ and $\Gamma_{\alpha^{24}\text{Mg}}$ are the total and partial width for the resonance under examination. Therefore, if N_i is the area of the i -th peak in the THM cross section described by Eq. (4.8) and ω_i is the statistical factor [163], the strength $(\omega\gamma)_i$ of the i -th resonance is given in arbitrary units by:

$$(\omega\gamma)_i = \frac{1}{2\pi} \omega_i N_i \frac{\Gamma^{s.p.}}{p^{27}\text{Al}} \frac{d\sigma_{d({}^{27}\text{Al},n){}^{28}\text{Si}}^{s.p.}}{d\Omega_{\mathbf{k}_{n^{28}\text{Si}}}} \quad (4.9)$$

where the superscript *s.p.* is used to indicate that single-particle wave functions should be used in the calculation of the parameters, therefore no spectroscopic factors appear.

The ${}^2\text{H}({}^{27}\text{Al}, \alpha{}^{24}\text{Mg})n$ reaction was measured at the INFN-LNS Tandem (Catania, Italy) using a 80-MeV ${}^{27}\text{Al}$ beam delivered onto a CD_2 target. The beam energy was chosen to span the ${}^{27}\text{Al}-p$ energy range between the threshold and ~ 1.5 MeV for normalization of the THM strengths (Eq. (4.9)) to the resonance strengths in the literature (see [127–129]). Also, the overlap with an energy region where resonance strengths are known made it possible to carry out validity tests of the method and constrain model parameters.

Fig. 4.5 shows the result of the THM measurement. While the ${}^2\text{H}({}^{27}\text{Al}, \alpha{}^{24}\text{Mg})n$ QF cross section is dominated by a clear resonant pattern, in agreement with what expected from the literature. Focusing first on the energy region of astrophysical interest around 100 keV, as marked by the red arrow in the figure, a clear resonance at about 85 keV is apparent, corresponding to the 84.3 keV

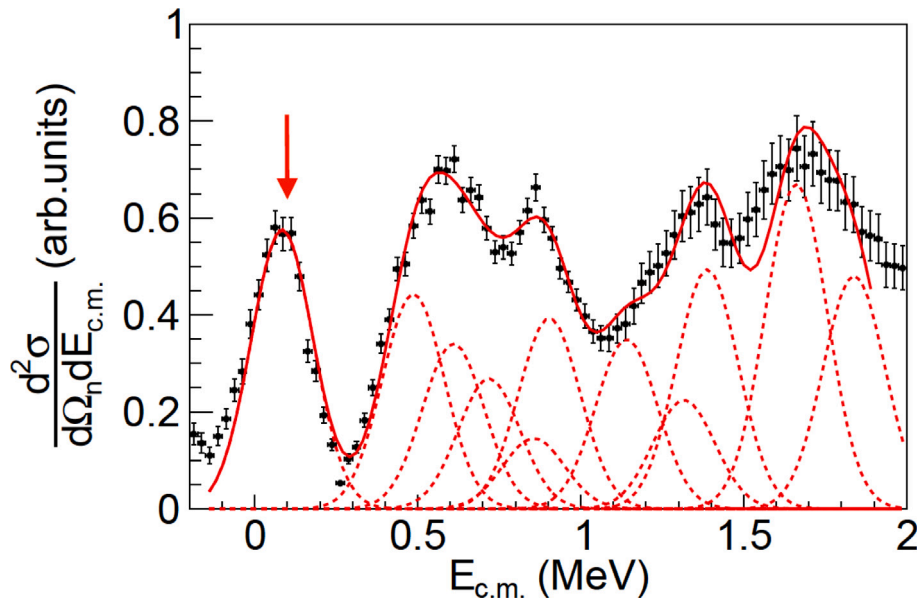


Fig. 4.5. Double differential cross section of the ${}^2\text{H}({}^{27}\text{Al}, \alpha{}^{24}\text{Mg})n$ reaction (black symbols). The red solid line is the result of the fitting using eq.A5 of [29]. Dashed lines are used to highlight the contribution of each resonance. The red arrow marks the energy region of astrophysical interest. Source: The figure is adapted from Ref. [129].

1^- resonance in [162], for which only an upper limit was available. Using Eq. (4.9) and normalizing the strength to those of the resonances at 903.54 keV and 1388.8 keV (to minimize the normalization error [115,166]) for the first time a value of the strength was obtained: $1.67 \pm 0.32 \times 10^{-14}$ eV, well within the upper limit $\omega\gamma \leq 2.60 \times 10^{-13}$ eV in [162]. For the other resonances below about 300 keV, more stringent upper limits than in the latter compilation were introduced, while the THM resonance strengths of states above 300 keV were found to be in good agreement with those in [162], confirming the validity of the method and indicating the presence of negligible systematic errors in comparison with the precision.

Using the narrow-resonance approximation and the Monte Carlo code RatesMC (see [167]), we calculated the reaction rate [129] that turned out to be ~ 3 times lower than in [162] at the temperatures where the MgAl cycle is especially important, around 0.1 GK. These results suggest that the MgAl cycle would not be closed at such temperatures, the (p, α) channel having a lower probability than so far adopted. Though further studies of the ${}^{27}\text{Al}(p, \gamma){}^{28}\text{Si}$ reaction are ongoing, being the latter more relevant for astrophysical considerations, preliminary calculations of AGB star nucleosynthesis were performed. They show that the THM ${}^{27}\text{Al}(p, \alpha){}^{24}\text{Mg}$ reaction rate increases the ${}^{27}\text{Al}$ yield in stars experiencing soft hot-bottom burning up to $\sim 25\%$, for solar metallicity in the $4 - 5 M_{\odot}$ mass domain [129].

4.3.5. The Coulomb-free p - p scattering cross section and the fundamental symmetries in the NN interaction

A recent application to the fundamental symmetries in the NN interactions originated from a previous work whose aim was to investigate the suppression of the Coulomb amplitude when the THM is applied to scattering processes [168,169]. In particular, the pp scattering was selected because of the presence of a characteristic minimum in the cross section around a center of mass energy of 200 keV, attributed to the interference between nuclear and Coulomb forces. The quasi-free scattering of protons below 1 MeV, extracted from the ${}^2\text{H}(p, pp)n$ reaction via the Trojan Horse Method (THM) did not show this minimum, a feature that was interpreted as a clear signature of suppression of Coulomb effects, also thanks to a sound theoretical development to determine the shape of the HOES pp scattering cross section. Strengthened by this result, the quasi-free scattering of protons below 1 MeV, has been used to obtain the first experimental estimation of the 1S_0 Coulomb-free scattering length and effective range for the proton-proton interaction. In fact, the Coulomb effects need to be theoretically removed from experimental p - p data to reveal the strong interaction contribution to the scattering length. Thus, one starts from the uncorrected p - p scattering length using available p - p scattering world data quoted as -7.8063 ± 0.0026 fm [170] and ends to the nuclear p - p scattering length applying sophisticated theoretical tools that can introduce considerable model dependence. The outcome can be as low as -14.9 ± 0.3 fm [171] or up to values ranging from -16.0 ± 0.3 fm [172] to -17.5 ± 0.3 fm [173]. The scatter of about 2.5 fm between the corrected values can be seen as a systematic uncertainty coming from theory. Moreover, the model corrections bring an increase in the relative uncertainty of almost two orders of magnitude.

An almost model-independent quantity is the short-range 1S_0 scattering length, where only the long-range Coulomb contribution is subtracted. This has been determined in [174]: it represents the first direct experimental outcome of the Coulomb free p - p scattering length and effective range. To arrive at this result, the s-wave effective-range expansion was used to fit the data, whose

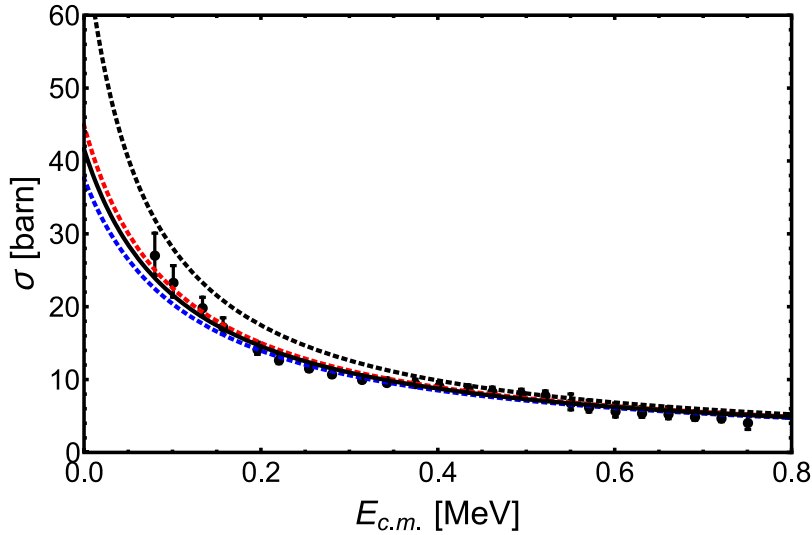


Fig. 4.6. Experimental quasi-free p-p scattering cross section after removal of the residual Coulomb interaction (black solid circles). Error bars indicate $\pm 1\sigma$ uncertainties. The result of the fit using Eq. (4.11) is shown as solid black line, while the dotted red, blue and black lines refer to the same equation for $n-n$, $p-p$ and $n-p$ scatterings, respectively, using current accepted values for nuclear a and r_0 parameters.

Source: The figure is adapted from Ref. [174].

fundamental equations are:

$$k \cot \delta = -\frac{1}{a} + \frac{1}{2}r_0k^2, \quad (4.10)$$

where k denotes the relative momentum of the NN pair and a and r_0 are the scattering length and the effective range parameters, respectively.

The s-wave NN scattering cross section is given by

$$\sigma_{tot} = \frac{4\pi}{\left(\frac{1}{a} - \frac{1}{2}r_0k^2\right)^2 + k^2}. \quad (4.11)$$

The fit was carried out using a Bayesian approach, taking a and r_0 as free parameters of the model. In particular, a Markov Chain Monte Carlo (MCMC) method was used by means of the *emcee* Python library [175], which is based on the Goodman & Weare algorithm described in [176]. To account for the large historical dispersion of a , a weakly informative flat prior distribution in the interval $(-25 \text{ fm}, -15 \text{ fm})$ was taken. A Gaussian prior distribution was chosen for r_0 with centroid at 2.80 fm corresponding to the weighted average of the current accepted values from the three NN combinations. See [174] for further details. The numbers resulting from the procedure are $a_{pp} = -18.17^{+0.52}_{-0.58} \text{ fm}$ and $r_0 = 2.80 \pm 0.05_{stat} \pm 0.001_{syst} \text{ fm}$. The result of the fit is shown in Fig. 4.6 as solid black line with Coulomb free THM p-p scattering data given as black solid circles. Dotted red, blue and black lines in the same figure refer to Eq. (4.11) with current accepted values for nuclear scattering length and effective range parameters from $n-n$, $p-p$ and $n-p$ scatterings, respectively.

We found that the extracted value of a_{pp} includes contributions from the short-range electromagnetic interaction [174]. Interestingly, even in the low-energy regime where the interacting protons exhibit point-like behavior, the s-wave phase shift δ of the nucleon-nucleon (NN) interaction in Eq. (4.10) incorporates all the effects arising from short-range interactions. Consequently, the current analysis of the HOES cross section provides direct insight into the complete short-range $p-p$ interaction, characterized by its distinctive values of a and r_0 .

The charge symmetry breaking of the short-range interaction and the universal window. Our methodology incorporates the concept of a universal window that applies to the nucleon-nucleon (NN) system. The universal or unitary window refers to a specific region characterized by the presence of a shallow state with an energy close to the threshold. In this region, the two-body scattering length, denoted as ‘ a ’, reaches values that are close to infinity. When ‘ a ’ is large, the shallow state can either be real ($a > 0$) or virtual ($a < 0$), and its energy is determined by the scattering length according to $E \simeq \hbar^2/ma^2$. The shallow nature of this state becomes apparent when comparing its energy to a typical energy of the system, \hbar/ml^2 , where l represents a typical length, such as the interaction range. When the ratio l/a is much smaller than 1, it indicates that the system is located within the unitary window and experiences a universal behavior, meaning that the system’s dynamics are largely unaffected by the specifics of the interaction. Instead, it is primarily influenced by the long-range behavior, allowing for a description based on only a few parameters [177]. By exploiting the characteristics of the universal window, we have developed a model that takes into account the short-range interaction between two protons being parameterized with a two-parameter Gaussian interaction for nucleon-nucleon (NN) interactions, specifically

applicable to s-wave interactions in the spin singlet channel, as given by:

$$V_{NN}(r) = V_0 e^{-r^2/r_G^2} + \frac{e_{NN}^2}{r}, \quad (4.12)$$

with $NN \equiv nn, np, pp$ and $e_{pp}^2 = e^2$ and zero otherwise. For more details on this construction and on how parameters have been set, please refer to [174]. The model gives the value $a_{pp}^{sr} = -17.6 \pm 0.4$ fm, in agreement within experimental errors with the THM estimate. Recently a new calculation has been performed using a model based on the Eckart potential [178] to capture both nuclear and electromagnetic contributions and for which the shape parameters are zero. The model produces the value $a_{pp}^{sr} = -17.9 \pm 0.5$ fm, absolutely compatible with the one obtained using the Gaussian interaction. We conclude that this technique provides us with parameters to evaluate the charge symmetry breaking of the short-range interaction as a whole. This breakthrough prompts the proposal of a novel paradigm in the study of charge symmetry breaking, aligning with the current understanding that, on a fundamental level, the charge dependence of nuclear forces arises from differences in the masses of up and down quarks and electromagnetic interactions among quarks.

4.3.6. Status of the $^{12}\text{C}+^{12}\text{C}$ fusion measurements and the THM experiment

The $^{12}\text{C}+^{12}\text{C}$ fusion is a critical phenomenon in various scenarios involving carbon-rich environments. One notable example is its impact on the late-stage evolution and nucleosynthesis of intermediate-mass and massive stars ($\geq 8 M_{\odot}$) [179]. It also influences the lower mass threshold for carbon ignition, which distinguishes between the progenitors of white dwarfs, novae, and type Ia supernovae on one hand, and those of core-collapse supernovae, neutron stars, and stellar-mass black holes on the other. This reaction is considered the ignition process for type Ia supernovae and superbursts, particularly if resonances are found to contribute within the Gamow peak [180]. Furthermore, it affects the weak component of the s-process, responsible for producing elements ranging from iron to strontium. Quiescent carbon burning occurs at temperatures ranging from 0.8 to 1.2 GK, corresponding to sub-Coulomb center-of-mass energies of 1 to 3 MeV, where the cross-section rapidly decreases below the nanobarn range. Consequently, the cross-section of this process has never been measured below a center-of-mass energy ($E_{c.m.}$) of 2 MeV. The compound nucleus (CN) ^{24}Mg is formed at an excitation energy above the $^{12}\text{C}+^{12}\text{C}$ decay threshold.

The primary channels involved in $^{12}\text{C} + ^{12}\text{C}$ fusion at astrophysical energies are those that emit protons and α particles. These channels have been studied by detecting the charged particles and/or the γ decay. Among them, the most significant branching occurs during the de-excitation of the first excited states of ^{23}Na and ^{20}Ne , as well as their ground states. Measuring the $^{12}\text{C} + ^{12}\text{C}$ cross-section at low energies presents significant challenges due to the exponential decrease in cross-section, resulting in a very low counting rate. Thus, it is crucial to carefully account for any natural or beam-induced background to ensure accurate measurements. A detailed explanation of these challenges can be found in Ref. [181], which provides the first measurement of the cross-section down to $E_{c.m.} = 2.14$ MeV, the lowest energy ever reached for this reaction. The obtained astrophysical S-factor reveals new resonances below 3 MeV, including a substantial increase at the lowest energies. This discovery has stimulated further experimental investigations. Here, we summarize recent studies that present the total S-factor as the final result. In Ref. [182], a measurement was conducted using a sphere array of 100 Compton-suppressed Ge detectors in coincidence with silicon detectors. This measurement pushed down to $E_{c.m.} = 2.84$ MeV and 2.96 MeV for the proton and α channels, respectively. Significant progress in direct experiments was made in the study presented in [183], where a measurement down to $E_{c.m.} = 2.2$ MeV was reported. This was achieved using the particle- γ coincidence technique. Charged particles were detected using annular silicon strip detectors, while γ -ray detection was performed using an array of $\text{LaBr}_3(\text{Ce})$ scintillators. Further advancements were published in [184], where similar techniques were employed on thick targets. Specifically, p and α particles were detected using a silicon detector array, while γ -ray detection was carried out using a high-efficiency HPGe detector. Recent results from this collaboration are reported in [185]. Significant target deterioration caused by beam accumulation highlights an urgent need for new target technology for such experiments. Another measurement of proton and alpha particles at $E_{c.m.} > 2.5$ MeV [186], challenges the typical assumption of isotropic angular distributions.

The hindrance effect. The challenges associated with accurately predicting the low-energy extrapolation of fusion reactions involving $^{12}\text{C}+^{12}\text{C}$ and other light ions were further complicated by the suggestion that the low-energy cross section might be reduced due to a “hindrance” effect, defined as the steepening of the exponential slope of the fusion excitation function at deep sub-barrier energies [187]. The “hindrance” in the fusion cross section appears to be a systematic behavior for reactions with $Q_{val} < 0$ [188,189] and it can be attributed to various factors, including the incompressibility of nuclear matter [190]. Alternative explanations for the sudden decrease in cross section data towards very low energies in heavy ion fusion systems include deformation, which has been observed in medium-mass systems at very low sub-Coulomb energies [191–193], as well as a possible cluster-structure effect, as shown in [194,195]. However, the extent of this effect in light ion fusion systems having $Q_{val} > 0$, is not clear, and in particular, in reactions like $^{12,13}\text{C}+^{12,13}\text{C}$ or $^{16}\text{O}+^{16}\text{O}$, has not been experimentally verified [196]. In particular, results from [196] rules out the existence of the maximum in the astrophysical S(E) factor predicted by the hindrance model, while confirming its rising trend towards lower energies. The “hindrance” effect is not confirmed theoretically either, as it is not observed in time-dependent Hartree–Fock (TDHF) calculations [193] or in a combination of mean-field and cluster models [197]. The hindrance factor in $^{12}\text{C}+^{12}\text{C}$ fusion is predicted to have a significant impact on the low-energy extrapolation of the cross section, as given by several stellar model simulations [198–201].

While hindrance may reduce the overall transmission probability through the Coulomb barrier, it cannot be considered in isolation and needs to be examined in the context of possible low-energy resonances. Due to the extremely rapid decline in the low cross section, it is unlikely that direct experimental measurements of fusion will provide significant insights into very low energies, despite ongoing efforts by the experimental community.

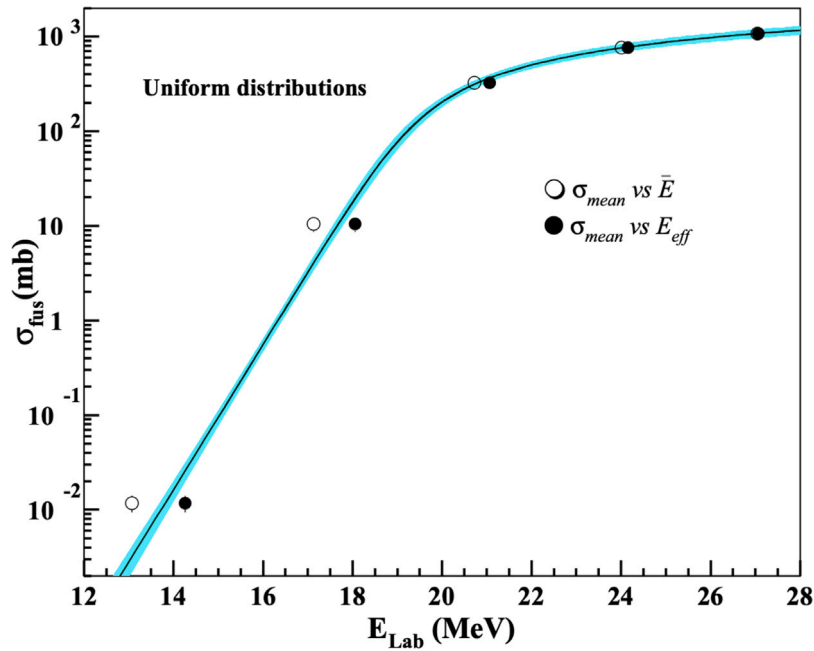


Fig. 4.7. Fusion excitation function for ${}^6\text{Li}+{}^{120}\text{Sn}$ vs. \bar{E} (open symbols) and E_{eff} (closed symbols), respectively. The solid black line represents the result of the deconvolution procedure [202], while the blue shaded region indicates the uncertainty associated with the procedure.

It is also important to remind here that an experimental challenge in measuring low energy fusion cross sections, where one has a very strong energy dependence of the cross section due to Coulomb barrier penetrability, is to associate the mean measured cross section with a properly determined effective interaction energy ER. If this is not carefully done, one generates an uncertainty in the extracted excitation function and, as a consequence, also on the presence of possible “hindrance” effects. Indeed, as discussed in detail in [202], each measured cross section is a mean value of the cross section, averaged over the probability $D(E,t)$ of finding a beam particle of energy E inside the target of thickness t . $D(E,t)$, in turn, depends on the beam energy distribution before the target, on the energy loss and straggling processes inside the target and also on the target uniformity. This last point depends on the type of target chemical composition and on the used deposition procedures and may have non negligible effects [202]. As demonstrated in [202], plotting the experimentally determined mean cross section as a function of an effective energy E_{eff} , obtained by weighting the beam energy in the target with the exponentially varying cross section, can lead to an incorrect determination of the excitation function. When dealing with homogeneous targets, it is expected that the effective energy (E_{eff}) will consistently shift towards higher values compared to the simple mean beam energy (\bar{E}). This shift occurs due to the weighted average considering the exponential growth of the cross-section. This phenomenon is illustrated in Fig. 4.7, which displays the measured sub-barrier fusion excitation function for ${}^6\text{Li}+{}^{120}\text{Sn}$ plotted against \bar{E} (open symbols) and E_{eff} (closed symbols), respectively. The solid black line represents the outcome of the deconvolution procedure [202], while the blue shaded region indicates the associated uncertainty linked to the procedure.

When non-uniformities are present in the target, even predicting this shift becomes more complex, and it has been observed that the magnitude of the shift varies from one target to another. Unfortunately, the above aspects are often not thoroughly discussed in published papers, leaving potential doubts on the uncertainties affecting the final results. For these reasons, it would be useful for the community if future experimental studies on this interesting topic will report more details on all of the above aspects.

The ${}^{12}\text{C}+{}^{12}\text{C}$ THM measurement. To overcome the limitations imposed by the low counting rate, an indirect measurement was performed using the Trojan Horse Method (THM) [203]. The measurement relies on the quasi-free (QF) kinematics of ${}^{14}\text{N} + {}^{12}\text{C}$ with ${}^2\text{H}$ as the spectator, which leads to ${}^{12}\text{C} + {}^{12}\text{C}$ reactions. The α or p particles were detected in coincidence with the spectator d particle using silicon telescopes on either side of the beam directions, covering the angular regions of the QF kinematics for the relevant breakup process. The THM measurement provided the two-body cross section for four channels: ${}^{20}\text{Ne}+\alpha_0$, ${}^{20}\text{Ne}+\alpha_1$, ${}^{23}\text{Na}+p_0$ and ${}^{23}\text{Na}+p_1$ in the entire astrophysical region of interest from $E_{c.m.} = 2.7$ MeV down to 0.8 MeV, revealing well-resolved resonance structures. These THM results were normalized to available direct data at $E_{c.m.} = 2.5\text{--}2.63$ MeV. The normalization error for the obtained results is 5%. Details can be found in [203].

The results are shown in Fig. 4.8 in terms of total modified $S(E)$ factor, $S(E)^*$ [30]. The black middle line represents the best fit curve while the gray band is the result of modified R-matrix calculations with lower and upper values of the resonance parameters as resulting from their uncertainties. Several existing direct data points below $E_{c.m.} = 4$ MeV are presented as follows: gray filled circles [181], purple filled triangles [204], blue empty squares [205], blue filled stars [206], blue filled triangles [207], red filled

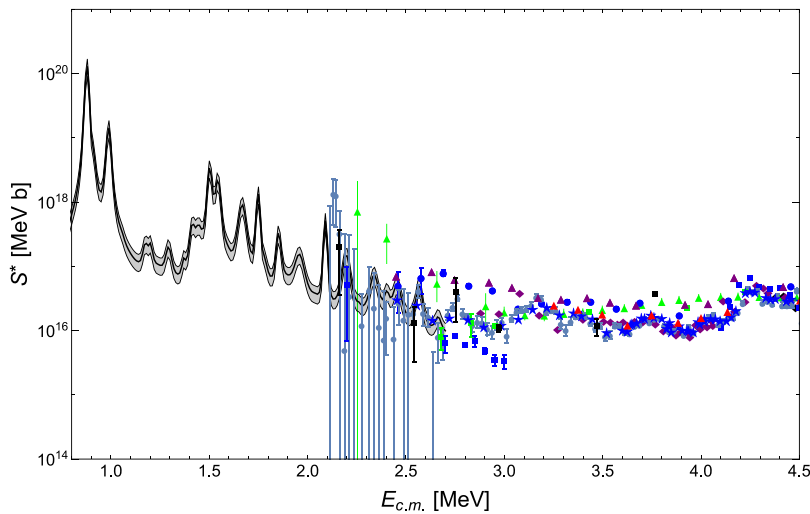


Fig. 4.8. THM total $S(E)^*$ factor (black solid line). The gray band represents the region spanned by modified R-matrix calculations with lower and upper values of the resonance parameters. Available direct data in the $E_{c.m.}$ range below 4 MeV are reported as gray filled circles [181], purple filled triangles [204], blue empty squares [205], blue filled stars [206], blue filled triangles [207], red filled diamonds [208], green filled triangles [209], green filled squares [182], black filled squares [183] and blue filled squares [184].

diamonds [208], green filled triangles [209], green filled squares [182], black filled squares [183], and blue filled squares [184]. It is worth noting that, except for the data from [181,183,184], the lower energy limit of these data points is determined by the background caused by hydrogen contamination in the targets. When excluding these instances, the agreement between the THM data and the direct data is apparent, within the experimental uncertainties, except for the direct data's low-energy limit around 2.14 MeV. Contrary to the claim of a strong resonance at that energy, the THM data suggest the presence of a nearby resonance at 2.095 MeV. This finding aligns with spectroscopy studies documented in [210,211], which demonstrate a pronounced dip at 2.14 MeV and no notably robust alpha state around 2.1 MeV. Additionally, the agreement remains satisfactory with data down to an energy of $E_{c.m.} = 2.15$ MeV from [212] for the $^{12}\text{C}(^{12}\text{C}, p_{0,1})^{23}\text{N}$ reactions. The obtained result is also consistent within experimental errors with the total $S(E)^*$ from recent studies [182–184], although the upper limit for the proton channel below $E_{c.m.} = 3$ MeV reported in [184] is significantly lower than the other results.

Following these results [203], theoretical calculations [213] based on a distorted wave Born approximation (DWBA) approach were presented. The authors' claim was the need to include Coulomb distortions through the introduction of a renormalization factor. This has the effect of lowering the THM astrophysical factors by many orders of magnitude, regardless of the existence of resonances and in apparent contradiction with the experimental data. However, the convergence of the calculations involving a transfer to an unbound system is not obvious and from a careful examination, it turns out that, on top of other things, the numerical stability of the proposed theory is not guaranteed. This implies that results are very sensitive to details of the model space and the calculated trend of the THM $S(E)^*$ is questionable. Theory calculations employing the Feynman path-integral method [214] have produced $S(E)$ factor values that exhibit agreement with the THM (two-step multichannel) results. However, these values are inconsistent with the Coulomb correction applied to the THM results in [213]. This discrepancy serves as a cautionary note regarding extrapolation procedures that do not take into account the contributions from resonant states. In [215], coupled channel calculations effectively characterize the $^{12}\text{C}+^{12}\text{C}$ fusion resonances near the Coulomb barrier energies. They incorporate a weak absorption mechanism that depends on angular momentum and has been adjusted to match the experimental fusion data. A more recent study [216] utilized the antisymmetrized molecular dynamics (AMD) model combined with R-matrix to investigate the behavior of the ^{24}Mg CN using different cluster configurations. The study indicates the presence of prominent molecular states formed by the combination of ^{12}C and ^{12}C nuclei. These states subsequently undergo fragmentation, resulting in numerous narrower resonances, primarily consisting of 0^+ and 2^+ states, due to the influence of channel coupling. These results align with the THM experimental spectrum of multiple states observed at low energies, though significantly lower than the current experimental trend of the $S(E)$ factor. However, calculations still need to include other contributions, such as the non-resonant one or potential interference effects.

Impact of the $^{12}\text{C}+^{12}\text{C}$ THM rate in astrophysics. Fig. 4.9 illustrates the THM reaction rate divided by the reference rate from [217] at relevant temperatures.

Below 2 GK, the rate experiences a significant increase, ranging from a factor of 1.18 at 1.2 GK to more than 25 at 0.5 GK. In the regime of hydrostatic carbon burning, which spans from 0.6 to 1.2 GK, this rate increase has implications for the ignition of carbon in massive stars. Stellar modeling studies presented in [199] indicate that for a 25 solar mass star undergoing core carbon burning, the ignition temperature and density would decrease by approximately 10% and 30% respectively. The substantial increase observed at 0.5 GK, primarily driven by the resonant structure around $E_{c.m.} = 1.5$ MeV, aligns with the conjectured value proposed in [218]. This value suggests that theoretical superburst ignition depths in accreting neutron stars could be reduced by a factor

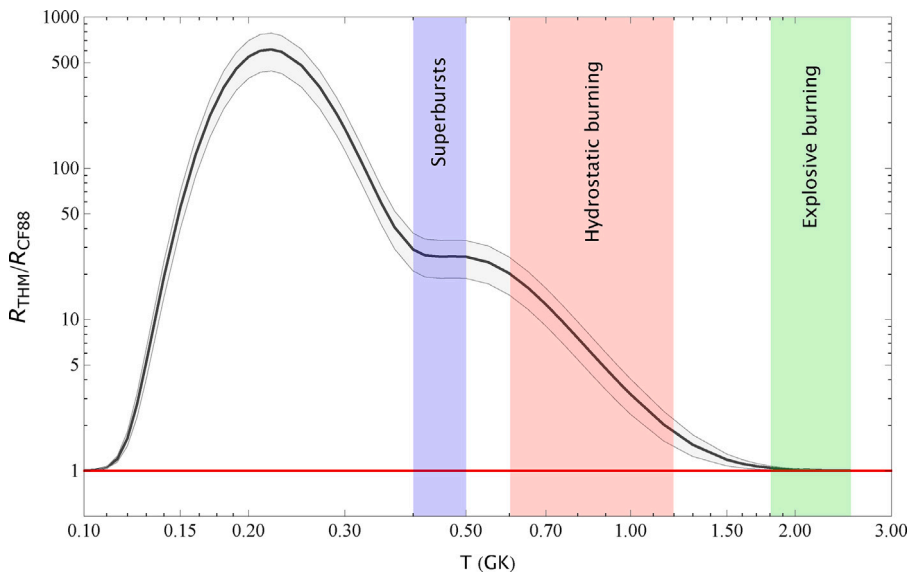


Fig. 4.9. Ratio between the total THM $^{12}\text{C}+^{12}\text{C}$ reaction rate (black line) from [203] and the reference one (red line) from [217]. The gray shading defines the region spanned considering the $\pm 1\sigma$ uncertainties. The designated color shades represent typical temperature ranges associated with carbon burning in various scenarios: the light blue shade corresponds to superbursts occurring in accreting neutron stars, the light red shade represents hydrostatic carbon burning in massive stars, and the light green shade refers to explosive carbon burning.

Source: The figure is adapted from Ref. [30].

of 2, assuming a realistic range of crust thermal conductivities and core Urca neutrino emissivities. This change is consistent with the superburst ignition depths inferred from observations, implying that carbon burning can indeed trigger superbursts. Recent investigations conducted in [219] explore the impact of the new carbon fusion cross-sections on Type Ia Supernovae. The progenitor systems of these supernovae, which are not yet fully understood, include the popular double-degenerate (DD) scenario, attributing Type Ia Supernovae to mergers of white dwarf binaries. The resonance-induced decrease in the carbon burning ignition temperature may facilitate accretion-induced collapse and increase the birthrate of Galactic neutron stars. Consequently, the contribution of the DD scenario to the Type Ia Supernovae rate becomes even smaller. The effects of the THM reaction rate on the upper bound for the progenitor mass of carbon-oxygen white dwarfs (M_{up}) and the lower bound for the progenitor mass of normal Type II supernovae (M^*) have been analyzed in [220]. The results show that M_{up} is reduced from 8 to 7.5 solar masses, while M^* approaches 10 solar masses. Recently, we explored the impact of the $^{12}\text{C}+^{12}\text{C}$ THM measurement on the compactness of a star [200]. Specifically, we examined how this measurement affects the binding energy of the inner mantle during the onset of core collapse. The findings reveal a significant alteration in the relationship between compactness and initial mass compared to previous results obtained by using the classical reference cross section given in [217]. In this case, we observe a non-monotonic but well-defined behavior, and there is no scattering of the compactness around the main trend. This occurrence has potential implications for the possibility of stellar explosions.

5. Advances addressing next challenges

In advanced stages of stellar nucleosynthesis, the study of reactions between medium to heavy nuclei is crucial. The study of these reactions faces significant challenges due to the presence of the Coulomb barrier, as the astrophysical energies involved are typically several MeV below it. Multiple decay channels contribute to the each reaction, usually tackled through the γ -particle coincidence technique to reduce the background. This technique prevents access to the exit channels where the reaction products are in their ground states. In this context, the Trojan Horse Method (THM) is regarded as the sole viable approach to investigate and gain access to these desired exit channels. To successfully apply the Trojan Horse Method (THM) in these cases, it is first necessary to carefully select appropriate Trojan Horse nuclei that can transfer composite clusters like ^{12}C , ^{16}O , and ^{22}Ne . After the well-known $^{12}\text{C}+^{12}\text{C}$ fusion reactions, other relevant processes such as $^{12}\text{C}+^{16}\text{O}$, $^{16}\text{O}+^{16}\text{O}$, and $^{22}\text{Ne}(\alpha, n)$ are currently being investigated. These studies require parallel efforts from both experimental and theoretical perspectives. From the experimental standpoint, it is essential to verify the accuracy of the factorization of the reaction cross section compared to more sophisticated approaches that consider the three-body nature of the final states and fully account for the final state interactions between the nuclei. Consequently, experimental setups and data analysis must be conducted meticulously and selectively. Strict kinematic conditions need to be imposed, and only a fraction of the available data can be utilized to satisfy the specific requirements of cross section factorization while still obtaining sufficient statistical information. Ongoing advancements in theory are currently being evaluated starting from the ‘‘Surrogate Method’’, aiming to incorporate distorted waves in a coherent manner, particularly in processes described as transfers to the continuum. These developments seek to enhance the understanding and description of the studied reactions. In the next paragraphs, a taste of such advancements is given.

5.1. Astrophysical cross sections from the surrogate method

5.1.1. Reminder of the surrogate method

The surrogate method (SRM) provides an alternative method to indirectly extract cross sections for a process of the form $x + A \rightarrow c + C$ from the auxiliary (“surrogate”) reaction $a + A \rightarrow b + c + C$. The method assumes that the two processes take place via the formation of an intermediate CN B that subsequently decays into the desired final channel, i.e., $a + A \rightarrow b + B^* \rightarrow b + c + C$. A detailed review of the method can be found in Ref. [221]. A brief outline is provided here. Following Bohr’s hypothesis, it is assumed that in these reactions the formation and decay of a CN take place independently of each other. For the process of interest, this allows us to write the cross section as:

$$\sigma(x + A \rightarrow c + C) = \sum_{J_T, \pi} \sigma_{x+A \rightarrow B}^{CN}(E_{ex}, J_T, \pi) G_{c+C}^{CN}(E_{ex}, J_T, \pi), \quad (5.1)$$

where $\sigma_{x+A \rightarrow B}^{CN}(E_{ex}, J_T, \pi)$ is the cross section for the CN formation for a given angular momentum J_T , parity π and excitation energy E_{ex} and $G_{c+C}^{CN}(E_{ex}, J_T, \pi)$ the branching ratio for the decay in the channel $c + C$. The objective of the surrogate method is to experimentally determine or constrain the decay probabilities $G_{c+C}^{CN}(E_{ex}, J_T, \pi)$, which are often difficult to calculate accurately.

In the surrogate reaction, the same B^* nucleus is formed and the decay product of interest ($c + C$) is measured in coincidence with the outgoing particle b . The probability for this process can be written as:

$$P_{S,c+C}(E_{ex}) = \sum_{J_T, \pi} F_S^{CN}(E_{ex}, J_T, \pi) G_{c+C}^{CN}(E_{ex}, J_T, \pi), \quad (5.2)$$

where the subscript S denotes the specific surrogate reaction (in our case, the transfer reaction $a + A \rightarrow b + c + C$), $F_S^{CN}(E_{ex}, J_T, \pi)$ is the probability of forming B^* in this surrogate reaction (with specific values of E_{ex} , J and π) and $G_{c+C}^{CN}(E_{ex}, J_T, \pi)$ is the same branching ratio appearing in the direct reaction (5.1). The probability $P_{S,c+C}(E_{ex})$ can be obtained experimentally as the ratio between the number of coincidences between the b particle and the decay particle c , $N_{S,c+C}$, and the total number of surrogate events, N_S , i.e.:

$$P_{S,c+C}^{exp}(E_{ex}) = \frac{N_{S,c+C}}{N_S \times \epsilon_{c+C}}, \quad (5.3)$$

where ϵ_{c+C} is the efficiency of detecting the exit-channel $c + C$ for the reactions in which b is detected.

Ideally, if a reliable prediction of $F_S^{CN}(E_{ex}, J_T, \pi)$ is possible, with an accurate determination of $P_{S,c+C}^{exp}(E_{ex})$ for a range of energies and angles of b , it might be possible to extract $G_{c+C}^{CN}(E_{ex}, J_T, \pi)$ which can then be used to calculate the desired cross section using (5.1). In practice, this approach is not always feasible due to the lack of some of this required information and the approach has relied on additional approximations. In particular, most practical applications have made use of the so-called “Weisskopf–Ewing approximation”, which assumes that the branching ratios $G_{c+C}^{CN}(E_{ex}, J_T, \pi)$ are independent of the angular momentum and spin, giving rise to the simplified cross section:

$$\sigma_{(x+A \rightarrow c+C)}(E) = \sigma_{x+A \rightarrow B}^{CN}(E_{ex}) G_{c+C}^{CN}(E_{ex}), \quad (5.4)$$

where $\sigma_{x+A \rightarrow B}^{CN}(E_{ex})$ is to be understood as the CN cross section summed over all possible J_T, π values. Applying the same approximation to the surrogate reaction, and using $\sum_{J_T, \pi} F_S^{CN}(E_{ex}, J_T, \pi) = 1$ we have

$$P_{S,c+C}(E_{ex}) = G_{c+C}^{CN}(E_{ex}), \quad (5.5)$$

allowing the determination of the desired cross section as

$$\sigma_{x+A \rightarrow c+C}(E) = \sigma_{x+A \rightarrow B}^{CN}(E_{ex}) P_{S,c+C}(E_{ex}), \quad (5.6)$$

which avoids the need of the probabilities $F_S^{CN}(E_{ex}, J_T, \pi)$.

5.1.2. Determination of the formation probability in the IAV model

When the Weisskopf–Ewing assumption is not fulfilled, one needs to return to the more general expression (5.2), which depends on the formation probabilities $F_S^{CN}(E_{ex}, J_T, \pi)$. In some recent applications of the SRM method [222], the authors propose to evaluate this quantity with the help of the Ichimura–Austern–Vincent (IAV) model [223]. This model was originally devised to evaluate the singles cross section for inclusive breakup reactions of the form $a + A \rightarrow b + B^*$ in which only the b particle is detected in the final channel. The model has been recently revisited and applied by several groups [224–227]. We give a brief description here and refer the reader to the latter references for further details. We consider the scattering of a two-body projectile ($a = b + x$) off a target A . We assume that b behaves as a spectator so that the $b + A$ interaction is described with some optical potential, while the $x + A$ interaction is given by a microscopic potential. Therefore, the full Hamiltonian of the system is expressed as

$$H = T_{aA} + V_{xA}(\vec{r}_x, \xi_A) + U_{bA}(\vec{r}_{bA}) + T_{bx} + V_{bx}(\vec{r}_{bx}), \quad (5.7)$$

where ξ_A denotes the degrees of freedom of the target nucleus and T_{aA} , T_{bx} are kinetic energy operators for the $a + A$ and $b + x$ relative motions, respectively. The interactions V_{xA} and U_{bA} are the microscopic and optical potential between $x + A$ and $b + A$, respectively.

In DWBA, the differential breakup cross section for the population of an excited state of the $x + A$ system as a function of the angle of the observed fragment b and the kinetic energy of the final channel E_{bB} is given by

$$\frac{d^2\sigma}{d\Omega_b dE_{bB}} = \frac{2\pi}{\hbar v_i} \rho(E_{bB}) \sum_f \delta(E_{aA} - E_{bB} - B_a - E_{xA}) |\langle \chi_{bB}^{(-)}(\vec{k}_b) \Phi_{xA}^f | V_{\text{post}} | \chi_{aA} \phi_a \phi_A \rangle|^2, \quad (5.8)$$

where $\rho(E_{bB})$ is the density of states of b particles, where $V_{\text{post}} = V_{bx} + U_{bA} - U_{bB}$ with U_{bB} an auxiliary and, in principle, arbitrary potential generating the distorted wave $\chi_{bB}^{(-)}$, $\Phi_{xA}^f(\vec{r}_x, \xi_A)$ are the states of the $x + A$ system, $\phi_a(\vec{r}_{bx})$ and $\phi_A(\xi_A)$ represent the ground state wave functions of the projectile and target, respectively, and χ_{aA} is a distorted wave, solution of a potential $U_a(\vec{R})$, typically describing $a + A$ elastic scattering. The delta function ensures energy conservation, with $E_i = E_f = E_{bB} + E_{xA} \equiv E$. By expressing the energy-conserving delta function in Eq. (5.8) as the imaginary part of an energy denominator, the sum over final $x + A$ states can be performed using completeness of these states, leading to a closed-form expression for the inclusive breakup cross section. For many applications, it is convenient to separate the elastic breakup (EBU) and nonelastic breakup (NEB) cross sections, distinguishing the situation in which the target is left in its ground state from the case in which it undergoes some kind of excitation. This separation can be formally done using the techniques proposed by Kasano and Ichimura [228]. The final formula for the NEB part results

$$\frac{d^2\sigma^{\text{NEB}}}{d\Omega_b dE_{bB}} = -\frac{2\pi}{\hbar v_i} \rho(E_{bB}) \langle \varphi_x(\vec{k}_b) | W_{xA} | \varphi_x(\vec{k}_b) \rangle, \quad (5.9)$$

where v_i is the relative velocity in the entrance channel, W_{xA} is the imaginary part of the $x + A$ optical potential U_{xA} and $\varphi_x(\vec{k}_b, \vec{r}_x)$ the so-called x -channel wave function

$$\varphi_x(\vec{k}_b, \vec{r}_x) = G_{xA}^{\text{opt}(+)} \langle \vec{r}_x \phi_b \chi_b^{(-)}(\vec{k}_b) | V_{\text{post}} | \chi_a^{(+)} \phi_a \rangle \quad (5.10)$$

with

$$G_{xA}^{\text{opt}(+)}(E - E_{bB}) = \frac{1}{(E^+ - E_{bB} - T_{xA} - U_{xA})} \quad (5.11)$$

The $\varphi_x(\vec{k}_b, \vec{r}_x)$ function describes the relative motion between the captured particle (x) and the target, when the spectator particle b is scattered with momentum \vec{k}_b . Asymptotically, this function has the usual spherical outgoing wave behavior.

The NEB accounts for breakup processes that involve any kind of nonelastic process of the $x + A$ system, including transfer to bound states, projectile dissociation ($a = b + x$) accompanied by target excitation or the formation of some $A + x$ CN. In the present work, we are interested in this latter process. This suggests that, for practical applications of the method, one might replace the full imaginary part W_{xA} by a short-ranged imaginary potential that simulates the $x + A$ fusion. Work is currently in progress to implement the aforementioned strategy to extract cross sections of astrophysical interest combining the SRM and IAV models. These results can provide valuable insights that may lead to refinements and advancements in THM theory.

6. Summary and outlook

In this comprehensive review, we delve into two commonly employed indirect techniques for extracting information about astrophysical reactions, the ANC and the THM, which utilize transfer reactions to determine reaction cross sections that are relevant in the field of nuclear astrophysics. The ANC method primarily focuses on determining the normalization of the tail of the overlap function. It is particularly useful for evaluating the direct capture reaction rate associated with a specific nuclear level. The THM offers a means of determining the reaction rate for rearrangement reactions by extracting the cross section for a binary process using a surrogate ‘‘Trojan Horse’’ particle. This method provides valuable insights into such reactions without directly measuring them. We have presented the theoretical formulations of these methods in a comprehensive and instructive manner, highlighting their adaptability to experimental requirements. While the employed approximations have proven successful, further investigations using refined approaches in future calculations can explore their validity in greater detail. Both the ANC and THM have demonstrated their effectiveness in various experiments related to astrophysical phenomena. Here we have provided a sample deriving from recent experimental works. Looking ahead, with the emergence of next-generation rare isotope facilities, the ANC and THM are poised to become even more powerful tools. These methods will play a crucial/unique role in addressing new challenges in nuclear astrophysics, such as the study of neutron captures on unstable nuclei or, apparently more trivially, decay channels that involve nuclei in their ground states where the typical γ -particle coincidence technique to reduce the background cannot be applied. This last plays a role of primary importance in astrophysical reactions between medium-heavy ions that are crucial in late evolutionary stages of massive stars in terms of energy generation and production of heavy elements. By utilizing these techniques, researchers can make significant advancements in understanding the intricate processes that occur in stellar environments.

Declaration of competing interest

The authors declare that they have no known competing financial interests or personal relationships that could have appeared to influence the work reported in this paper.

Acknowledgments

This work has been supported by the European Union (ChETEC-INFRA, project no. 101008324), the U.S. DOE grants DE-FG02-08ER41533, and the PRIN project ‘‘urka’’ 2022rjlwhn.

References

- [1] D.D. Clayton, *Principles of Stellar Evolution and Nucleosynthesis*, McGraw-Hill Book Company, 1968.
- [2] C.E. Rolfs, W.S. Rodney, *Cauldrons in the Cosmos*, University of Chicago Press, USA, 1988.
- [3] E.G. Adelberger, A. García, R.G.H. Robertson, K.A. Snover, A.B. Balantekin, K. Heeger, M.J. Ramsey-Musolf, D. Bemmerer, A. Junghans, C.A. Bertulani, J.W. Chen, H. Costantini, P. Prati, M. Couder, E. Uberseder, M. Wiescher, R. Cyburt, B. Davids, S.J. Freedman, M. Gai, D. Gazit, L. Gialanella, G. Imbriani, U. Greife, M. Hass, W.C. Haxton, T. Itahashi, K. Kubodera, K. Langanke, D. Leitner, M. Leitner, P. Vetter, L. Winslow, L.E. Marcucci, T. Motobayashi, A. Mukhamedzhanov, R.E. Tribble, K.M. Nollett, F.M. Nunes, T.S. Park, P.D. Parker, R. Schiavilla, E.C. Simpson, C. Spitaleri, F. Strieder, H.P. Trautvetter, K. Suemmerer, S. Typel, *Rev. Modern Phys.* 83 (1) (2011) 195–246, <http://dx.doi.org/10.1103/RevModPhys.83.195>, arXiv:1004.2318.
- [4] C. Iliadis, *Nuclear Physics of the Stars*, Wiley, Weinheim, 2007.
- [5] C. Bertulani, P. Danielewicz, *Introduction to Nuclear Reactions*, second ed., Taylor & Francis, Bristol, UK, 2021.
- [6] H. Assenbaum, K. Langanke, C. Rolfs, Z. Phys. A At. Nucl. 327 (1987) 461–468, <http://dx.doi.org/10.1007/BF01289572>.
- [7] F. Strieder, C. Rolfs, C. Spitaleri, P. Corvisiero, *Naturwissenschaften* 88 (2001) 461–467, <http://dx.doi.org/10.1007/s001140100267>.
- [8] G. Fiorentini, R. Kavanagh, C. Rolfs, Z. Phys. A Hadron. Nucl. 350 (1995) 289–301, <http://dx.doi.org/10.1007/BF01291186>.
- [9] C. Iliadis, *Phys. Rev. C* 107 (4) (2023) 044610, <http://dx.doi.org/10.1103/PhysRevC.107.044610>, arXiv:2304.03383.
- [10] C. Bertulani, A. Gade, *Phys. Rep.* 485 (6) (2010) 195–259, <http://dx.doi.org/10.1016/j.physrep.2009.09.002>, URL <https://www.sciencedirect.com/science/article/pii/S037015730900252X>.
- [11] M. Aliotta, K. Langanke, *Front. Phys.* 10 (2022) 1–9, <http://dx.doi.org/10.3389/fphy.2022.942726>.
- [12] P. Descouvemont, D. Baye, *Rep. Progr. Phys.* 73 (3) (2010) 036301, <http://dx.doi.org/10.1088/0034-4885/73/3/036301>, arXiv:1001.0678.
- [13] H.J. Assenbaum, K. Langanke, C. Rolfs, Z. Phys. A Hadron. Nucl. 327 (4) (1987) 461–468.
- [14] A. Tumino, C. Spitaleri, C. Bertulani, A.M. Mukhamedzhanov, *Few-Body Syst.* 54 (7) (2013) 869–875, <http://dx.doi.org/10.1007/s00601-013-0690-5>.
- [15] R. Tribble, C. Bertulani, M. La Cognata, A. Mukhamedzhanov, C. Spitaleri, *Rep. Progr. Phys.* 77 (10) (2014) 106901, <http://dx.doi.org/10.1088/0034-4885/77/10/106901>.
- [16] T. Aumann, C. Bertulani, *Prog. Part. Nucl. Phys.* 112 (2020) 103753, <http://dx.doi.org/10.1016/j.pnpnp.2019.103753>.
- [17] A. Tumino, C.A. Bertulani, M.L. Cognata, L. Lamia, R.G. Pizzone, S. Romano, S. Typel, *Ann. Rev. Nucl. Part. Sci.* 71 (2021) 345–376, <http://dx.doi.org/10.1146/annurev-nucl-102419-033642>.
- [18] A. Tumino, S. Typel, in: I. Tanihata, H. Toki, T. Kajino (Eds.), *Handbook of Nuclear Physics*, 2022, pp. 1–32, http://dx.doi.org/10.1007/978-981-15-8818-1_1-1.
- [19] A.M. Mukhamedzhanov, L.D. Blokhintsev, *Eur. Phys. J. A* 58 (2) (2022) 29, <http://dx.doi.org/10.1140/epja/s10050-021-00651-0>.
- [20] G. Baur, C. Bertulani, H. Rebel, *Nucl. Phys. A* 458 (1) (1986) 188–204, [http://dx.doi.org/10.1016/0375-9474\(86\)90290-3](http://dx.doi.org/10.1016/0375-9474(86)90290-3).
- [21] S. Typel, H. Wolter, *Few-Body Syst.* 29 (2000) 75–93, <http://dx.doi.org/10.1007/s006010070010>.
- [22] C. Spitaleri, et al., *Phys. Rev. C* 63 (2001) 055801, <http://dx.doi.org/10.1103/PhysRevC.63.055801>.
- [23] S. Typel, G. Baur, *Ann. Phys.* 305 (2003) 228–265, [http://dx.doi.org/10.1016/S0003-4916\(03\)00060-5](http://dx.doi.org/10.1016/S0003-4916(03)00060-5), arXiv:nucl-th/0208069.
- [24] A.M. Mukhamedzhanov, et al., *Eur. Phys. J. A* 27 (S1) (2006) 205–215, <http://dx.doi.org/10.1016/j.nuclphysa.2006.12.051>, arXiv:nucl-th/0509035.
- [25] C. Spitaleri, in: R. Cherubini, P. Dalpiaz, B. Minetti (Eds.), “Quasi-Free Reactions at Low Energy”, *Problems of Fundamental Modern Physics II*, World Scientific, 1991, <http://dx.doi.org/10.1142/1154>.
- [26] G. Baur, *Phys. Lett. B* 178 (1986) 135–138, [http://dx.doi.org/10.1016/0370-2693\(86\)91483-8](http://dx.doi.org/10.1016/0370-2693(86)91483-8).
- [27] A. Kadyrov, I. Bray, A. Mukhamedzhanov, A. Stelbovics, *Ann. Physics* 324 (7) (2009) 1516–1546, <http://dx.doi.org/10.1016/j.aop.2009.02.003>, URL <https://www.sciencedirect.com/science/article/pii/S0003491609000463>. July 2009 Special Issue.
- [28] A.M. Mukhamedzhanov, L.D. Blokhintsev, B.F. Irgaziev, A.S. Kadyrov, M. La Cognata, C. Spitaleri, R.E. Tribble, *J. Phys. G* 35 (2008) 014016, <http://dx.doi.org/10.1088/0954-3899/35/1/014016>, arXiv:0708.0658.
- [29] M. La Cognata, et al., *Astrophys. J.* 708 (2010) 796–811, <http://dx.doi.org/10.1088/0004-637X/708/1/796>.
- [30] A. Tumino, et al., *Nature* 557 (2018) 687–690, <http://dx.doi.org/10.1038/s41586-018-0149-4>.
- [31] A. Mukhamedzhanov, *Phys. Rev. C* 84 (2011) 044616, <http://dx.doi.org/10.1103/PhysRevC.84.044616>, arXiv:1108.4663.
- [32] M. La Cognata, et al., *Ap. J. L.* 739 (2011) L54, <http://dx.doi.org/10.1088/2041-8205/739/2/L54>.
- [33] A.M. Lane, R.G. Thomas, *Rev. Modern Phys.* 30 (1958) 257–353, <http://dx.doi.org/10.1103/RevModPhys.30.257>.
- [34] M.S. Hussein, *Eur. Phys. J. A* 53 (5) (2017) 110, <http://dx.doi.org/10.1140/epja/i2017-12321-7>, arXiv:1705.06305.
- [35] C.A. Bertulani, M.S. Hussein, S. Typel, *Phys. Lett. B* 776 (2018) 217–221, <http://dx.doi.org/10.1016/j.physletb.2017.11.050>, arXiv:1707.04563.
- [36] L.D. Faddeev, *Zh. Eksp. Teor. Fiz.* 39 (1960) 1459–1467.
- [37] A. Mukhamedzhanov, R. Tribble, *Phys. Rev. C* 59 (1999) 3418–3424, <http://dx.doi.org/10.1103/PhysRevC.59.3418>.
- [38] A. Mukhamedzhanov, H. Clark, C. Gagliardi, Y.-W. Lui, L. Trache, R. Tribble, H. Xu, X.G. Zhou, V. Burjan, J. Cejpek, V. Kroha, F. Carstoiu, *Phys. Rev. C* 56 (1997) 1302–1312, <http://dx.doi.org/10.1103/PhysRevC.56.1302>.
- [39] I. Thompson, *Comput. Phys. Rep.* 7 (4) (1988) 167–212, [http://dx.doi.org/10.1016/0167-7977\(88\)90005-6](http://dx.doi.org/10.1016/0167-7977(88)90005-6), URL <https://www.sciencedirect.com/science/article/pii/0167797788900056>.
- [40] V. Burjan, M. Gulino, Z. Hons, V. Kroha, M. McCleskey, J. Mrázek, N. Nguyen, F.M. Nunes, S. Piskor, S. Romano, M.L. Sergi, C. Spitaleri, R.E. Tribble, *Eur. Phys. J. A* 55 (7) (2019) 114, <http://dx.doi.org/10.1140/epja/i2019-12801-8>.
- [41] G. Kiss, M. La Cognata, C. Spitaleri, R. Yarmukhamedov, I. Wiedenhöver, L. Baby, S. Cherubini, A. Cvetinović, G. D’Agata, P. Figuera, G. Guardo, M. Gulino, S. Hayakawa, I. Indelicato, L. Lamia, M. Lattuada, F. Mudd, S. Palmerini, R. Pizzone, G. Rapisarda, S. Romano, M. Sergi, R. Sparta, O. Trippella, A. Tumino, M. Anastasiou, S. Kuvín, N. Rijal, B. Schmidt, S. Igamov, S. Sakuta, K. Tursumakhatov, Z. Fülöp, G. Gyürky, T. Szücs, Z. Halász, E. Somorjai, Z. Hons, J. Mrázek, R. Tribble, A. Mukhamedzhanov, *Phys. Lett. B* 807 (2020) 135606, <http://dx.doi.org/10.1016/j.physletb.2020.135606>.
- [42] N.K. Timofeyuk, R. Johnson, A. Mukhamedzhanov, *Phys. Rev. Lett.* 91 (2003) 232501, <http://dx.doi.org/10.1103/PhysRevLett.91.232501>, arXiv:nucl-th/0311049. Erratum: *Phys. Rev. Lett.* 97 (2006) 069904.
- [43] L. Trache, A. Azhari, F. Carstoiu, H. Clark, C. Gagliardi, Y. Lui, A. Mukhamedzhanov, X. Tang, N. Timofeyuk, R. Tribble, *Phys. Rev. C* 67 (2003) 062801, <http://dx.doi.org/10.1103/PhysRevC.67.062801>, arXiv:nucl-ex/0304016.
- [44] M. McCleskey, A.M. Mukhamedzhanov, L. Trache, R.E. Tribble, A. Banu, V. Eremenko, V.Z. Goldberg, Y.-W. Lui, E. McCleskey, B.T. Roeder, A. Spiridon, F. Carstoiu, V. Burjan, Z. Hons, I. Thompson, *Phys. Rev. C* 89 (4) (2014) 044605, <http://dx.doi.org/10.1103/PhysRevC.89.044605>.
- [45] G. D’Agata, A.I. Kilic, V. Burjan, J. Mrázek, V. Glagolev, V. Kroha, G.L. Guardo, M. La Cognata, L. Lamia, S. Palmerini, R.G. Pizzone, G.G. Rapisarda, S. Romano, M.L. Sergi, R. Sparta, C. Spitaleri, I. Siváček, A. Tumino, *Phys. Rev. C* 103 (2021) 015806, <http://dx.doi.org/10.1103/PhysRevC.103.015806>, URL <https://link.aps.org/doi/10.1103/PhysRevC.103.015806>.
- [46] C. Abia, R.P. Hedrosa, I. Domínguez, O. Straniero, *Astron. Astrophys.* 599 (2017) A39, <http://dx.doi.org/10.1051/0004-6361/201629969>.
- [47] S. Palmerini, O. Trippella, M. Busso, *Mon. Not. R. Astron. Soc.* 467 (1) (2017) 1193–1201, <http://dx.doi.org/10.1093/mnras/stx137>, arXiv:https://academic.oup.com/mnras/article-pdf/467/1/1193/10489548/stx137.pdf.
- [48] M. Wiescher, H.W. Becker, J. Görres, K.U. Kettner, H.P. Trautvetter, W.E. Kieser, C. Rolfs, R.E. Azuma, K.P. Jackson, J.W. Hammer, *Nucl. Phys. A* 349 (1) (1980) 165–216, [http://dx.doi.org/10.1016/0375-9474\(80\)90451-0](http://dx.doi.org/10.1016/0375-9474(80)90451-0), URL <https://www.sciencedirect.com/science/article/pii/0375947480904510>.

- [49] R.B. Vogelaar, T.R. Wang, S.E. Kellogg, R.W. Kavanagh, *Phys. Rev. C* 42 (1990) 753–757, <http://dx.doi.org/10.1103/PhysRevC.42.753>, URL <https://link.aps.org/doi/10.1103/PhysRevC.42.753>.
- [50] F.R. Pantaleo, A. Boeltzig, A. Best, R. Perrino, M. Aliotta, J. Balibrea-Correa, F. Barile, D. Bemmerer, C. Brogгинi, C.G. Bruno, R. Buompane, A. Cacioli, F. Cavanna, T. Chillery, G.F. Ciani, P. Corvisiero, L. Csedreki, T. Davinson, R.J. deBoer, R. Depalo, G. D'Erasmus, A. Di Leva, Z. Elekes, F. Ferraro, E.M. Fiore, A. Formicola, Z. Fülöp, G. Gervino, A. Guglielmetti, C. Gustavino, G. Gyürky, G. Imbriani, M. Junker, I. Kochanek, M. Lugaro, E. Masha, R. Menegazzo, V. Mossa, V. Paticchio, D. Piatti, P. Prati, D. Rapagnani, L. Schiavulli, K. Stöckel, O. Straniero, T. Szücs, M.P. Takács, D. Trezzi, M. Wiescher, S. Zavatarelli, LUNA Collaboration Collaboration, *Phys. Rev. C* 104 (2021) 025802, <http://dx.doi.org/10.1103/PhysRevC.104.025802>, URL <https://link.aps.org/doi/10.1103/PhysRevC.104.025802>.
- [51] M.Q. Buckner, C. Iliadis, J.M. Cesaratto, C. Howard, T.B. Clegg, A.E. Champagne, S. Daigle, *Phys. Rev. C* 86 (2012) 065804, <http://dx.doi.org/10.1103/PhysRevC.86.065804>, URL <https://link.aps.org/doi/10.1103/PhysRevC.86.065804>.
- [52] V. Burjan, Z. Hons, V. Kroha, J. Mrázek, Š. Piškor, A.M. Mukhamedzhanov, L. Trache, R.E. Tribble, M. La Cognata, L. Lamia, R.G. Pizzone, S. Romano, C. Spitaleri, A. Tumino, *Eur. Phys. J. A* 55 (114) (2019) <http://dx.doi.org/10.1140/epja/i2019-12801-8>.
- [53] J. Verotte, G. Berrier-Ronsin, J. Kalifa, R. Tamisier, *Nucl. Phys. A* 390 (2) (1982) 285–313, [http://dx.doi.org/10.1016/0375-9474\(82\)90162-2](http://dx.doi.org/10.1016/0375-9474(82)90162-2), URL <https://www.sciencedirect.com/science/article/pii/0375947482901622>.
- [54] T. H.-J., P. Lezoch, U. Strohhusch, *Nucl. Phys. A* 462 (2) (1987) 333–357, [http://dx.doi.org/10.1016/0375-9474\(87\)90551-3](http://dx.doi.org/10.1016/0375-9474(87)90551-3), URL <https://www.sciencedirect.com/science/article/pii/0375947487905513>.
- [55] C.M. Perey, F.G. Perey, *At. Data Nucl. Data Tables* 17 (1) (1976) 1–101, [http://dx.doi.org/10.1016/0092-640X\(76\)90007-3](http://dx.doi.org/10.1016/0092-640X(76)90007-3), URL <https://www.sciencedirect.com/science/article/pii/0092640X76900073>.
- [56] R.G. Pizzone, R. Sparta, C.A. Bertulani, C. Spitaleri, M. La Cognata, J. Lalmansingh, L. Lamia, A. Mukhamedzhanov, A. Tumino, *Astrophys. J.* 786 (2) (2014) 112, <http://dx.doi.org/10.1088/0004-637X/786/2/112>, arXiv:1403.4909.
- [57] G.G. Kiss, M. La Cognata, C. Spitaleri, R. Yarmukhamedov, I. Wiedenhöver, L.T. Baby, S. Cherubini, A. Cvetinović, G. D'Agata, P. Figuera, G.L. Guardo, M. Gulino, S. Hayakawa, I. Indelicato, L. Lamia, M. Lattuada, F. Muddò, S. Palmerini, R.G. Pizzone, G.G. Rapisarda, S. Romano, M.L. Sergi, R. Sparta, O. Trippella, A. Tumino, M. Anastasiou, S.A. Kuvin, N. Rijal, B. Schmidt, S.B. Igamov, S.B. Sakuta, K.I. Tursunmakhmatov, Z. Fülöp, G. Gyürky, T. Szücs, Z. Halász, E. Somorjai, Z. Hons, J. Mrázek, R.E. Tribble, A.M. Mukhamedzhanov, *Phys. Lett. B* 807 (2020) 135606, <http://dx.doi.org/10.1016/j.physletb.2020.135606>.
- [58] P. Descouvemont, A. Adahchour, C. Angulo, A. Coc, E. Vangioni-Flam, *At. Data Nucl. Data Tables* 88 (1) (2004) 203–236, <http://dx.doi.org/10.1016/j.adt.2004.08.001>, arXiv:astro-ph/0407101.
- [59] Q.I. Tursunmakhmatov, R. Yarmukhamedov, *Phys. Rev. C* 85 (4) (2012) 045807, <http://dx.doi.org/10.1103/PhysRevC.85.045807>, arXiv:0905.2026.
- [60] G. Kiss, M. La Cognata, R. Yarmukhamedov, K. Tursunmakhmatov, I. Wiedenhöver, L. Baby, S. Cherubini, A. Cvetinović, G. D'Agata, P. Figuera, G. Guardo, M. Gulino, S. Hayakawa, I. Indelicato, L. Lamia, M. Lattuada, F. Muddò, S. Palmerini, R. Pizzone, G. Rapisarda, S. Romano, M. Sergi, R. Sparta, C. Spitaleri, O. Trippella, A. Tumino, M. Anastasiou, S. Kuvin, N. Rijal, B. Schmidt, S. Igamov, S. Sakuta, Z. Fülöp, G. Gyürky, T. Szücs, Z. Halász, E. Somorjai, Z. Hons, J. Mrázek, R. Tribble, A. Mukhamedzhanov, *Phys. Rev. C* 104 (2021) 015807, <http://dx.doi.org/10.1103/PhysRevC.104.015807>, URL <https://link.aps.org/doi/10.1103/PhysRevC.104.015807>.
- [61] L. Bouchet, E. Jourdain, J.-P. Roques, *Astrophys. J.* 801 (2) (2015) 142, <http://dx.doi.org/10.1088/0004-637X/801/2/142>.
- [62] J. José, A. Coc, M. Hernandez, *Astrophys. J.* 560 (2) (2001) 897, <http://dx.doi.org/10.1086/322979>.
- [63] N. Prantzos, R. Diehl, *Phys. Rep.* 267 (1) (1996) 1–69, [http://dx.doi.org/10.1016/0370-1573\(95\)00055-0](http://dx.doi.org/10.1016/0370-1573(95)00055-0), URL <https://www.sciencedirect.com/science/article/pii/0370157395000550>.
- [64] M. Wiescher, J. Görres, F.-K. Thielemann, H. Ritter, *Astron. Astrophys.* 160 (1986) 56–72, URL <https://articles.adsabs.harvard.edu/pdf/1986A%26A...160...56W>.
- [65] H. Herndl, J. Görres, M. Wiescher, B.A. Brown, L. Van Wormer, *Phys. Rev. C* 52 (1995) 1078–1094, <http://dx.doi.org/10.1103/PhysRevC.52.1078>, URL <https://link.aps.org/doi/10.1103/PhysRevC.52.1078>.
- [66] J.A. Caggiano, D. Bazin, V. Benenson, B. Davids, R. Ibbotson, H. Scheit, B.M. Sherrill, M. Steiner, J. Yurkon, A.F. Zeller, B. Blank, M. Chartier, J. Greene, J.A. Nolen, A.H. Wuosmaa, M. Bhattacharya, A. Garcia, M. Wiescher, *Phys. Rev. C* 64 (2001) 025802, <http://dx.doi.org/10.1103/PhysRevC.64.025802>, URL <https://link.aps.org/doi/10.1103/PhysRevC.64.025802>.
- [67] Y. Togano, T. Gomi, T. Motobayashi, Y. Ando, N. Aoi, H. Baba, K. Demichi, Z. Elekes, N. Fukuda, Z. Fülöp, U. Futakami, H. Hasegawa, Y. Higurashi, K. Ieki, N. Imai, M. Ishihara, K. Ishikawa, N. Iwasa, H. Iwasaki, S. Kanno, Y. Kondo, T. Kubo, S. Kubono, M. Kunibu, K. Kurita, Y.U. Matsuyama, S. Michimasa, T. Minemura, M. Miura, H. Murakami, T. Nakamura, M. Notani, S. Ota, A. Saito, H. Sakurai, M. Serata, S. Shimoura, T. Sugimoto, E. Takeshita, S. Takeuchi, K. Ue, K. Yamada, Y. Yanagisawa, K. Yoneda, A. Yoshida, *Phys. Rev. C* 84 (2011) 035808, <http://dx.doi.org/10.1103/PhysRevC.84.035808>, URL <https://link.aps.org/doi/10.1103/PhysRevC.84.035808>.
- [68] J. Marganiec, S. Beceiro Novo, S. Typel, C. Langer, C. Wimmer, H. Alvarez-Pol, T. Aumann, K. Boretzky, E. Casarejos, A. Chatillon, D. Cortina-Gil, U. Datta-Pramanik, Z. Elekes, Z. Fülöp, D. Galaviz, H. Geissel, S. Giron, U. Greife, F. Hammache, M. Heil, J. Hoffman, H. Johansson, O. Kiselev, N. Kurz, K. Larsson, T. Le Bleis, Y.A. Litvinov, K. Mahata, C. Muentz, C. Nociforo, W. Ott, S. Paschalis, R. Plag, W. Prokopowicz, C. Rodríguez Tajés, D.M. Rossi, H. Simon, M. Staniou, J. Stroth, K. Stümmerer, A. Wagner, F. Wamers, H. Weick, M. Wiescher, R3B Collaboration Collaboration, *Phys. Rev. C* 93 (2016) 045811, <http://dx.doi.org/10.1103/PhysRevC.93.045811>, URL <https://link.aps.org/doi/10.1103/PhysRevC.93.045811>.
- [69] B. Guo, Z.H. Li, X.X. Bai, W.P. Liu, N.C. Shu, Y.S. Chen, *Phys. Rev. C* 73 (2006) 048801, <http://dx.doi.org/10.1103/PhysRevC.73.048801>, URL <https://link.aps.org/doi/10.1103/PhysRevC.73.048801>.
- [70] N.K. Timofeyuk, P. Descouvemont, I.J. Thompson, *Phys. Rev. C* 78 (2008) 044323, <http://dx.doi.org/10.1103/PhysRevC.78.044323>, URL <https://link.aps.org/doi/10.1103/PhysRevC.78.044323>.
- [71] F. Meurders, A. Van Der Steld, *Nucl. Phys. A* 230 (2) (1974) 317–328, [http://dx.doi.org/10.1016/0375-9474\(74\)90310-8](http://dx.doi.org/10.1016/0375-9474(74)90310-8), URL <https://www.sciencedirect.com/science/article/pii/0375947474903108>.
- [72] N.K. Timofeyuk, R.C. Johnson, A.M. Mukhamedzhanov, *Phys. Rev. Lett.* 91 (2003) 232501, <http://dx.doi.org/10.1103/PhysRevLett.91.232501>, URL <https://link.aps.org/doi/10.1103/PhysRevLett.91.232501>.
- [73] V. Burjan, J. Mrázek, G. D'Agata, *Front. Astron. Space Sci.* 7 (2020) <http://dx.doi.org/10.3389/fspas.2020.562466>, URL <https://www.frontiersin.org/articles/10.3389/fspas.2020.562466>.
- [74] L.J. Sun, X.X. Xu, S.Q. Hou, C.J. Lin, J. José, J. Lee, J.J. He, Z.H. Li, J.S. Wang, C.X. Yuan, F. Herwig, J. Keegans, T. Budner, D.X. Wang, H.Y. Wu, P.F. Liang, Y.Y. Yang, Y.H. Lam, P. Ma, F.F. Duan, Z.H. Gao, Q. Hu, Z. Bai, J.B. Ma, J.G. Wang, F.P. Zhong, C.G. Wu, D.W. Luo, Y. Jiang, Y. Liu, D.S. Hou, R. Li, N.R. Ma, W.H. Ma, G.Z. Shi, G.M. Yu, D. Patel, S.Y. Jin, Y.F. Wang, Y.C. Yu, Q.W. Zhou, P. Wang, L.Y. Hu, X. Wang, H.L. Zang, P.J. Li, Q.Q. Zhao, H.M. Jia, L. Yang, P.W. Wen, Yang, M. Pan, X.Y. Wang, Z.G. Hu, R.F. Chen, M.L. Liu, W.Q. Yang, Y.M. Zhao, *Phys. Lett. B* 802 (2020) 135213, <http://dx.doi.org/10.1016/j.physletb.2020.135213>, URL <https://www.sciencedirect.com/science/article/pii/S0370269320300174>.
- [75] L.J. Sun, X.X. Xu, C.J. Lin, J. Lee, S.Q. Hou, C.X. Yuan, Z.H. Li, J. José, J.J. He, J.S. Wang, D.X. Wang, H.Y. Wu, P.F. Liang, Y.Y. Yang, Y.H. Lam, P. Ma, F.F. Duan, Z.H. Gao, Q. Hu, Z. Bai, J.B. Ma, J.G. Wang, F.P. Zhong, C.G. Wu, D.W. Luo, Y. Jiang, Y. Liu, D.S. Hou, R. Li, N.R. Ma, W.H. Ma, G.Z. Shi, G.M. Yu, D. Patel, S.Y. Jin, Y.F. Wang, Y.C. Yu, Q.W. Zhou, P. Wang, L.Y. Hu, X. Wang, H.L. Zang, P.J. Li, Q.Q. Zhao, L. Yang, P.W. Wen, F. Yang, H.M. Jia, G.L. Zhang, M. Pan, X.Y. Wang, H.H. Sun, Z.G. Hu, R.F. Chen, M.L. Liu, W.Q. Yang, Y.M. Zhao, H.Q. Zhang, RIBLL Collaboration Collaboration, *Phys. Rev. C* 99 (2019) 064312, <http://dx.doi.org/10.1103/PhysRevC.99.064312>, URL <https://link.aps.org/doi/10.1103/PhysRevC.99.064312>.

- [76] A. Azhari, V. Burjan, F. Carstoiu, C. Gagliardi, V. Kroha, A. Mukhamedzhanov, F. Nunes, X. Tang, L. Trache, R. Tribble, *Phys. Rev. C* 63 (2001) 055803, <http://dx.doi.org/10.1103/PhysRevC.63.055803>.
- [77] C. Gagliardi, R. Tribble, A. Azhari, Y.-W.L. H.L. Clark, A. Mukhamedzhanov, A. Sattarov, L. Trache, V. Burjan, J. Cejpek, V. Kroha, S. Piskor, J. Vincour, *Phys. Rev. C* 59 (1999) 1149–1153, <http://dx.doi.org/10.1103/PhysRevC.59.1149>, arXiv:nucl-ex/9811005.
- [78] P. Bertone, A. Champagne, M. Boswell, C. Iliadis, S. Hale, V. Hansper, D. Powell, *Phys. Rev. C* 66 (2002) 055804, <http://dx.doi.org/10.1103/PhysRevC.66.055804>.
- [79] N. Imai, N. Aoi, S. Kubono, D. Beaumel, K. Abe, S. Kato, T. Kubo, K. Kumagai, M. Kurokawa, X. Liu, A. Mengoni, S. Michimasa, H. Ohnuma, H. Sakurai, P. Strasser, T. Teranishi, M. Ishihara, *Phys. Lett.* 688 (2001) 281–284, [http://dx.doi.org/10.1016/S0375-9474\(01\)00715-1](http://dx.doi.org/10.1016/S0375-9474(01)00715-1).
- [80] S. Kubono, K. Abe, S. Kato, T. Teranishi, M. Kurokawa, X. Liu, N. Imai, K. Kumagai, P. Strasser, M.H. Tanaka, Y. Fuchi, C.S. Lee, Y.K. Kwon, L. Lee, J.H. Ha, Y.K. Kim, *Phys. Rev. Lett.* 90 (2003) 062501, <http://dx.doi.org/10.1103/PhysRevLett.90.062501>.
- [81] T. Motobayashi, T. Takei, S. Kox, C. Perrin, F. Merchez, D. Rebreyend, K. Ieki, H. Murakami, Y. Ando, N. Iwasa, M. Kurokawa, S. Shirato, J. Ruan, T. Ichihara, T. Kubo, N. Inabe, A. Goto, S. Kubono, S. Shimoura, M. Ishihara, *Phys. Lett. B* 264 (1991) 259–263, [http://dx.doi.org/10.1016/0370-2693\(91\)90345-Q](http://dx.doi.org/10.1016/0370-2693(91)90345-Q).
- [82] B. Skorodumov, G. Rogachev, P. Boutachkov, A. Arahamian, V.Z. Goldberg, A. Mukhamedzhanov, S. Almaraz, H. Amro, F.D. Becchetti, S. Brown, Y. Chen, H. Jiang, J.J. Kolata, L.O. Lamm, M. Quinn, A. Woehr, *Phys. Rev. C* 75 (2007) 024607, <http://dx.doi.org/10.1103/PhysRevC.75.024607>.
- [83] A. Mukhamedzhanov, A. Banu, P. Bem, V. Burjan, C. Gagliardi, V. Goldberg, Z. Hons, V. Kroha, M. La Cognata, Š. Piskoř, R. Pizzone, S. Romano, E. Šimečková, C. Spitaleri, L. Trache, R. Tribble, *J. Phys.: Conf. Ser.* 202 (2010) 012017, <http://dx.doi.org/10.1088/1742-6596/202/1/012017>.
- [84] G.G. Kiss, M. La Cognata, R. Yarmukhamedov, K. Tursunmakhatov, I. Wiedenhöver, L. Baby, S. Cherubini, A. Cvetinović, G. D'Agata, P. Figuera, et al., *Phys. Rev. C* 104 (1) (2021) 015807.
- [85] C. Spitaleri, A. Mukhamedzhanov, L. Blokhintsev, M. La Cognata, R. Pizzone, A. Tumino, *Phys. At. Nucl.* 74 (2011) 1725–1739, <http://dx.doi.org/10.1134/S1063778811110184>.
- [86] A. Tumino, C. Spitaleri, S. Cherubini, M. Gulino, M. La Cognata, L. Lamia, R.G. Pizzone, S.M.R. Puglia, G.G. Rapisarda, S. Romano, M.L. Sergi, R. Spartà, *Few-Body Syst.* 54 (2013) 745–753, <http://dx.doi.org/10.1007/s00601-012-0407-1>.
- [87] C. Spitaleri, M. La Cognata, L.L. R.G., Pizzone, A. Tumino, *Eur. Phys. J. A* 55 (9) (2019) 161, <http://dx.doi.org/10.1140/epja/i2019-12833-0>.
- [88] A. Tumino, C. Spitaleri, A. Di Pietro, P. Figuera, M. Lattuada, A. Musumarra, M.G. Pellegriti, R.G. Pizzone, S. Romano, C. Rolfs, S. Tudisco, S. Typel, *Phys. Rev. C* 67 (2003) 065803, <http://dx.doi.org/10.1103/PhysRevC.67.065803>, URL <https://link.aps.org/doi/10.1103/PhysRevC.67.065803>.
- [89] M. Sergi, C. Spitaleri, M. La Cognata, A. Coc, A. Mukhamedzhanov, S.V. Burjan, S. Cherubini, V. Crucillà, M. Gulino, F. Hammache, Z. Hons, B. Irgaziev, G. Kiss, V. Kroha, L. Lamia, R. Pizzone, S. Puglia, G. Rapisarda, S. Romano, N. de Séréville, E. Somorjai, S. Tudisco, A. Tumino, *Phys. Rev. C* 82 (2010) 032801, <http://dx.doi.org/10.1103/PhysRevC.82.032801>.
- [90] M.L. Sergi, C. Spitaleri, M. La Cognata, L. Lamia, R.G. Pizzone, G.G. Rapisarda, X.D. Tang, B. Bucher, M. Couder, P. Davies, R. deBoer, X. Fang, L. Lamm, C. Ma, M. Notani, S. O'Brien, D. Roberson, W. Tan, M. Wiescher, B. Irgaziev, A. Mukhamedzhanov, J. Mrazek, V. Kroha, *Phys. Rev. C* 91 (6) (2015) 065803, <http://dx.doi.org/10.1103/PhysRevC.91.065803>.
- [91] R. Pizzone, C. Bertulani, L. Lamia, M. La Cognata, M. Sergi, R. Spartà, A. Tumino, *Eur. Phys. J. A* 56 (2020) 283, <http://dx.doi.org/10.1140/epja/s10050-020-00285-8>.
- [92] S. Cherubini, M. Gulino, C. Spitaleri, G. Rapisarda, M. La Cognata, L. Lamia, R. Pizzone, S. Romano, S. Kubono, H. Yamaguchi, S. Hayakawa, Y. Wakabayashi, N. Iwasa, S. Kato, T. Komatsubara, T. Teranishi, A. Coc, d.N. Séréville, F. Hammache, G. Kiss, S. Bishop, D. Binh, *Phys. Rev. C* 92 (2015) 015805, <http://dx.doi.org/10.1103/PhysRevC.92.015805>, URL <https://link.aps.org/doi/10.1103/PhysRevC.92.015805>.
- [93] R.G. Pizzone, B.T. Roeder, M. McCleskey, L. Trache, R.E. Tribble, C. Spitaleri, C.A. Bertulani, S. Cherubini, M. Gulino, I. Indelicato, M.L. Cognata, L. Lamia, G.G. Rapisarda, R. Spartà, *Eur. Phys. J. A* 52 (2) (2016) 24, <http://dx.doi.org/10.1140/epja/i2016-16024-3>.
- [94] A. Tumino, R. Spartà, C. Spitaleri, A. Mukhamedzhanov, S. Typel, R. Pizzone, E. Tognelli, S. Degl'Innocenti, V. Burjan, V. Kroha, et al., *Astrophys. J.* 785 (2) (2014) 96.
- [95] A. Cvetinović, C. Spitaleri, R. Spartà, G. Rapisarda, S. Puglia, M. La Cognata, S. Cherubini, G. Guardo, M. Gulino, L. Lamia, et al., *Phys. Rev. C* 97 (6) (2018) 065801.
- [96] G. Rapisarda, C. Spitaleri, A. Cvetinović, R. Spartà, S. Cherubini, G. Guardo, M. Gulino, M. La Cognata, L. Lamia, R. Pizzone, et al., *Eur. Phys. J. A* 54 (11) (2018) 189.
- [97] C. Spitaleri, M. Aliotta, S. Cherubini, M. Lattuada, D. Miljanic, S. Romano, N. Soic, M. Zadro, R. Zappala, *Phys. Rev. C* 60 (1999) 055802, <http://dx.doi.org/10.1103/PhysRevC.60.055802>.
- [98] A. Tumino, C. Spitaleri, M.L. Sergi, V. Kroha, V. Burjan, S. Cherubini, Z. Fülöp, M. La Cognata, L. Lamia, J. Novác, R.G. Pizzone, S. Romano, E. Somorjai, S. Tudisco, J. Vincour, *Eur. Phys. J. A* 27 (2006) 243–248, <http://dx.doi.org/10.1140/epja/i2006-08-038-1>.
- [99] Q.-G. Wen, C.-B. Li, S.-H. Zhou, Q.-Y. Meng, J. Zhou, X.-M. Li, S.-Y. Hu, Y.-Y. Fu, C. Spitaleri, A. Tumino, R.G. Pizzone, G. Rapisarda, *Phys. Rev. C* 78 (2008) 035805, <http://dx.doi.org/10.1103/PhysRevC.78.035805>.
- [100] L. Lamia, C. Spitaleri, N. Carlin, S. Cherubini, M.G.D. Szanto, M. Gulino, M. La Cognata, M.G. Munhoz, R.G. Pizzone, S.M.R. Puglia, G.G. Rapisarda, S. Romano, M.L. Sergi, A.S. de Toledo, S. Tudisco, A. Tumino, *Il Nuovo Cimento* 31 (4) (2008) 423–431, <http://dx.doi.org/10.1393/ncc/i2009-10303-2>.
- [101] G. Rapisarda, C. Spitaleri, A. Cvetinović, R. Spartà, S. Cherubini, G.L. Guardo, M. Gulino, M. La Cognata, L. Lamia, R.G. Pizzone, S. Romano, M.L. Sergi, A. Tumino, *Eur. Phys. J. A* 54 (11) (2018) 189, <http://dx.doi.org/10.1140/epja/i2018-12622-3>.
- [102] A. Cvetinović, C. Spitaleri, R. Spartà, G. Rapisarda, S. Puglia, M. La Cognata, S. Cherubini, G. Guardo, M. Gulino, L. Lamia, R. Pizzone, S. Romano, M. Sergi, A. Tumino, *Phys. Rev. C* 97 (2018) 065801, <http://dx.doi.org/10.1103/PhysRevC.97.065801>, URL <https://link.aps.org/doi/10.1103/PhysRevC.97.065801>.
- [103] C. Spitaleri, L. Lamia, A. Tumino, R.G. Pizzone, S. Cherubini, A.D. Zoppo, P. Figuera, M. La Cognata, A. Musumarra, M.G. Pellegriti, A. Rinollo, C. Rolfs, S. Romano, S. Tudisco, *Phys. Rev. C* 69 (2004) 055806, <http://dx.doi.org/10.1103/PhysRevC.69.055806>; *Phys. Rev. C* 73 (2006) 049905;
- [104] L. Lamia, C. Spitaleri, V. Burjan, N. Carlin, S. Cherubini, V. Crucillà, M.G. Munhoz, M.G.D. Santo, M. Gulino, Z. Hons, G. Kiss, V. Kroha, S. Kubono, M. La Cognata, C. Li, J. Mrazek, A. Mukhamedzhanov, R. Pizzone, S. Puglia, Q. Wen, G. Rapisarda, C. Rolfs, S. Romano, M. Sergi, E. Somorjai, F. Souza, A.S. de Toledo, G. Tabacaru, A. Tumino, Y. Wakabayashi, H. Yamaguchi, S.-H. Zhou, *J. Phys. G: Nucl. Part. Phys.* 39 (1) (2011) 015106, <http://dx.doi.org/10.1088/0954-3899/39/1/015106>.
- [105] M. La Cognata, S. Romano, C. Spitaleri, S. Cherubini, V. Crucillà, M. Gulino, L. Lamia, R.G. Pizzone, A. Tumino, R. Tribble, C. Fu, V.Z. Goldberg, A.M. Mukhamedzhanov, D. Schmidt, G. Tabacaru, L. Trache, B. Irgaziev, *Phys. Rev. C* 76 (2007) 065804, <http://dx.doi.org/10.1103/PhysRevC.76.065804>.
- [106] M. La Cognata, C. Spitaleri, A. Mukhamedzhanov, A. Banu, S. Cherubini, A. Coc, V. Crucillà, B. Irgaziev, M. Gulino, B. Irgaziev, G.G. Kiss, L. Lamia, J. Mrazek, R.G. Pizzone, S.M.R. Puglia, G.G. Rapisarda, S. Romano, M.L. Sergi, G. Tabacaru, L. Trache, R.E. Tribble, W. Trzaska, A. Tumino, *Astrophys. J.* 708 (1) (2009) 796–811, <http://dx.doi.org/10.1088/0004-637x/708/1/796>.
- [107] M. La Cognata, C. Spitaleri, A. Tumino, S. Typel, S. Cherubini, L. Lamia, A. Musumarra, R. Pizzone, A. Rinollo, C. Rolfs, S. Romano, D. Schürmann, F. Strieder, *Phys. Rev. C* 72 (2005) 065802, <http://dx.doi.org/10.1103/PhysRevC.72.065802>.
- [108] A. Rinollo, et al., *Nucl. Phys. A* 758 (2005) 146–149, <http://dx.doi.org/10.1016/j.nuclphysa.2005.05.030>.
- [109] C. Spitaleri, M. Aliotta, P. Figuera, M. Lattuada, R. Pizzone, S. Romano, A. Tumino, C. Rolfs, L. Gialanella, F. Strieder, S. Cherubini, A. Musumarra, D. Miljanic, S. Typel, H. Wolter, *Eur. Phys. J. A* 7 (2000) 181–187, <http://dx.doi.org/10.1007/PL00013592>.

- [110] A. Tumino, C. Spitaleri, C. Bonomo, S. Cherubini, P. Figuera, M. Gulino, M. La Cognata, L. Lamia, A. Musumarra, M.G. Pellegriti, R.G. Pizzone, A. Rinollo, S. Romano, *Eur. Phys. J. A* 25 (2005) 649–650, <http://dx.doi.org/10.1140/epjad/i2005-06-085-1>.
- [111] M. Gulino, C. Spitaleri, S. Cherubini, V. Crucillà, M. La Cognata, L. Lamia, R. Pizzone, S. Romano, M. Sergi, A. Tumino, L. Chengbo, Z. Elekes, E. Somorjai, V. Burjan, V. Kroha, A. Mukhamedzhanov, *J. Phys. G: Nucl. Part. Phys.* 37 (12) (2010) 125105, <http://dx.doi.org/10.1088/0954-3899/37/12/125105>.
- [112] A. Tumino, C. Spitaleri, A. Mukhamedzhanov, G. Rapisarda, S. Cherubini, V. Crucillà, Z. Elekes, Z. Fülöp, M. Gulino, G. Gyürky, G. Kiss, M. La Cognata, L. Lamia, F. Mudò, R. Pizzone, S. Romano, M. Sergi, E. Somorjai, *Phys. Rev. Lett.* 98 (2007) 252502, <http://dx.doi.org/10.1103/PhysRevLett.98.252502>, URL <https://link.aps.org/doi/10.1103/PhysRevLett.98.252502>.
- [113] A. Tumino, C. Spitaleri, A. Mukhamedzhanov, G.G. Rapisarda, L. Campajola, S. Cherubini, V. Crucillà, Z. Elekes, Z. Fülöp, L. Gialanella, M. Gulino, G. Gyürky, G. Kiss, M. La Cognata, L. Lamia, A. Ordine, R.G. Pizzone, S. Romano, M.L. Sergi, E. Somorjai, *Phys. Rev. C* 78 (2008) 064001, <http://dx.doi.org/10.1103/PhysRevC.78.064001>.
- [114] A. Tumino, C. Spitaleri, A. Mukhamedzhanov, S. Typel, M. Aliotta, V. Burjan, M.G. del Santo, G. Kiss, V. Kroha, Z. Hons, M. La Cognata, L. Lamia, J. Mrazek, R. Pizzone, S. Piskor, G. Rapisarda, S. Romano, M. Sergi, R. Spartà, *Phys. Lett. B* 700 (2) (2011) 111–115, <http://dx.doi.org/10.1016/j.physletb.2011.05.001>, URL <https://www.sciencedirect.com/science/article/pii/S0370269311004813>.
- [115] I. Indelicato, M. La Cognata, C. Spitaleri, V. Burjan, S. Cherubini, M. Gulino, S. Hayakawa, Z. Hons, V. Kroha, L. Lamia, M. Mazzocco, J. Mrazek, R.G. Pizzone, S. Romano, E. Strano, D. Torresi, A. Tumino, *Astrophys. J.* 845 (1) (2017) 19, <http://dx.doi.org/10.3847/1538-4357/aa7de7>.
- [116] M. La Cognata, C. Spitaleri, O. Trippella, G.G. Kiss, G.V. Rogachev, A.M. Mukhamedzhanov, M. Avila, G.L. Guardo, E. Koshchii, A. Kuchera, L. Lamia, S.M.R. Puglia, S. Romano, D. Santiago, R. Spartà, *Astrophys. J.* 777 (2) (2013) 143, <http://dx.doi.org/10.1088/0004-637x/777/2/143>.
- [117] R. Pizzone, G. D'Agata, M. La Cognata, I. Indelicato, C. Spitaleri, S. Blagus, S. Cherubini, P. Figuera, L. Grassi, G.L. Guardo, M. Gulino, S. Hayakawa, R. Kshetri, L. Lamia, M. Lattuada, T. Mijatović, M. Milin, D.M. D., L. Preolec, G.G. Rapisarda, S. Romano, M.L. Sergi, N. Skukan, N. Soić, V. Tokić, A. Tumino, M. Uroić, *Astrophys. J.* 836 (1) (2017) 57, <http://dx.doi.org/10.3847/1538-4357/836/1/57>.
- [118] M. La Cognata, R.G. Pizzone, J. José, M. Hernanz, S. Cherubini, M. Gulino, G.G. Rapisarda, C. Spitaleri, *Astrophys. J.* 846 (1) (2017) 65, <http://dx.doi.org/10.3847/1538-4357/aa845f>.
- [119] G. Guardo, C. Spitaleri, L. Lamia, R. Spartà, N. Carlin, S. Cherubini, G.G.D. Santo, I. Indelicato, M. La Cognata, D. Lattuada, S. Messina, M. Munhoz, S.P.R. Pizzone, G. Rapisarda, S. Romano, M. Sergi, F. Souza, A.S. de Toledo, S. Tudisco, A. Tumino, *Eur. Phys. J. A* 55 (2019) 211, <http://dx.doi.org/10.1140/epja/i2019-12914-0>.
- [120] R. Spartà, L. Lamia, M. La Cognata, C. Spitaleri, G.G. Rapisarda, G.L. Guardo, S. Cherubini, G. D'Agata, A. Di Pietro, P. Figuera, M. Gulino, D. Lattuada, M. Lattuada, S. Palmerini, R.G. Pizzone, S. Romano, M.L. Sergi, A. Tumino, S. Typel, *Eur. Phys. J. A* 57 (2021) 170, <http://dx.doi.org/10.1140/epja/s10050-021-00481-0>.
- [121] L. Lamia, C. Spitaleri, C.A. Bertulani, S.Q. Hou, M. La Cognata, R.G. Pizzone, S. Romano, M.L. Sergi, A. Tumino, *Astrophys. J.* 850 (2) (2017) 175, <http://dx.doi.org/10.3847/1538-4357/aa965c>.
- [122] L. Lamia, M. Mazzocco, R.G. Pizzone, S. Hayakawa, M. La Cognata, C. Spitaleri, C.A. Bertulani, A. Boiano, C. Boiano, C. Broggin, A. Caciolli, S. Cherubini, G. D'Agata, H. da Silva, R. Depalo, F. Galtarossa, G.L. Guardo, M. Gulino, I. Indelicato, M. La Commara, G. La Rana, R. Menegazzo, J. Mrazek, A. Pakou, C. Parascandolo, D. Piatti, D. Pierroutsakou, S.M.R. Puglia, S. Romano, G.G. Rapisarda, A.M. Sánchez-Benítez, M.L. Sergi, O. Sgouros, F. Soramel, V. Soukera, R. Spartà, E. Strano, D. Torresi, A. Tumino, H. Yamaguchi, G.L. Zhang, *Astrophys. J.* 879 (1) (2019) 23, <http://dx.doi.org/10.3847/1538-4357/ab2234>.
- [123] S. Hayakawa, M. La Cognata, L. Lamia, H. Yamaguchi, D. Kahl, K. Abe, H. Shimizu, L. Yang, O. Beliuskina, S.M. Cha, K.Y. Chae, S. Cherubini, P. Figuera, Z. Ge, M. Gulino, J. Hu, A. Inoue, N. Iwasa, A. Kim, D. Kim, G. Kiss, S. Kubono, M. La Commara, M. Lattuada, E.J. Lee, J.Y. Moon, S. Palmerini, C. Parascandolo, S.Y. Park, V.H. Phong, D. Pierroutsakou, R.G. Pizzone, G.G. Rapisarda, S. Romano, C. Spitaleri, X.D. Tang, O. Trippella, A. Tumino, N.T. Zhang, *Astrophys. J. Lett.* 915 (1) (2021) L13, <http://dx.doi.org/10.3847/2041-8213/ac061f>.
- [124] G. D'Agata, R.G. Pizzone, M. La Cognata, I. Indelicato, C. Spitaleri, S. Palmerini, O. Trippella, D. Vescovi, S. Blagus, S. Cherubini, P. Figuera, L. Grassi, G.L. Guardo, M. Gulino, S. Hayakawa, R. Kshetri, L. Lamia, M. Lattuada, T. Mijatović, M. Milin, D. Miljanić, L. Preolec, G.G. Rapisarda, S. Romano, M.L. Sergi, N. Skukan, N. Soć, V. Tokić, A. Tumino, M. Uroić, *Astrophys. J.* 860 (1) (2018) 61, <http://dx.doi.org/10.3847/1538-4357/aac207>.
- [125] A. Oliva, G. Guardo, L. Lamia, S. Cherubini, A. Cvetinovic, G. D'Agata, N. de Sereville, A. Di Pietro, P. Figuera, M. Gulino, F. Hammache, S. Hayakawa, I. Indelicato, M. La Cognata, M.L. Commara, D. Lattuada, M. Lattuada, G. Manicò, M. Mazzocco, S. Messina, S. Palmerini, R. Pizzone, M. Pumo, G. Rapisarda, S. Romano, M. Sergi, N. Soić, R. Spartà, C. Spitaleri, A. Tumino, *Il Nuovo Cimento C* 43 (2020) 111, <http://dx.doi.org/10.1393/ncc/i2020-20111-7>.
- [126] R. Pizzone, C. Spampinato, R. Spartà, M. Couder, W. Tan, V. Burjan, G. D'Agata, G.L. Guardo, M. La Cognata, L. Lamia, J. Mrazek, S. Palmerini, S. Typel, A. Tumino, M. Wiescher, S. Anguilar, D. Bardayan, D. Blankstein, L. Boccioni, L. Callahan, S.M. Cha, K.Y. Chae, A.M. Clark, B. Frenzt, M.R. Hall, A. Gula, S. Henderson, R. Kelmar, M.S. Kwag, I. Indelicato, M.L. Commara, D. Lattuada, Q. Liu, J. Long, M. Mazzocco, A. Majumdar, S. McGuinness, A. Nelson, A.A. Oliva, P. O'Malley, P.M. Prajapati, G.G. Rapisarda, S. Romano, M.L. Sergi, C. Seymour, M. Skulski, C. Spitaleri, J. Wilkinson, *Eur. Phys. J. A* 56 (2020) 199, <http://dx.doi.org/10.1140/epja/s10050-020-00212-x>.
- [127] S. Palmerini, et al., *Eur. Phys. J. Plus* 136 (2021) 898, <http://dx.doi.org/10.1140/epjp/s13360-021-01872-4>.
- [128] M. La Cognata, S. Palmerini, P. Adsley, F. Hammache, A. Di Pietro, P. Figuera, R. Alba, S. Cherubini, F. Dell'Agli, G. Guardo, M. Gulino, L. Lamia, D. Lattuada, C. Maiolino, A. Oliva, R. Pizzone, P. Prajapati, S. Romano, D. Santonocito, R. Spartà, M. Sergi, A. Tumino, *Phys. Lett. B* 826 (2022) 136917, <http://dx.doi.org/10.1016/j.physletb.2022.136917>, URL <https://www.sciencedirect.com/science/article/pii/S037026932200051X>.
- [129] M. La Cognata, S. Palmerini, P. Adsley, F. Hammache, A. Di Pietro, P. Figuera, F. Dell'Agli, R. Alba, S. Cherubini, G.L. Guardo, M. Gulino, L. Lamia, D. Lattuada, C. Maiolino, A. Oliva, R.G. Pizzone, P.M. Prajapati, G.G. Rapisarda, S. Romano, D. Santonocito, R. Spartà, M.L. Sergi, A. Tumino, P. Ventura, *Astrophys. J.* 941 (1) (2022) 96, <http://dx.doi.org/10.3847/1538-4357/ac9c5e>.
- [130] R.H. Cyburt, B.D. Fields, K.A. Olive, T.-H. Yeh, *Rev. Modern Phys.* 88 (1) (2016) 015004, <http://dx.doi.org/10.1103/RevModPhys.88.015004>, arXiv:1505.01076.
- [131] L. Lamia, C. Spitaleri, R.G. Pizzone, E. Tognelli, A. Tumino, S. Degl'Innocenti, P.G. Prada Moroni, M. La Cognata, L. Pappalardo, M.L. Sergi, *Astrophys. J.* 768 (1) (2013) 65, <http://dx.doi.org/10.1088/0004-637X/768/1/65>.
- [132] C. Li, Q. Wen, A. Tumino, Y. Fu, J. Zhou, S. Zhou, Q. Meng, C. Spitaleri, R.G. Pizzone, L. Lamia, *Phys. Rev. C* 95 (2017) 035804, <http://dx.doi.org/10.1103/PhysRevC.95.035804>, URL <https://link.aps.org/doi/10.1103/PhysRevC.95.035804>.
- [133] M.L. Cognata, C. Spitaleri, A. Tumino, S. Typel, S. Cherubini, L. Lamia, A. Musumarra, R.G. Pizzone, A. Rinollo, C. Rolfs, S. Romano, D. Schürmann, F. Strieder, *Phys. Rev. C* 72 (2005) 065802, <http://dx.doi.org/10.1103/PhysRevC.72.065802>, URL <https://link.aps.org/doi/10.1103/PhysRevC.72.065802>.
- [134] L. Lamia, C. Spitaleri, M. La Cognata, S. Palmerini, R.G. Pizzone, *Astron. Astrophys.* 541 (2012) A158, <http://dx.doi.org/10.1051/0004-6361/201219014>.
- [135] R. Pizzone, R. Spartà, C. Bertulani, C. Spitaleri, M. La Cognata, J. Lalamsingh, L. Lamia, A. Mukhamedzhanov, A. Tumino, *Astrophys. J.* 786 (2) (2014) 112.
- [136] R. Pizzone, C. Spampinato, R. Spartà, M. Couder, W. Tan, V. Burjan, G. D'Agata, G. Guardo, M. La Cognata, L. Lamia, et al., *Eur. Phys. J. A* 56 (8) (2020) 199.
- [137] R. Spartà, R.G. Pizzone, C.A. Bertulani, S. Hou, L. Lamia, A. Tumino, *Front. Astron. Space Sci.* 7 (2020) 560149.
- [138] C.A. Bertulani, T. Kajino, *Prog. Part. Nucl. Phys.* 89 (2016) 56–100, <http://dx.doi.org/10.1016/j.pnpnp.2016.04.001>, arXiv:1604.03197.
- [139] A. Coc, E. Vangioni, *Int. J. Mod. Phys. E* 26 (8) (2017) 1741002, <http://dx.doi.org/10.1142/S0218301317410026>, arXiv:1707.01004.
- [140] S.Q. Hou, J.J. He, S. Kubono, Y.S. Chen, *Phys. Rev. C* 91 (5) (2015) 055802, <http://dx.doi.org/10.1103/PhysRevC.91.055802>, arXiv:1502.03961.

- [141] M. Barbagallo, A. Musumarra, L. Cosentino, E. Maugeri, S. Heinitz, A. Mengoni, R. Dressler, D. Schumann, F. Käppeler, N. Colonna, P. Finocchiaro, M. Ayrano, L. Damone, N. Kivel, O. Aberle, S. Altstadt, J. Andrzejewski, L. Audouin, M. Bacak, J. Balibrea-Correa, S. Barros, V. Bécáres, F. Bečvář, C. Beinrucker, E. Berthoumieux, J. Billowes, D. Bosnar, M. Brugger, M. Caamaño, M. Calviani, F. Calviño, D. Cano-Ott, R. Cardella, A. Casanovas, D.M. Castelluccio, F. Cerutti, Y.H. Chen, E. Chiaveri, G. Cortés, M.A. Cortés-Giraldo, S. Cristallo, M. Diakaki, C. Domingo-Pardo, E. Dupont, I. Duran, B. Fernandez-Dominguez, A. Ferrari, P. Ferreira, W. Furman, S. Ganesan, A. García-Rios, A. Gawlik, T. Glodariu, K. Göbel, I.F. Gonçalves, E. González-Romero, E. Griesmayer, C. Guerrero, F. Gunsing, H. Harada, T. Heftrich, J. Heyse, D.G. Jenkins, E. Jericha, T. Katabuchi, P. Kavrgin, A. Kimura, M. Kokkoris, M. Krtička, E. Leal-Cidoncha, J. Lerendegui, C. Lederer, H. Leeb, S. Lo Meo, S.J. Lonsdale, R. Losito, D. Macina, J. Marganec, T. Martínez, C. Massimi, P. Mastinu, M. Mastromarco, A. Mazzone, E. Mendoza, P.M. Milazzo, F. Mingrone, M. Mirea, S. Montesano, R. Nolte, A. Oprea, A. Pappalardo, N. Patronis, A. Pavlik, J. Perkowski, M. Piscopo, A. Plompen, I. Porras, J. Praena, J. Quesada, K. Rajeev, T. Rauscher, R. Reifarth, A. Riego-Perez, P. Rout, C. Rubbia, J. Ryan, M. Sabate-Gilarte, A. Saxena, P. Schillebeeckx, S. Schmidt, P. Sedyshev, A.G. Smith, A. Stamatopoulos, G. Tagliente, J.L. Tain, A. Tarifeño-Saldivia, L. Tassan-Got, A. Tsinganis, S. Valenta, G. Vannini, V. Variale, P. Vaz, A. Ventura, V. Vlachoudis, R. Vlastou, J. Vollaie, A. Wallner, S. Warren, M. Weigand, C. Weiß, C. Wolf, P.J. Woods, T. Wright, P. Žugec, n TOF Collaboration, *Phys. Rev. Lett.* 117 (15) (2016) 152701, <http://dx.doi.org/10.1103/PhysRevLett.117.152701>, [arXiv:1606.09420](https://arxiv.org/abs/1606.09420).
- [142] L. Damone, M. Barbagallo, M. Mastromarco, A. Mengoni, L. Cosentino, E. Maugeri, S. Heinitz, D. Schumann, R. Dressler, F. Käppeler, N. Colonna, P. Finocchiaro, J. Andrzejewski, J. Perkowski, A. Gawlik, O. Aberle, S. Altstadt, M. Ayrano, L. Audouin, M. Bacak, J. Balibrea-Correa, J. Ballof, V. Bécáres, F. Bečvář, C. Beinrucker, G. Bellia, A.P. Bernardes, E. Berthoumieux, J. Billowes, M.J.G. Borge, D. Bosnar, A. Brown, M. Brugger, M. Busso, M. Caamaño, F. Calviño, M. Calviani, D. Cano-Ott, R. Cardella, A. Casanovas, D.M. Castelluccio, R. Catherall, F. Cerutti, Y.H. Chen, E. Chiaveri, J.G.M. Correia, G. Cortés, M.A. Cortés-Giraldo, S. Cristallo, M. Diakaki, M. Dietz, C. Domingo-Pardo, A. Dorsival, E. Dupont, I. Duran, B. Fernandez-Dominguez, A. Ferrari, P. Ferreira, W. Furman, S. Ganesan, A. García-Rios, S. Gilardoni, T. Glodariu, K. Göbel, I.F. Gonçalves, E. González-Romero, T.D. Goodacre, E. Griesmayer, C. Guerrero, F. Gunsing, H. Harada, T. Heftrich, J. Heyse, D.G. Jenkins, E. Jericha, K. Johnston, Y. Kadi, A. Kalamara, T. Katabuchi, P. Kavrgin, A. Kimura, N. Kivel, U. Köster, M. Kokkoris, M. Krtička, D. Kurtulgil, E. Leal-Cidoncha, C. Lederer-Woods, H. Leeb, J. Lerendegui-Marco, S. Lo Meo, S.J. Lonsdale, R. Losito, D. Macina, J. Marganec, B. Marsh, T. Martínez, F. Marsh, D. Massimi, P. Mastinu, F. Matteucci, A. Mazzone, E. Mendoza, P.M. Milazzo, F. Mingrone, M. Mirea, A. Musumarra, A. Negret, R. Nolte, A. Oprea, N. Patronis, A. Pavlik, L. Piersanti, M. Piscopo, A. Plompen, I. Porras, J. Praena, J.M. Quesada, D. Radeck, K. Rajeev, T. Rauscher, R. Reifarth, A. Riego-Perez, S. Rothe, P. Rout, C. Rubbia, J. Ryan, M. Sabate-Gilarte, A. Saxena, J. Schell, P. Schillebeeckx, S. Schmidt, P. Sedyshev, C. Seiffert, A.G. Smith, N.V. Sosnin, A. Stamatopoulos, T. Stora, G. Tagliente, J.L. Tain, A. Tarifeño-Saldivia, L. Tassan-Got, A. Tsinganis, S. Valenta, G. Vannini, V. Variale, P. Vaz, A. Ventura, V. Vlachoudis, R. Vlastou, A. Wallner, S. Warren, M. Weigand, C. Weiß, C. Wolf, P.J. Woods, T. Wright, P. Žugec, n TOF Collaboration, *Phys. Rev. Lett.* 121 (4) (2018) 042701, <http://dx.doi.org/10.1103/PhysRevLett.121.042701>, [arXiv:1803.05701](https://arxiv.org/abs/1803.05701).
- [143] M. Gai, E.E. Kading, M. Hass, K.M. Nolle, S.R. Stern, T. Stora, A. Weiss, *European Physical Journal Web of Conferences*, in: *European Physical Journal Web of Conferences*, vol. 227, 2020, p. 01007, <http://dx.doi.org/10.1051/epjconf/202022701007>.
- [144] P.E. Koehler, C.D. Bowman, F.J. Steinkruger, D.C. Moody, G.M. Hale, J.W. Stamer, S.A. Wender, R.C. Haight, P.W. Lisowski, W.L. Talbert, *Phys. Rev. C* 37 (3) (1988) 917–926, <http://dx.doi.org/10.1103/PhysRevC.37.917>.
- [145] I. Tomandl, J. Vacić, U. Köster, L. Viererbl, E.A. Maugeri, S. Heinitz, D. Schumann, M. Ayrano, J. Ballof, R. Catherall, K. Chrysalidis, T. Day Goodacre, D. Fedorov, V. Fedosseev, K. Johnston, B. Marsh, S. Rothe, J. Schell, C. Seiffert, *Phys. Rev. C* 99 (1) (2019) 014612, <http://dx.doi.org/10.1103/PhysRevC.99.014612>.
- [146] S. Kubono, Y. Yanagisawa, T. Teranishi, S. Kato, Y. Kishida, S. Michimasa, Y. Ohshiro, S. Shimoura, K. Ue, S. Watanabe, N. Yamazaki, *Eur. Phys. J. A* 13 (1–2) (2002) 217–220.
- [147] Y. Yanagisawa, S. Kubono, T. Teranishi, K. Ue, S. Michimasa, M. Notani, J.J. He, Y. Ohshiro, S. Shimoura, S. Watanabe, N. Yamazaki, H. Iwasaki, S. Kato, T. Kishida, T. Morikawa, Y. Mizoi, *Nucl. Instrum. Methods Phys. Res. A* 539 (2005) 74–83, <http://dx.doi.org/10.1016/j.nima.2004.09.041>.
- [148] H. Yamaguchi, S. Hayakawa, N.R. Ma, H. Shimizu, L. Yang, D. Kahl, K. Abe, T. Suhara, N. Iwasa, A. Kim, D.H. Kim, S.M. Cha, M.S. Kwag, J.H. Lee, E.J. Lee, K.Y. Chae, Y. Wakabayashi, N. Imai, N. Kitamura, P. Lee, J.Y. Moon, K.B. Lee, C. Akers, H.S. Jung, N.N. Duy, L.H. Khiem, C.S. Lee, S. Cherubini, M. Gulino, C. Spitaleri, G.G. Rapisarda, L. Cognata, L. Lamia, S. Romano, A. Coc, N. de Sereville, F. Hammache, G. Kiss, S. Bishop, T. Teranishi, T. Kawabata, Y.K. Kwon, D.N. Binh, *Journal of Physics Conference Series*, in: *Journal of Physics Conference Series*, vol. 1643, 2020, 012069, <http://dx.doi.org/10.1088/1742-6596/1643/1/012069>.
- [149] A. Krauss, H.W. Becker, H.P. Trautvetter, C. Rolfs, K. Brand, *Nucl. Phys. A* 465 (1) (1987) 150–172, [http://dx.doi.org/10.1016/0375-9474\(87\)90302-2](http://dx.doi.org/10.1016/0375-9474(87)90302-2).
- [150] U. Greife, F. Gorris, M. Junker, C. Rolfs, D. Zahnow, *Z. Phys. A Hadron. Nucl.* 351 (1) (1995) 107–112, <http://dx.doi.org/10.1007/BF01292792>.
- [151] R.E. Brown, N. Jarmie, *Phys. Rev. C* 41 (4) (1990) 1391–1400, <http://dx.doi.org/10.1103/PhysRevC.41.1391>.
- [152] R.L. Schulte, M. Cosack, A.W. Obst, J.L. Weil, *Nucl. Phys. A* 192 (3) (1972) 609–624, [http://dx.doi.org/10.1016/0375-9474\(72\)90093-0](http://dx.doi.org/10.1016/0375-9474(72)90093-0).
- [153] C. Angulo, M. Arnould, M. Rayet, P. Descouvemont, D. Baye, C. Leclercq-Willain, A. Coc, S. Barhoumi, P. Aguer, C. Rolfs, R. Kunz, J.W. Hammer, A. Mayer, T. Paradellis, S. Kossionides, C. Chronidou, K. Spyrou, S. degl'Innocenti, G. Fiorentini, B. Ricci, S. Zavatarelli, C. Providencia, H. Wolters, J. Soares, C. Grama, J. Rahighi, A. Shoter, M. Lamehi Rachti, *Nucl. Phys. A* 656 (1) (1999) 3–183, [http://dx.doi.org/10.1016/S0375-9474\(99\)00030-5](http://dx.doi.org/10.1016/S0375-9474(99)00030-5).
- [154] R.H. Cyburt, *Phys. Rev. D* 70 (2) (2004) 023505, <http://dx.doi.org/10.1103/PhysRevD.70.023505>, [arXiv:astro-ph/0401091](https://arxiv.org/abs/astro-ph/0401091).
- [155] A. Coc, E. Vangioni, *Journal of Physics Conference Series*, in: *Journal of Physics Conference Series*, vol. 202, 2010, 012001, <http://dx.doi.org/10.1088/1742-6596/202/1/012001>.
- [156] R.J. Cooke, M. Pettini, C.C. Steidel, *Astrophys. J.* 855 (2) (2018) 102.
- [157] V. Mossa, K. Stöckel, F. Cavanna, F. Ferraro, M. Aliotta, F. Barile, D. Bemmerer, A. Best, A. Boeltzig, C. Brogini, et al., *Nature* 587 (7833) (2020) 210–213.
- [158] J. Moscoso, R.S. de Souza, A. Coc, C. Iliadis, *Astrophys. J.* 923 (1) (2021) 49.
- [159] K. Lind, S.E. Kopusov, C. Battistini, A.F. Marino, G. Ruchti, A. Serenelli, C.C. Worley, A. Alves-Brito, M. Asplund, P.S. Barklem, T. Bensby, M. Bergemann, S. Blanco-Cuaresma, A. Bragaglia, B. Edvardsson, S. Feltzing, P. Gruyters, U. Heiter, P. Jofre, A.J. Korn, T. Nordlander, N. Ryde, C. Soubiran, G. Gilmore, S. Randich, A.M.N. Ferguson, R.D. Jeffries, A. Vallenari, C. Allende Prieto, E. Pancino, A. Recio-Blanco, D. Romano, R. Smiljanic, M. Bellazzini, F. Damiani, V. Hill, P. de Laverny, R.J. Jackson, C. Lardo, S. Zaggia, *Astron. Astrophys.* 575 (2015) L12, <http://dx.doi.org/10.1051/0004-6361/201425554>.
- [160] G.S.D. Costa, J.E. Norris, D. Yong, *Astrophys. J.* 769 (1) (2013) 8, <http://dx.doi.org/10.1088/0004-637X/769/1/8>.
- [161] E. Carretta, A. Bragaglia, S. Lucatello, R.G. Gratton, V. D'Orazi, A. Sollima, *Astron. Astrophys.* 615 (2018) A17, <http://dx.doi.org/10.1051/0004-6361/201732324>.
- [162] C. Iliadis, R. Longland, A.E. Champagne, A. Coc, *Nucl. Phys. A* 841 (1–4) (2010) 251–322, <http://dx.doi.org/10.1016/j.nuclphysa.2010.04.010>, [arXiv:1004.4149](https://arxiv.org/abs/1004.4149).
- [163] C. Iliadis, *Nuclear physics of stars*, 2015, <http://dx.doi.org/10.1002/9783527692668>.
- [164] R. Diehl, H. Haloain, K. Kretschmer, G.G. Lichti, V. Schönfelder, A.W. Strong, A. von Kienlin, W. Wang, P. Jean, J. Knödseder, J.-P. Roques, G. Weidenspointner, S. Schanne, D.H. Hartmann, C. Winkler, C. Wunderer, *Nature* 439 (7072) (2006) 45–47, <http://dx.doi.org/10.1038/nature04364>, [arXiv:astro-ph/0601015](https://arxiv.org/abs/astro-ph/0601015).
- [165] E. Groopman, E. Zinner, S. Amari, F. Gyngard, P. Hoppe, M. Jadhav, Y. Lin, Y. Xu, K. Marhas, L.R. Nittler, *Astrophys. J.* 809 (1) (2015) 31, <http://dx.doi.org/10.1088/0004-637X/809/1/31>.

- [166] M. La Cognata, S. Palmerini, C. Spitaleri, I. Indelicato, A.M. Mukhamedzhanov, I. Lombardo, O. Trippella, *Astrophys. J.* 805 (2) (2015) 128, <http://dx.doi.org/10.1088/0004-637X/805/2/128>.
- [167] R. Longland, C. Iliadis, A.E. Champagne, J.R. Newton, C. Ugalde, A. Coc, R. Fitzgerald, *Nucl. Phys. A* 841 (1–4) (2010) 1–30, <http://dx.doi.org/10.1016/j.nuclphysa.2010.04.008>, arXiv:1004.4136.
- [168] A. Tumino, C. Spitaleri, A. Mukhamedzhanov, G.G. Rapisarda, S. Cherubini, V. Crucillà, Z. Elekes, Z. Fülöp, M. Gulino, G. Gyürky, G. Kiss, M. La Cognata, L. Lamia, F. Mudó, R.G. Pizzone, S. Romano, M.L. Sergi, E. Somorjai, *Phys. Rev. Lett.* 98 (25) (2007) 252502, <http://dx.doi.org/10.1103/PhysRevLett.98.252502>.
- [169] A. Tumino, C. Spitaleri, A. Mukhamedzhanov, G.G. Rapisarda, L. Campajola, S. Cherubini, V. Crucillà, Z. Elekes, Z. Fülöp, L. Gialanella, M. Gulino, G. Gyürky, G. Kiss, M.L. Cognata, L. Lamia, A. Ordine, R.G. Pizzone, S. Romano, M.L. Sergi, E. Somorjai, *Phys. Rev. C* 78 (6) (2008) 064001, <http://dx.doi.org/10.1103/PhysRevC.78.064001>.
- [170] M. Piarulli, L. Giralanda, R. Schiavilla, R.N. Pérez, J.E. Amaro, E.R. Arriola, *Phys. Rev. C* 91 (2) (2015) 024003, <http://dx.doi.org/10.1103/PhysRevC.91.024003>, arXiv:1412.6446.
- [171] S.-I. Ando, J.W. Shin, C.H. Hyun, S.-W. Hong, *Phys. Rev. C* 76 (6) (2007) 064001, <http://dx.doi.org/10.1103/PhysRevC.76.064001>, arXiv:0704.2312.
- [172] E. Epelbaum, W. Glöckle, U.-G. Meißner, *Nucl. Phys. A* 747 (2) (2005) 362–424, <http://dx.doi.org/10.1016/j.nuclphysa.2004.09.107>, arXiv:nucl-th/0405048.
- [173] M. Walzl, U.-G. Meißner, E. Epelbaum, *Nucl. Phys. A* 693 (3) (2001) 663–692, [http://dx.doi.org/10.1016/S0375-9474\(01\)00969-1](http://dx.doi.org/10.1016/S0375-9474(01)00969-1), arXiv:nucl-th/0010019.
- [174] A. Tumino, G.G. Rapisarda, M. La Cognata, A. Oliva, A. Kievsky, C.A. Bertulani, G. D'Agata, M. Gattobigio, G.L. Guardo, L. Lamia, D. Lattuada, R.G. Pizzone, S. Romano, M.L. Sergi, R. Spartà, M. Viviani, *Commun. Phys.* 6 (1) (2023) 106, <http://dx.doi.org/10.1038/s42005-023-01221-0>.
- [175] D. Foreman-Mackey, M.W. Hogg, D. Lang, J. Goodman, *Publ. Astron. Soc. Pac.* 125 (925) (2013) 306, <http://dx.doi.org/10.1086/670067>, arXiv:1202.3665.
- [176] J. Goodman, J. Weare, *Commun. Appl. Math. Comput. Sci.* 5 (1) (2010) 65–80, <http://dx.doi.org/10.2140/camcos.2010.5.65>.
- [177] E. Braaten, H.W. Hammer, *Phys. Rep.* 428 (5–6) (2006) 259–390, <http://dx.doi.org/10.1016/j.physrep.2006.03.001>, arXiv:cond-mat/0410417.
- [178] A. Tumino, A. Kievsky, G.G. Rapisarda, M. La Cognata, A. Oliva, C.A. Bertulani, G. D'Agata, M. Gattobigio, G.L. Guardo, L. Lamia, D. Lattuada, R.G. Pizzone, S. Romano, M.L. Sergi, R. Spartà, M. Viviani, *Few-Body Systems* 66 (1) (2024) 5, <http://dx.doi.org/10.1007/s00601-024-01975-5>.
- [179] M.E. Bennett, R. Hirschi, M. Pignatari, S. Diehl, C. Fryer, F. Herwig, A. Hungerford, K. Nomoto, G. Rockefeller, F.X. Timmes, M. Wiescher, *Mon. Not. R. Astron. Soc.* 420 (4) (2012) 3047–3070, <http://dx.doi.org/10.1111/j.1365-2966.2012.20193.x>, arXiv:1201.1225.
- [180] M.C. Chen, F. Herwig, P.A. Denissenkov, B. Paxton, *Mon. Not. R. Astron. Soc.* 440 (2) (2014) 1274–1280, <http://dx.doi.org/10.1093/mnras/stu108>, arXiv:1310.1898.
- [181] T. Spillane, F. Raiola, C. Rolfs, D. Schurman, F. Strieder, S. Zeng, H. Becker, C. Bordeanu, L. Gialanella, M. Romano, J. Schweitzer, *Phys. Rev. Lett.* 98 (2007) 122501, <http://dx.doi.org/10.1103/PhysRevLett.98.122501>.
- [182] C.L. Jiang, D. Santiago-Gonzalez, S. Almaraz-Calderon, K.E. Rehm, B.B. Back, K. Auranen, M.L. Avila, A.D. Ayangeakaa, S. Bottoni, M.P. Carpenter, C. Dickerson, B. DiGiovine, J.P. Greene, C.R. Hoffman, R.V.F. Janssens, B.P. Kay, S.A. Kuvin, T. Lauritsen, R.C. Pardo, J. Sethi, D. Seweryniak, R. Talwar, C. Ugalde, S. Zhu, D. Bourgin, S. Courtin, F. Haas, M. Heine, G. Fruet, D. Montanari, D.G. Jenkins, L. Morris, A. Lefebvre-Schuhl, M. Alcorta, X. Fang, X.D. Tang, B. Bucher, C.M. Deibel, S.T. Marley, *Phys. Rev. C* 97 (2018) 012801, <http://dx.doi.org/10.1103/PhysRevC.97.012801>, URL <https://link.aps.org/doi/10.1103/PhysRevC.97.012801>.
- [183] G. Fruet, S. Courtin, M. Heine, D.G. Jenkins, P. Adsley, A. Brown, R. Canavan, W.N. Catford, E. Charon, D. Curien, S. Della Negra, J. Duprat, F. Hammache, J. Lesrel, G. Lotay, A. Meyer, D. Montanari, L. Morris, M. Moukaddam, J. Nippert, Z. Podolyák, P.H. Regan, I. Ribaud, M. Richer, M. Rudigier, R. Shearman, N. de Séville, C. Stodel, *Phys. Rev. Lett.* 124 (19) (2020) 192701, <http://dx.doi.org/10.1103/PhysRevLett.124.192701>.
- [184] W.P. Tan, A. Boeltzig, C. Dulal, R.J. deBoer, B. Frentz, S. Henderson, K.B. Howard, R. Kelmar, J.J. Kolata, J. Long, K.T. Macon, S. Moylan, G.F. Peaslee, M. Renaud, C. Seymour, G. Seymour, B. Vande Kolk, M. Wiescher, E.F. Aguilera, P. Amador-Valenzuela, D. Lizcano, E. Martinez-Quiroz, *Phys. Rev. Lett.* 124 (19) (2020) 192702, <http://dx.doi.org/10.1103/PhysRevLett.124.192702>, arXiv:2005.03196.
- [185] W.P. Tan, A. Gula, K. Lee, A. Majumdar, S. Moylan, O. Olivas-Gomez, Shahina, M. Wiescher, E.F. Aguilera, D. Lizcano, E. Martinez-Quiroz, J.C. Morales-Rivera, *Phys. Rev. C* 110 (3) (2024) 035808, <http://dx.doi.org/10.1103/PhysRevC.110.035808>.
- [186] L. Morales-Gallegos, M. Aliotta, L. Gialanella, A. Best, C.G. Bruno, R. Buompane, T. Davinson, M. De Cesare, A. Di Leva, A. D'Onofrio, J.G. Duarte, L.R. Gasques, G. Imbriani, G. Porzio, D. Rapagnani, M. Romoli, F. Terrasi, *Eur. Phys. J. A* 60 (1) (2024) 11, <http://dx.doi.org/10.1140/epja/s10050-024-01233-6>.
- [187] C.L. Jiang, H. Esbensen, K.E. Rehm, B.B. Back, R.V.F. Janssens, J.A. Caggiano, P. Collon, J. Greene, A.M. Heinz, D.J. Henderson, I. Nishinaka, T.O. Pennington, D. Seweryniak, *Phys. Rev. Lett.* 89 (2002) 052701, <http://dx.doi.org/10.1103/PhysRevLett.89.052701>, URL <https://link.aps.org/doi/10.1103/PhysRevLett.89.052701>.
- [188] C.L. Jiang, K.E. Rehm, H. Esbensen, R.V. Janssens, B.B. Back, C.N. Davids, J.P. Greene, D.J. Henderson, C.J. Lister, R.C. Pardo, T. Pennington, D. Peterson, D. Seweryniak, B. Shumard, S. Sinha, X.D. Tang, I. Tanihata, S. Zhu, P. Collon, S. Kurtz, M. Paul, *Phys. Rev. C* 71 (4) (2005) 044613, <http://dx.doi.org/10.1103/PhysRevC.71.044613>, arXiv:nucl-ex/0412043.
- [189] C.L. Jiang, B.B. Back, H. Esbensen, R.V. Janssens, K.E. Rehm, *Phys. Rev. C* 73 (1) (2006) 014613, <http://dx.doi.org/10.1103/PhysRevC.73.014613>, arXiv:nucl-ex/0508001.
- [190] Ş. Mişicu, H. Esbensen, *Phys. Rev. Lett.* 96 (11) (2006) 112701, <http://dx.doi.org/10.1103/PhysRevLett.96.112701>, arXiv:nucl-th/0602064.
- [191] G. Montagnoli, A.M. Stefanini, *Eur. Phys. J. A* 53 (8) (2017) 169, <http://dx.doi.org/10.1140/epja/i2017-12350-2>, arXiv:1707.07583.
- [192] B.B. Back, H. Esbensen, C.L. Jiang, K.E. Rehm, *Rev. Modern Phys.* 86 (2014) 317–360, <http://dx.doi.org/10.1103/RevModPhys.86.317>, URL <https://journals.aps.org/rmp/abstract/10.1103/RevModPhys.86.317>.
- [193] K. Godbey, C. Simenel, A.S. Umar, *Phys. Rev. C* 100 (2019) 024619, <http://dx.doi.org/10.1103/PhysRevC.100.024619>, URL <https://journals.aps.org/prc/abstract/10.1103/PhysRevC.100.024619>.
- [194] D. Torresi, C. Wheldon, T. Kokalova, S. Bailey, A. Boiano, C. Boiano, M. Fischella, M. Mazzocco, C. Parascandolo, D. Pierroutsakou, E. Strano, M. Zadro, M. Cavallaro, S. Cherubini, N. Curtis, A. Di Pietro, J. Fernández Garcia, P. Figuera, T. Glodariu, J. Grbosz, M. La Cognata, M. La Commara, M. Lattuada, D. Mengoni, R.G. Pizzone, C. Signorini, C. Stefanini, L. Stroe, C. Spitaleri, *Phys. Rev. C* 96 (2017) 044317, <http://dx.doi.org/10.1103/PhysRevC.96.044317>, URL <https://link.aps.org/doi/10.1103/PhysRevC.96.044317>.
- [195] M. La Cognata, M. Fischella, A.P. Di, P. Figuera, V. Goldberg, S. Cherubini, J.F. Garcia, M. Gulino, L. Lamia, D. Lattuada, et al., *Phys. Rev. C* 99 (3) (2019) 034301.
- [196] N. Zhang, X. Wang, D. Tudor, B. Bucher, I. Burducea, H. Chen, Z. Chen, D. Chesneau, A. Chilug, L. Gasques, et al., *Phys. Lett. B* 801 (2020) 135170.
- [197] A.S. Umar, K. Godbey, C. Simenel, *Phys. Rev. C* 107 (6) (2023) 064605, <http://dx.doi.org/10.1103/PhysRevC.107.064605>, arXiv:2305.17752.
- [198] L.R. Gasques, E.F. Brown, A. Chieffi, C.L. Jiang, M. Limongi, C. Rolfs, M. Wiescher, D.G. Yakovlev, *Phys. Rev. C* 76 (3) (2007) 035802, <http://dx.doi.org/10.1103/PhysRevC.76.035802>.
- [199] M. Pignatari, R. Hirschi, M. Wiescher, R. Gallino, M. Bennett, M. Beard, C. Fryer, F. Herwig, G. Rockefeller, F.X. Timmes, *Astrophys. J.* 762 (1) (2013) 31, <http://dx.doi.org/10.1088/0004-637X/762/1/31>, arXiv:1212.3962.
- [200] A. Chieffi, L. Roberti, M. Limongi, M. La Cognata, L. Lamia, S. Palmerini, R.G. Pizzone, R. Spartà, A. Tumino, *Astrophys. J.* 916 (2) (2021) 79, <http://dx.doi.org/10.3847/1538-4357/ac06ca>, arXiv:2106.00013.

- [201] E. Monribat, S. Martinet, S. Courtin, M. Heine, S. Ekström, D.G. Jenkins, A. Choplin, P. Adsley, D. Curien, M. Moukaddam, J. Nippert, S. Tsiatsiou, G. Meynet, *Astron. Astrophys.* 660 (2022) A47, <http://dx.doi.org/10.1051/0004-6361/202141858>, arXiv:2111.15224.
- [202] M. Fisichella, A.C. Shotton, A. Di Pietro, P. Figuera, M. Lattuada, C. Marchetta, V. Privitera, L. Romano, C. Ruiz, M. Zadro, *Phys. Rev. C* 92 (2015) 064611, <http://dx.doi.org/10.1103/PhysRevC.92.064611>, URL <https://link.aps.org/doi/10.1103/PhysRevC.92.064611>.
- [203] A. Tumino, C. Spitaleri, M.L. Cognata, S. Cherubini, G.L. Guardo, M. Gulino, S. Hayakawa, I. Indelicato, L. Lamia, H. Petrascu, et al., *Nature* 557 (2018) 687–690, <http://dx.doi.org/10.1038/s41586-018-0149-4>.
- [204] M.G. Mazarakis, W.E. Stephens, *Phys. Rev. C* 7 (4) (1973) 1280–1287, <http://dx.doi.org/10.1103/PhysRevC.7.1280>.
- [205] M.D. High, B. Čujec, *Nucl. Phys. A* 282 (1) (1977) 181–188, [http://dx.doi.org/10.1016/0375-9474\(77\)90179-8](http://dx.doi.org/10.1016/0375-9474(77)90179-8).
- [206] K.U. Kettner, H. Lorenz-Wirzba, C. Rolfs, *Z. Phys. A Hadron. Nucl.* 298 (1) (1980) 65–75, <http://dx.doi.org/10.1007/BF01416030>.
- [207] J.R. Patterson, H. Winkler, C.S. Zaidins, *Astrophys. J.* 157 (1969) 367, <http://dx.doi.org/10.1086/150073>.
- [208] H.W. Becker, K.U. Kettner, C. Rolfs, H.P. Trautvetter, *Z. Phys. A Hadron. Nucl.* 303 (1981) 305–312, <http://dx.doi.org/10.1007/BF01421528>.
- [209] L. Barrón-Palos, E.F. Aguilera, J. Aspiazu, A. Huerta, E. Martínez-Quiroz, R. Monroy, E. Moreno, G. Murillo, M.E. Ortiz, R. Policroniades, A. Varela, E. Chávez, *Nucl. Phys. A* 779 (2006) 318–332, <http://dx.doi.org/10.1016/j.nuclphysa.2006.09.004>.
- [210] R. Abegg, C.A. Davis, *Phys. Rev. C* 43 (6) (1991) 2523–2540, <http://dx.doi.org/10.1103/PhysRevC.43.2523>.
- [211] A. Caciolli, G. Calzolari, M. Chiari, A. Climent-Font, G. Garcia, F. Lucarelli, S. Nava, *Nucl. Instrum. Methods Phys. Res. B* 266 (8) (2008) 1392–1396, <http://dx.doi.org/10.1016/j.nimb.2007.11.025>.
- [212] J. Zickefoose, A. Di Leva, F. Strieder, L. Gialanella, G. Imbriani, N. De Cesare, C. Rolfs, J. Schweitzer, T. Spillane, O. Straniero, F. Terrasi, *Phys. Rev. C* 97 (6) (2018) 065806, <http://dx.doi.org/10.1103/PhysRevC.97.065806>.
- [213] A.M. Mukhamedzhanov, D.Y. Pang, A.S. Kadyrov, *Phys. Rev. C* 99 (6) (2019) 064618, <http://dx.doi.org/10.1103/PhysRevC.99.064618>.
- [214] A. Bonasera, J.B. Natowitz, *Phys. Rev. C* 102 (6) (2020) 061602, <http://dx.doi.org/10.1103/PhysRevC.102.061602>, arXiv:2011.05130.
- [215] L.R. Gasques, L.C. Chamon, G.P. Cessel, *Eur. Phys. J. A* 58 (6) (2022) 102, <http://dx.doi.org/10.1140/epja/s10050-022-00751-5>.
- [216] Y. Taniguchi, M. Kimura, *Phys. Lett. B* 849 (2024) 138434, URL <https://doi.org/10.1016/j.physletb.2023.138434>.
- [217] G.R. Caughlan, W.A. Fowler, *At. Data Nucl. Data Tables* 40 (1988) 283, [http://dx.doi.org/10.1016/0092-640X\(88\)90009-5](http://dx.doi.org/10.1016/0092-640X(88)90009-5).
- [218] R.L. Cooper, A.W. Steiner, E.F. Brown, *Astrophys. J.* 702 (1) (2009) 660–671, <http://dx.doi.org/10.1088/0004-637X/702/1/660>, arXiv:0903.3994.
- [219] K. Mori, M.A. Famiano, T. Kajino, M. Kusakabe, X. Tang, *Mon. Not. R. Astron. Soc.: Lett.* 482 (1) (2018) L70–L74, <http://dx.doi.org/10.1093/mnras/sly188>, arXiv:https://academic.oup.com/mnras/article-pdf/482/1/L70/54700039/mnras_482_1_l70.pdf.
- [220] O. Straniero, L. Piersanti, I. Dominguez, A. Tumino, On the mass of supernova progenitors: The role of the $^{12}\text{C} + ^{12}\text{C}$ reaction, 2019, pp. 7–11.
- [221] J.E. Escher, J.T. Harke, F.S. Dietrich, N.D. Scielzo, I.J. Thompson, W. Younes, *Rev. Mod. Phys.* 84 (2012) 353–397, <http://dx.doi.org/10.1103/RevModPhys.84.353>, <https://link.aps.org/doi/10.1103/RevModPhys.84.353>.
- [222] A. Ratkiewicz, J.A. Cizewski, J.E. Escher, G. Potel, J.T. Harke, R.J. Casperson, M. McCleskey, R.A.E. Austin, S. Burcher, R.O. Hughes, B. Manning, S.D. Pain, W.A. Peters, S. Rice, T.J. Ross, N.D. Scielzo, C. Shand, K. Smith, *Phys. Rev. Lett.* 122 (2019) 052502, <http://dx.doi.org/10.1103/PhysRevLett.122.052502>, <https://link.aps.org/doi/10.1103/PhysRevLett.122.052502>.
- [223] M. Ichimura, N. Austern, C.M. Vincent, *Phys. Rev. C* 32 (1985) 431–439, <http://dx.doi.org/10.1103/PhysRevC.32.431>.
- [224] J. Lei, A.M. Moro, *Phys. Rev. C* 92 (2015) 044616, <http://dx.doi.org/10.1103/PhysRevC.92.044616>.
- [225] G. Potel, F.M. Nunes, I.J. Thompson, *Phys. Rev. C* 92 (2015) 034611, <http://dx.doi.org/10.1103/PhysRevC.92.034611>.
- [226] B.V. Carlson, R. Capote, M. Sin, *Few-Body Systems* 57 (2016) 307–314, <http://dx.doi.org/10.1007/s00601-016-1054-8>.
- [227] G. Potel, et al., *Eur. Phys. J. A* 53 (9) (2017) 178, <http://dx.doi.org/10.1140/epja/i2017-12371-9>.
- [228] A. Kasano, M. Ichimura, *Phys. Lett. B* 115 (1982) 81, [http://dx.doi.org/10.1016/0370-2693\(82\)90800-0](http://dx.doi.org/10.1016/0370-2693(82)90800-0).